Copyright Warning & Restrictions

The copyright law of the United States (Title 17, United States Code) governs the making of photocopies or other reproductions of copyrighted material.

Under certain conditions specified in the law, libraries and archives are authorized to furnish a photocopy or other reproduction. One of these specified conditions is that the photocopy or reproduction is not to be "used for any purpose other than private study, scholarship, or research." If a, user makes a request for, or later uses, a photocopy or reproduction for purposes in excess of "fair use" that user may be liable for copyright infringement,

This institution reserves the right to refuse to accept a copying order if, in its judgment, fulfillment of the order would involve violation of copyright law.

Please Note: The author retains the copyright while the New Jersey Institute of Technology reserves the right to distribute this thesis or dissertation

Printing note: If you do not wish to print this page, then select "Pages from: first page # to: last page #" on the print dialog screen

ABSTRACT

DECONTAMINATION OF THE PASSAIC RIVER SEDIMENTS USING ULTRASOUND WITH OZONE *NANO-BUBBLES*

by
Janitha Hewa Batagoda

The Passaic River is 129km long and flows through the northern New Jersey. During the mid-twentieth century, the U.S. census indicated that there were approximately 2,900 industries along the river bank. The amount of industries established next to the river indicated the inevitable river pollution, which was compounded by lenient environmental protection laws. One of the major contributors of the river pollution was Diamond Alkali Co., which started production of chemicals around 1951 at the 4km marker in the Passaic River.

In 1970, the United States Environmental Protection Agency (U.S. EPA) identified the Passaic River as the second most polluted river in the United States, where in 1983 a Diamond Alkali site investigation showed extremely high levels of hazardous chemicals. Contaminants in the river included PAHs, PCDD/F, PCBs, DDT, pesticides and their byproducts, and heavy metals including Hg, Cr, and Pb. This made the contaminated river eligible for cleanup funds under the federal Superfund program. Hence, the U.S. EPA initiated investigations to identify the severity of the river pollution. In 2016, the U.S. EPA proposed a cleanup program to mitigate the impact of the pollution in the river sediments.

Scrutinizing the U.S. EPA remediation plan brings up concerns that will impact the current condition of the river. The dredging exposing the contaminated sediments to freshwater, capping to prevent future dredging, and others such as dewatering and the transportation of the dredged sediments impacting the community during the cleanup are

some of the major concerns. Hence, identifying a better and complete technology to remediate the Passaic River's contaminated sediments is a necessity. This remediation plan should have the capability to be carried out in-situ, where the negative impacts from the current plan can be mitigated.

This research is on developing a novel in-situ technology to remediate the Passaic River sediments by using ultrasound and ozone *nano-bubbles*. The study identifies key parameters that will enhance the removal of organic and inorganic pollutants from the contaminated sediments. The key parameters that impact the proposed technology are temperature, pH level, ozone *nano-bubble* size, dissolved ozone concentration, ultrasound power, dwell time, and the duration of ultrasound treatment.

Each parameter is varied while observing its impact on the removal efficiency of organic and inorganic contaminants in contaminated sediments. The solution temperature has a direct impact on Ozone levels in water, where organic material removal indicates high removal efficiencies at low temperatures. The maximum removal efficiencies of organics were 92%. The inorganic contaminant used during the investigation is chromium. The removal efficiency of the chromium does not show a significant impact due to temperature, where the study shows a 98% removal efficiency. The test results show that the combination of ozone, *nano-bubbles*, and ultrasound to treat contaminated sediments is a reliable and implementable technology. The data obtained from the laboratory experiments can be used to develop a pilot scale study for possible field application.

DECONTAMINATION OF THE PASSAIC RIVER SEDIMENTS USING ULTRASOUND WITH OZONE *NANO-BUBBLES*

by
Janitha Hewa Batagoda

A Dissertation
Submitted to the Faculty of
New Jersey Institute of Technology
in Partial Fulfillment of the Requirements for the Degree of
Doctor of Philosophy in Civil Engineering

John A. Reif, Jr. Department of Civil and Environmental Engineering

May 2018

APPROVAL PAGE

DECONTAMINATION OF THE PASSAIC RIVER SEDIMENTS USING ULTRASOUND WITH OZONE *NANO-BUBBLES*

Janitha Hewa Batagoda

Dr. Jay N. Meegoda, Dissertation Advisor — Date
Professor of Civil and Environmental Engineering, NJIT

Dr. Taha Marhaba, Committee Member — Date
Professor of Civil and Environmental Engineering, NJIT

Dr. Wen Zhang, Committee Member — Date
Associate Professor of Civil and Environmental Engineering, NJIT

Dr. Larisa Kristopa, Committee Member — Date
Director of Materials Characterization Laboratory, NJIT

Dr. Bruno M. Goncalves da Silva, Committee Member — Date
Assistant Professor of Civil and Environmental Engineering, NJIT

Dr. Ivan Guzman, Committee Member — Date
Assistant Professor of New York City College of Technology

BIOGRAPHICAL SKETCH

Author: Janitha Hewa Batagoda

Degree: Doctor of Philosophy

Date: May 2018

Undergraduate and Graduate Education:

- Doctor of Philosophy in Civil Engineering,
  New Jersey Institute of Technology, Newark, NJ, 2018

- Master of Science in Civil Engineering,
  University of Moratuwa, Sri Lanka, 2011

- Bachelor of Science in Civil Engineering,
  University of Moratuwa, Sri Lanka, 2008

Major: Civil Engineering

Presentations and Publications:

Batagoda J. H., Meegoda, J. N., Aluthgun-Hewage, S., (2018). In-situ Remediation of Passaic River Sediments using Ultrasound and Ozone Nano-bubbles. *Proceedings of World Environmental & Water Resources Congress 2018*, Minneapolis, MN, USA.

Meegoda J. N., Batagoda J. H., Aluthgun-Hewage, S., (2017). Briefing: In-situ Decontamination of Sediments using Ozone *Nano-bubbles* and Ultrasound. *Journal of Environmental Engineering and Science*, 12 (1), pp. 1-3.

Meegoda J. N., Batagoda J. H., Aluthgun-Hewage, S., (2017). Decontaminate Passaic River Sediments using Ultrasound with Ozone Nano Bubbles. *Proceedings of the 19th International Conference on Soil Mechanics and Geotechnical Engineering*, Seoul, South Korea.

Kamolpornwijit W., Meegoda J. N., Batagoda J. H., (2017). Metal Extraction from Chromium Contaminated Soils. *Proceedings of the 19th International Conference on Soil Mechanics and Geotechnical Engineering*, Seoul, South Korea.

Kamolpornwijit W., Meegoda J. N., Batagoda J. H., (2017). A Detailed Laboratory Scale Feasibility Study of Recovering Metallic Iron and Chromium from Chromium Contaminated Soils. *Indian Geotechnical Journal*. 46(4), pp. 437-444.

Kamolpornwijit W., Meegoda J. N., Batagoda J. H., (2016). Detailed Laboratory Scale Feasibility Study of Recovering Metallic Iron and Chromium from Contaminated Soil. *International Conference on Soil and Environment* 2016, Bangalore

Meegoda J. N., & Batagoda J. H., (2016). A New Technology to Decontaminate Sediments Using Ultrasound with Ozone Nano Bubbles. *Geo-Chicago 2016: Sustainability, Energy, and the Geoenvironment*, pp- 14-18, August 2016.

Kamolpornwijit W., Meegoda J. N., Batagoda J. H., (2015). Engineering Properties of Chromium Contaminated Soils. *Geotechnical Engineering Journal of the SEAGS & AGSSEA.* 46 (4). pp – 8-15, ISSN 0046-5828

Jayasinghe C., & Batagoda J. H., (2013). The Effect of Building Planning Aspects on Indoor Air Quality. *International Journal of Civil Engineering, International Academy of Science, Engineering and Technology*. 2, pp- 9-28.

Batagoda J. H., & Jayasinghe C., (2010). Effect of Building Ventilation on Indoor Environment. *International Conference on Sustainable Built Environments (ICSBE 2010)* 12th-14th December 2010, Kandy, Sri Lanka.

Batagoda J. H., & Jayasinghe C., (2010). Demand Control Ventilation and Sri Lankan Application – A Case Study. *International Conference on Sustainable Built Environments (ICSBE 2010)* 12th-14th December 2010, Kandy, Sri Lanka.

මා දයාබර දෙමාපියන් වෙත පුදකරමි

To my parents

For their unlimited

Love and support

ACKNOWLEDGEMENT

I would like to extend my sincere gratitude to many people who supported and contributed towards the research study presented in this dissertation. This feat was unobtainable without my research supervisor, committee members, academic and non-academic staff, friends and family who helped in many ways during my research.

I want to convey my sincere gratitude to my research advisor professor Jay Meegoda for this opportunity join New Jersey Institute of Technology (NJIT) and study for my Ph.D. also for opportunities of research he provided me exposing me to many areas of research. His guidance and support throughout my research helped me to obtain and achieve many goals. I am grateful for the guidance and help of Dr. Wen Zhang throughout my research by letting me use equipment from the environmental laboratory. I would like to deeply thank Dr. Larisa Kristopa for her immense support by facilitating me to use the facilities of the York Center and her insight on analytical methods.

I would like to thank my dissertation committee members Dr. Taha Marhaba, Dr. Bruno M. Goncalves da Silva and Dr. Ivan Guzman for their constructive criticism and advice to improve my dissertation. I am grateful for their help and support provided throughout my research to be better at my research and teaching activities.

I acknowledge the National Science Foundation (NSF, Award Number: 1349089) for providing funding to purchase materials necessary to conduct this research. I am also grateful for the I-CORPs for providing me funding to travel for conferences to present my findings and to gain more experience by talking to peers.

I want to thank Mrs. Heidi Young, Mr. Steven George, and Mr. Andrew Flory for their help and support providing me necessary access to laboratories and purchasing

necessary materials and machinery to progress research. I would like to thank all my friends namely, Mr. Likun Hua, Ms. Shaini Dilsha and Ms. Wanyi Fu for their support while carrying out my studies and all the others who helped me in many ways.

Finally, I would like to thank my Father, Mr. Nandasena Batagoda and my Mother, Ms. Susantha Vithanage for their loving support and for keeping me motivated.

TABLE OF CONTENTS

TABLE OF CONTENTS
(Continued)

Chapter **Page**

TABLE OF CONTENTS
(Continued)

TABLE OF CONTENTS
(Continued)

Chapter **Page**

LIST OF TABLES

LIST OF FIGURES

LIST OF FIGURES
(Continued)

LIST OF FIGURES
(Continued)

LIST OF FIGURES
(Continued)

CHAPTER 1

INTRODUCTION

1.1 Problem Statement

1.1.1 Geology and Topography

The Passaic River was formed in north New Jersey at the end of the last ice age due to a massive proglacial lake (Lake Passaic). The Passaic River watershed is approximately 129 kilometers long and starts near Mendham, NJ. Its river basin drains almost 2,435 square kilometers in northeastern New Jersey and southeastern New York. The ancient native Indians used the river as a mode of transportation. The early settlers from Europe also used this river as a mode of transportation for food. Hints of these cultures and names of their settlements resonate throughout the region and remain as valuable windows into the area's history and human settlements. The development of the river as a transportation center and a port during the Civil War encouraged the use of the river as the transportation center and led to dredging of the river to enhance transportation. After the Civil War the industrialization of Newark and Paterson increased, creating additional industries closer to the Passaic River link. The industrial history of the Lower Passaic began in the late 1820s. Newark Bay was once a very common place for oyster reefs, which in the late 1880s was New York's most profitable fishery. The estuary provided jobs for thousands and food for many. The Dundee Dam, Dundee Lake, and Dundee Canal were built to encourage new boat transportation on the river. In the decades that followed, factories sprang up along the Lower Passaic River and drew power for their manufacturing operations from the Dundee Dam. It was once a rich ecosystem inhabited by a diverse and abundant community of

invertebrates and vertebrates with wetlands and tidal-creek habitats creating one highly diverse biological environment. The lower portion of the Passaic River beyond Dundee Dam is a tributary leading to Newark Bay and part of the New York-New Jersey Harbor estuary. The Lower Passaic was a heavily industrialized area. According to the 1939 Census, there were 2,900 manufacturing establishments in the watershed. The principal manufacturing· centers were Paterson, Passaic, Clifton, Bloomfield, Garfield, Kearny, and Newark. The major industries were engaged in dyeing and finishing of textiles, the manufacture of wearing apparel, food and kindred products, and the production of textile machinery, chemicals, paints and varnishes, electrical equipment, and leather goods.

From 1951 to 1969, the Diamond Alkali Company, known as the Diamond Shamrock Chemicals Company, operated a pesticide manufacturing plant at 80 Lister Avenue in Newark. The mid-1940s marked the beginning of manufacturing operations, including the production of Dichlorodiphenyltrichloroethane (DDT) and phenoxy herbicides. Between 1951 and 1969, the Diamond Alkali Company operated a chemical plant that manufactured herbicides 2,4,5-trichlorophenoxyacetic acid (2,4,5-T), chlorophenoxy acid and 2,4-dichlorophenoxyacetic acid (2,4-D). The compound 2,3,7,8-tetrachlorodibenzo-*p*-dioxin (TCDD), commonly referred to as dioxin, was produced as a by-product of the herbicide production process which the U. S. EPA categorizes as a likely carcinogen. Subsequent owners used the property until 1983, when sampling at the site and in the Passaic River revealed high levels of dioxin.

Most of the lower Passaic River was not dredged after the 1950s due to concerns of dumping sites for the dredged materials from the lower river basin. A historical review of water quality and sediment quality data reveals the significant presence of wide ranges

of toxic chemicals throughout the river, whose concentrations greatly exceed the sediment quality benchmarks and probable ecological stressors.

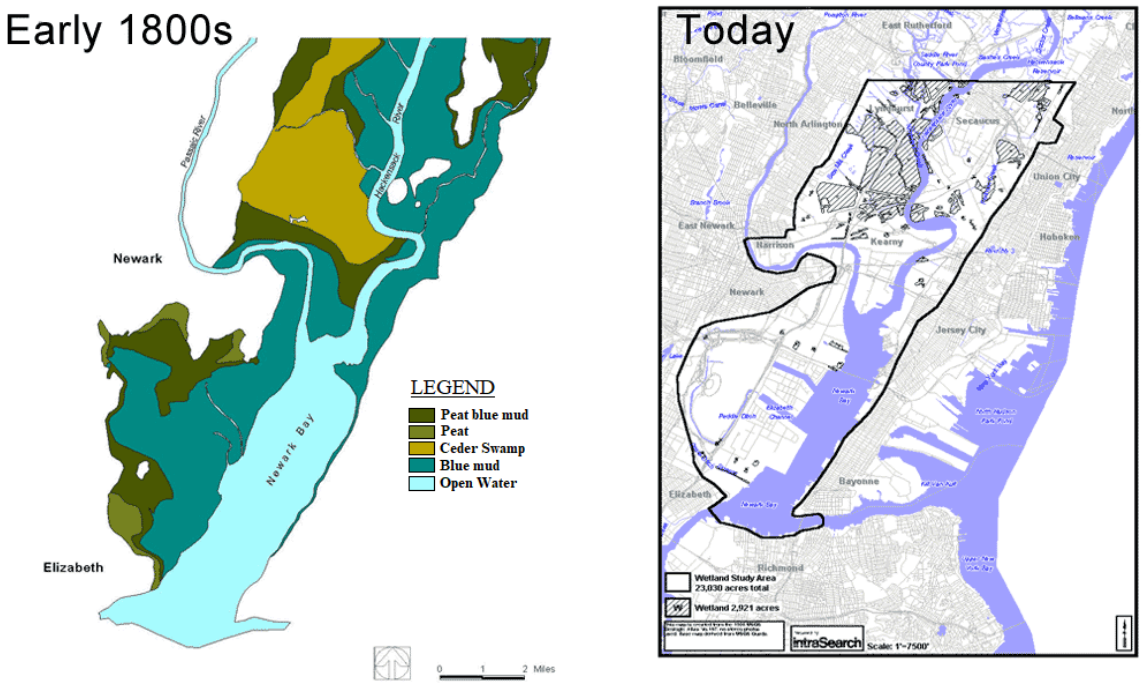

Figure 1.1 A comparison of the extent of wetlands in lower Passaic River environments early 1800s and today.
Source: Timothy J. Iannuzzi and David F. Ludwig Historical and Current Ecology of the Lower Passaic River BBL Sciences, 326 First St., Suite 200, Annapolis, MD 21403 http://www.urbanhabitats.org/v02n01/passaicriver_full.html. Accessed on December 20, 2017).

1.1.2 Present Day Passaic River

Industrial waste disposal, industrial sewage, and toxic chemical spills have greatly contaminated the Passaic River estuary and aquatic system including water and sediments. In 1970, the United States Environmental Protection Agency (U.S. EPA) declared the Passaic River as the second most polluted river in America. In 1983, hazardous levels of dioxins were identified during an investigation at the Diamond Alkali Company site. The production of Agent Orange during the Vietnam War and the dumping and leakage of the byproducts such as dioxins to the Passaic River were key detrimental incidents to the river

environment. The Division of Science, Research and Technology of the New Jersey Department of Environmental Protection Agency conducted an investigation of the polluted chemical plant site and found 1.2 ppm of 2,3,7,8-TCDD. The site was cleaned but later high dioxin levels were found in crabs and shellfish of Newark Bay. Dioxin concentrations in fish and crabs in the Passaic River are among the highest reported in any known scientific literature and are considered unsafe for human consumption. Fish and aquatic life are often better indicators of toxic contamination than sediments or water due to their propensity for the bioaccumulation of chemicals. Elevated levels of contaminants in the water and sediments may not be detectable, hence fish and aquatic life are always a better indicator of the degradation of the ecosystem due to contamination.

Over 100 of the industrial facilities have been identified as potentially responsible for discharging a range of contaminants into the river, including polychlorinated dibenzo-p-dioxins (PCDD), polychlorinated dibenzofurans (PCDF), polychlorinated biphenyl (PCB) mixtures, polyaromatic hydrocarbons (PAH) compounds, Dichlorodiphenyltrichloroethane (DDT), and other pesticides. The contaminants are not limited to organics; mercury, lead, and other metals are found in the river sediments. About 70 companies that operated those facilities which produced chemicals that polluted the river have formed the Cooperating Parties Group (CPG) and signed an agreement with the U.S. EPA to perform a remedial investigation/feasibility study plan for the Lower Passaic River Study Area Cooperating Parties Group under U.S. EPA. In 1984, U.S. EPA added the site to the National Priorities List, making the Passaic River eligible for cleanup funds under the federal Superfund program.

1.1.3 Current Remediation Plan

The addition of the Passaic River to the national priority list released U.S. EPA funding to prepare a remediation plan to restore the river ecosystem to an innocuous state allowing the locals and industries to use the river. The U.S. EPA recently proposed a $1.7 billion remediation plan that includes bank to bank dredging and capping. Capping of the dredged river bed consists of covering the dredged river bed with a mixture of sand and activated carbon. The sand and carbon were overlaid with a geotextile membrane finishing the capping. Sediments are dredged to a depth of 0.762m, except for the 3.22 km where navigation is enabled hence dredges to much greater depths and the dredged area will be capped without causing any additional flooding of the lowlands. The dredging will be done on the tidal portion of the river. The dredged sediment removal would involve mechanical dredging (bucket dredging), transporting the sediments to a processing facility for dewatering, transporting the processed dredged material for further treatment or placement, and backfilling or capping the dredged area. This U.S. EPA proposal involves dredging 3.29 million cubic meters of contaminated sediments and subsequent capping, dewatering, and transporting the dredged sediments to a secure disposal site; the project is expected to be completed in five years, making it one of the largest cleanups ever proposed by the U.S. EPA.

The proposed remediation plan is extremely expensive and comprises risks of resuspension of contaminants. The Lower Passaic River is a tidal river causing complications with the transportation of dredged sediments. In addition, as one of the most congested regions in the country, the U.S. EPA proposed plan has the potential to cause significant disruptions to economic and social growth of the region, with the closing

of several drawbridges to facilitate transport of dredged sediments and finding and operating a large dewatering facility in Newark. This will no doubt adversely impact the transfer of people, goods and service in, out, and across the region. The impact on the society due to the current plan includes closing bridges to traffic to move dredged sediments, and risks involve using the river for recreational activities such as rowing, boating, and fishing.

The research described in this thesis is directed towards developing an *in-situ* treatment method to decontaminate the heavily contaminated Passaic River sediments. The aim of this study is to use ultrasound and ozone *nano-bubbles* to develop a treatment technology that will remediate a variety of contaminants in the river sediments. The initial laboratory experiments showed promising results indicating the possibility to use ozone *nano-bubbles* and ultrasound to treat contaminated soil. The use of ozone which during decomposition in water releases oxygen, will allow the bioremediation of the sediments and restore the ecosystem. The use of this technology to decontaminate Passaic River sediments will eliminate the necessity to dredge, dewater, and transport contaminated soil to an offsite, which are major expenses in the U.S. EPA proposed remediation plan. This research work aims at laying the groundwork for the development of economically viable and environmentally sustainable *in-situ* treatment method to decontaminate heavily contaminated river sediments.

1.2 Scope of the Study

The proposed technology will combine ultrasound and ozone *nano-bubbles* as an integrated main treatment process in a multi-staged remediation technology. The ultrasound

transducers with varying power will be housed in a containment chamber which is made out of an anti-corrosive material. The chamber will include an ozone *nano-bubble* delivery system and a wastewater removal system that will include nanofiltration. The treatment will be performed inside the containment chamber and after treatment, waste water will be extracted from the chamber and filtered through a nanofiltration system. The rudimentary sketch of the containment chamber is shown in Figure 1.2.

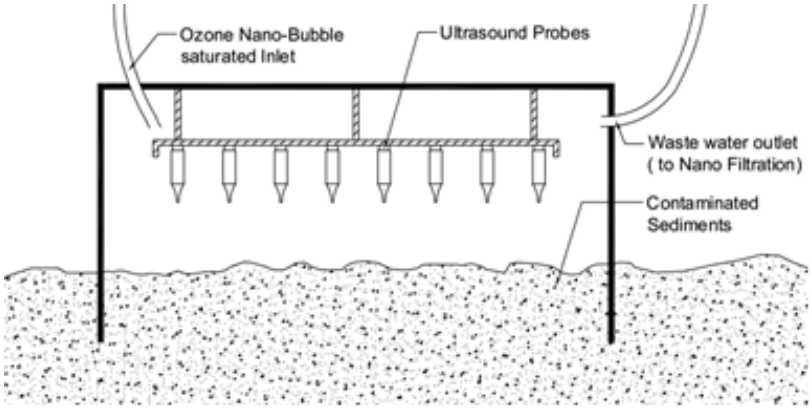

Figure 1.2 Rudimentary sketch of the containment chamber used for remediation.

The proposed containment chamber will be 3.5m×3.5m×1.5m (L×W×D), made out of anti-corrosive material. The ultrasound transducers will be arranged in a grid of 0.3m intervals to maximize the impact from the sonication. The chamber will be lowered to the sediments allowing it to sink into the contaminated sediments. The containment chamber will be filled with ozone *nano-bubble* saturated water while ultrasound is applied to the contaminated sediments. Desorb contaminants from the sediment due to ultrasound will be oxidized by ozone *nano-bubble* saturated water. During the ultrasound application, river sediments will be mixed with water containing ozone *nano-bubbles* to form a slurry. After ultrasound treatment, sediments are allowed to settle and the generated wastewater above the settled sediments inside the chamber will be extracted and treated through a

nanofiltration system on a barge which will allow the heavy metals to precipitate and other residual chemicals to be oxidized before recirculating it back into the containment chamber. The proposed flow chart for the field application is shown in Figure 1.3.

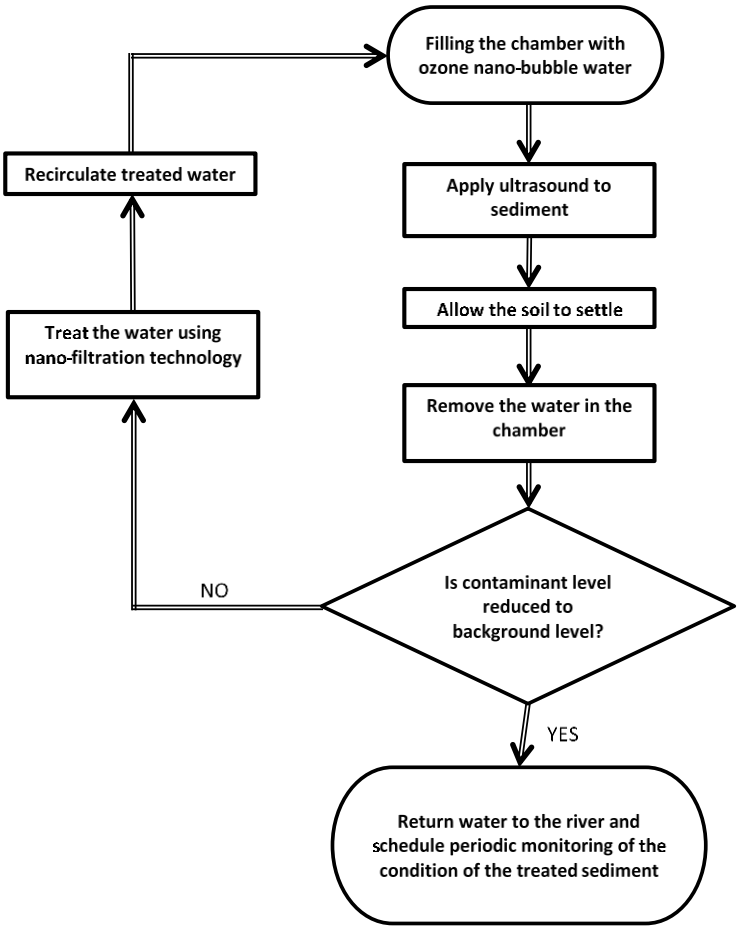

Figure 1.3 Flow chart for the field application.

1.3 Challenges and Objectives

Based on the requirement for developing a technology to decontaminate contaminated Passaic River sediments, the study focused in on a few major objectives listed below:

1 Use of ultrasound in decontamination of soil has been investigated in past research. However, the ultrasound with *nano-bubbles* had to be investigated.

2 The use of ozone *nano-bubbles* and the behavior of ozone *nano-bubbles* due to hydrodynamic cavitation of ultrasound needed further investigation.

3 The use of ultrasound and *nano-bubbles* as a single unit to remove heavy metals from the contaminated sediments needed further investigation.

4 Impact of ultrasound and ozone *nano-bubbles* on removal of organic in contaminated sediments needed further investigation.

5 The impact of temperature, pH, dissolved ozone level, ultrasound power, ultrasound dwell time, and duration of the treatment on this proposed technology needed further investigation.

CHAPTER 2

ULTRASOUND APPLICATION AND BEHAVIOR

2.1 Introduction

The application and use of sound waves with a frequency higher than 20 kHz is defined as ultrasound and is used in medical, industrial, scientific, and biological fields using a wide range of frequencies. Ultrasound is usually generated from piezoelectric crystals with frequencies ranging from 20 kHz to 100 MHz, where electrical signals matching the natural frequency of the crystal is applied to generate ultrasound.

The low frequency application from 20-100 kHz frequency range is used in medical imaging to industrial cleaning including sediment remediation (Meegoda et al., 2001, Meegoda et al., 2002). The mid frequency application from 200-400 kHz frequency range is used in particle separation (Aboobaker et al., 2003 and 2005). The high frequency application from 1-30 MHz frequency range is used in medical field to remove kidney stones, sono-chemistry to destroy chemicals and condition assessment of concrete culverts (Zou, 2018). The higher frequencies (above 1MHz) tend not to affect the medium of propagation and mostly used with low power levels (10W or less).

The most relevant application of ultrasound energy is its application to clean surfaces in the low frequency range. It is used in metals and electronics industry to remove oxide films, oil, grease, and other contaminants from solid surfaces. As practiced today, it is a batch process where parts to be cleaned are placed in vats containing a detergent solution. Ultrasound tanks range in size from laboratory size to several thousand gallons. It is also possible to install submersible ultrasound transducers into ordinary tanks or vats,

thereby converting them into ultrasound baths. In common use, the parts to be cleaned are placed in a bath filled with the cleaning solution and subjected to ultrasound vibration for 10-20 minutes. The liquid, often called detergent solution, is composed of water, surfactant, and other additives. Cavitation, vortex and micro-streaming produced by ultrasound energy removes contaminants adhered to the solid surface of the parts placed in the solution.

The propagation of ultrasound through the liquid will promote three different reactions in the liquid, heating of the liquid due to the dissipation of acoustic energy, formation of fluid flow and convection cells, and formation of gas/vapor bubbles (collapse, and coalescence). Ultrasound cleaning works by providing shear forces to remove the material adhered to a surface. This shear force is developed by cavitation. Ultrasound causes high-energy acoustic cavitation: that is, the formation of microscopic vapor bubbles in the low pressure (rarefied) part of the ultrasound wave. These bubbles collapse in the compression part of the wave creating very minute, but high energy movements of the solvent that result in localized high shear forces. During cavitational collapse, intense heating of the bubble occurs. These localized hot spots have temperatures of roughly 5000^0C, pressures of 500 atmospheres, and a lifetime of a few microseconds (Suslick, 1990). Shock waves from cavitation in liquid-solid slurries produce high-velocity inter-particle collisions, the impact of which is sufficient to melt most metals. Applications to chemical reactions exist in both liquid (homogeneous) and liquid-solid mixtures. Application of ultrasound energy to a soil slurry such as contaminated sediments causes acoustic cavitation. Shock waves from cavitation in liquid-solid slurries produce high-velocity inter-particle collisions, the impact of which is sufficient to desorb the contaminants from soil.

2.2 Heat Generation

The main two forms of energy that are entrenched within acoustic waves are the particle velocity of the medium and the potential energy gathered within the mass of the medium. When ultrasound is applied over a liquid medium the apparent heat generation due the creation and collapse of vapor bubbles in the liquid is monitored by many researchers (Nomura et al., 1993, Oh et al., 2002). The temperature rise in the liquid will considerable impacts on the material and chemical reactions in the solution. The mount of power applied during the generation of ultrasound which is applied to the liquid is a direct impact on how much heat is formed with in the liquid due to the dissipation of acoustic energy. Hence, the heat generated over the use of ultrasound must be investigated to ascertain the heat generated during sonication in water. The heat generated due to the mechanical energy dissipation from the transducers can be calculated using the calorimetric method (Manson and Lorimer, 1988).

Heat generated due to sonication in water can be calculated by the following formula, where P_l is the heat generated in water (power lost), $^{dT}/_{dt}$ rate of temperature rise (T – temperature, t-time), C_p is the specific heat capacity of water and the mass of the liquid M_l.

$$P_l = \left(^{dT}/_{dt}\right) C_p . M_l \tag{2.1}$$

2.3 Impact of Ultrasound on *Nano-bubbles* and Dissolved Gases

The ultrasound wave propagation through the liquid will have considerable impact on the bubbles in water and the dissolved gases. During the wave propagation, the liquid is subjected to the compression and expansion from the wave (Figure 2.1.a). Ultrasound waves consist of a cyclic succession of compression and rarefaction phase cycles divulged by transducer vibration (Tang 2003). Compression cycles exert a compressive pressure and force the water molecules and compress any air bubbles in the medium encouraging the gases in the bubbles to dissolve in the liquid. The expansion cycles exert a suction pressure which pulls the water molecules apart (Vajnhandl and Marechal 2005). When the suction pressure exceeds the surface tension of liquid in the rarefaction sections, small vapor and gas filled cavitation bubbles are formed (Chen 2012). These formed bubbles will be exposed to the next sessions of ultrasound waves. Hence, forcing the existing bubbles to react to each wave by compressing and expanding that can cause the bubble to either shrink or expand with in the liquid, where the process will encourage the bubbles to coalesce and to be large in size to move up the liquid. The captured process is shown in Figure 2.1.b.

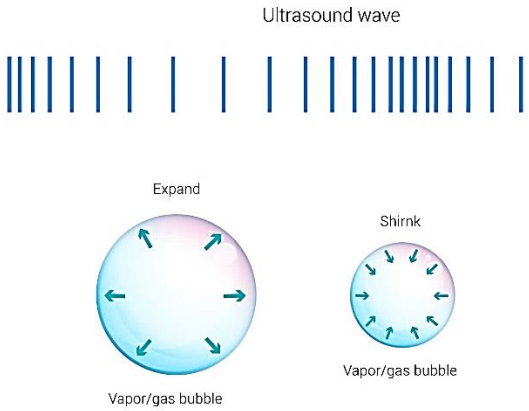

Figure 2.1.a Bubble expanding and shrinking under the ultrasound wave.

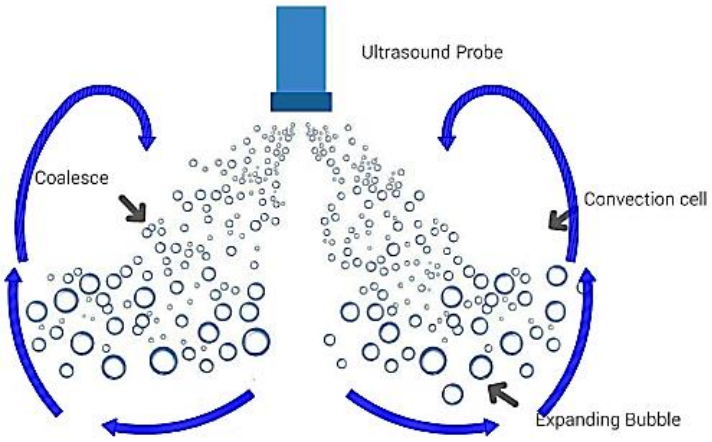

Figure 2.1.b Gas/vapor bubble formation under sonication in water.

The compression of the bubble shrinks the interfacial area of the bubble immensely which forces the gas diffusion outwards dissolving the gas into the liquid. When a bubble is compressed, its interfacial area shrinks greatly. Shock wave from sonication when travelling through water will push the *nano-bubble* close to each other. The action described as primary Bjerknes force and secondary Bjerknes force in a standing ultrasound wave. When the bubble in water is smaller than the resonant size, the secondary Bjerknes forces will act as the attraction forces allowing the bubbles to coalescence (Crum, 1975).

2.4 Materials and Methods

Ultrasound sonicator with a maximum power output of 1500W (Sonics & Materials, Inc., Model vibracell VC-1500, 240 Volts, Power 1500 Watts, and Frequency 20 KHz) was used as the source of the ultrasound. A 1.91cm tip diameter ultrasound probe (sonication transducer) was used as the source of ultrasound. Fluke 53II B thermometer (with an accuracy of 0.05% + 0.3°C) was used in the investigation to collect continuous real time temperature from the water samples.

The water samples were tested for dissolved oxygen by using a PASPORT optical dissolved oxygen sensor (model PS-2196). Conductivity of the samples were tested using PASPORT conductivity sensor (model PS-2196) and for a continuous reading, a PASCO wireless conductivity sensor was used (model PS-3210). The two instruments were checked against each other to adjust the calibration.

In order to analyze the sample for the dissolved ozone by using 4500-O_3 indigo Colorimetric method. The Thermo Scientific™ Evolution 201 and 220 UV-Vis spectrophotometer were used for the 4500-O_3 ozone analysis. Malvern Nano Zetasizer is used to measure the size of *nano-bubbles* and its zeta potentials. To analyze the *nano-bubble* size 12mm square polystyrene cuvettes used and to analyze the zeta potential Folded Capillary Zeta Cell (model DTS1070) is used.

2.5 Results and Discussion

2.5.1 Ultrasound Heat Generation

The heat generated during the sonication of a liquid has considerable impact on the test samples. Prolong sonication times will increase the temperature rise in water and it will promote a reduction in dissolved gases in water. During this study the importance of having gas saturated water is important. The contaminant treatment depends upon the amount of ozone gas dissolved in water and its capability to react with pollutants.

To identify the impact of sonication time and the amount of heat generated during the application of ultrasound, a set of experiments were performed by varying the ultrasound power. The dwell time was kept as a constant value. The dwell time for

ultrasound was 4 minutes by using a 1.91cm a variation of ultrasound power, 300W, 600W, 900W and 1200W. Figure 2.2 represents the experimental set up for the power output.

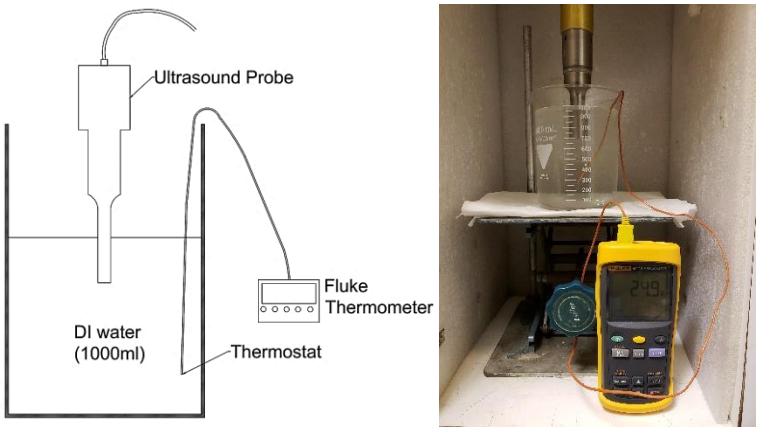

Figure 2.2 Experimental setup for temperature variation due to sonication.

The deionized water (DI water) was kept to stabilize for 24 hours prior to the experiments. The deionized water tends to absorb gases once discharged from the system where, Type I water will turn to Type II water during the transportation from DI filter to containers. Hence, assuming within 24 hours the water reaches stable levels by absorbing gases from the air, the water was kept in a 10-liter container. The testing was performed at room temperature (25^0C).

Figure 2.3 presents the data obtained by applying varying ultrasound power temperature normalized to 25^0C due to slight variation of the temperature in water. Sonication was performed in a beaker containing 1000ml of stabilized DI water. Looking at the lower ultrasound power the temperature increase was much lower compared to the high ultrasound power. The rate of change in temperature ($^{dT}/_{dt}$) in the low ultrasound power is 0.0299 ^{0}C/s.

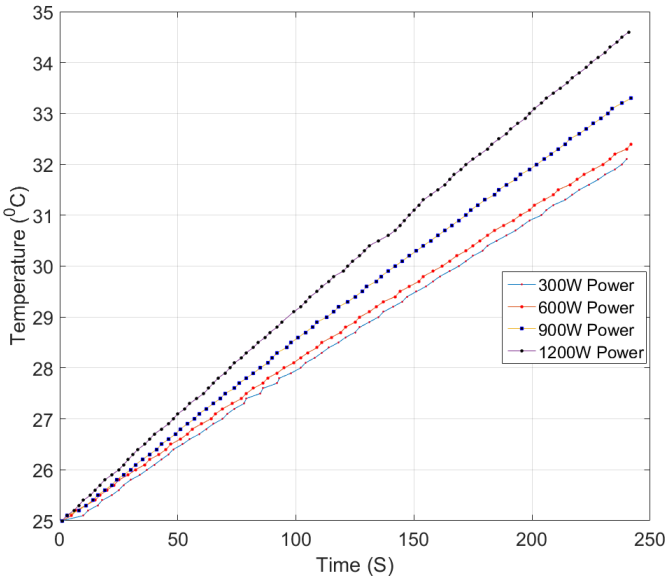

Figure 2.3 Temperature variation in water to different ultrasound power.

The rate of temperature changes for 300W, 600W, 900W, and 1200W ultrasound power levels were 0.0299 ^{0}C/s, 0.0306 ^{0}C/s, 0.0347 ^{0}C/s, 0.0399 ^{0}C/s. Hence, the obvious conclusion being having higher ultrasound power will escalate the rate of temperature change in the liquid subjected to sonication. Energy dissipated as heat was calculated to identify the energy lost during sonication. The observed energy lost during sonication at 150W, 300W, 600W, 900W, and 1200W are shown in Figure 2.4. The heat lost during sonication was calculated using Equation 2.1 where, the specific heat capacity of water was assumed as 4.179 J/g^{0}C.

Figure 2.4 Ultrasound energy lost as heat during sonication in liquid at 150W, 300W, 600W, 900W, and 1200W.

At low power levels (at 300W), the amount of energy lost as heat is 41.21% of the total energy produced and transferred from the sonication. Ultrasound wave propagation in the liquid generating shockwaves causes heat dissipation during the shock. Rapid reoccurrence of these shocks reduces the impact of sonication on liquid and solid particles. At higher power levels, such as 1200Ws, the energy lost is 13.87% from the total energy applied to the system. This allows the system to be subjected to high ultrasound intensities. Hence, by increasing the sonication power used during the study the impact from the energy lost as heat can be averted.

During the investigation of the power and heat generation in the liquid, each sample was tested for the conductivity and the dissolved oxygen concentrations 15 minutes after the sonication of 4 minutes. Table 2.1 presents the results obtained. The conductivity of the DI water was 10 µS/cm and the dissolved oxygen concentration was 8.74 mg/l.

Table 2.1 The Conductivity and Oxygen Concentration in DI Water After Sonication

Sonication power (W)	**Conductivity** (µS/cm)	**Dissolved oxygen** (mg/l)	**Reduction of oxygen** (mg/l)
300	10	7.24	1.5
600	10.5	6.79	1.95
900	10.5	6.65	2.09
1200	9	6.72	1.02

Increase in power did not make considerable impact on the conductivity of the DI water. However, the application of ultrasound had a considerable impact on the dissolved gases in water. The dissolved oxygen concentrations decreased with the increase of the ultrasound power. The ozone reduction at 1200W decreased, where the possible elucidation of the scenario being, ultrasound breaking the water molecule and forming oxygen and hydrogen per oxide that decomposes and become oxygen. The observation made during the investigation was backed by a study conducted by Ziembowicz et al. (2018). Researchers utilized a 20kHz ultrasound device to irradiate variations of increasing power and duration of the irradiation. At increased power intensities, the amount of hydrogen peroxide formed in the system increased where longer sonication times detected higher hydrogen peroxide levels.

2.5.2 Impact of Ultrasound on Soil

The forces generated during the ultrasound propagation through the liquid medium has the potential to break the bonds between the particle and any adsorption bonds between contaminants. These high shear forces contain the capability to change the properties of the soil including the particle size and the surface of the particle.

This impact was tested on 80g sample of soil that was subjected to a total sonication time of 100 minutes, where the sample was sonicated in segments of 4 minutes for each cycle. Particle size distribution of the soil that is been subjected to sonication was tested prior to the experiment. Figure 2.5 presents the particle size distribution of the soil sample prior to sonication and after sonication. The sonication was power kept at 300W and 1200W and the samples were kept in a 1000ml water suspension. A sample of 50g sonicated soil finer than US sieve number 200 (particle size < 75µm) was used to test the particle size distribution using the hydrometer test.

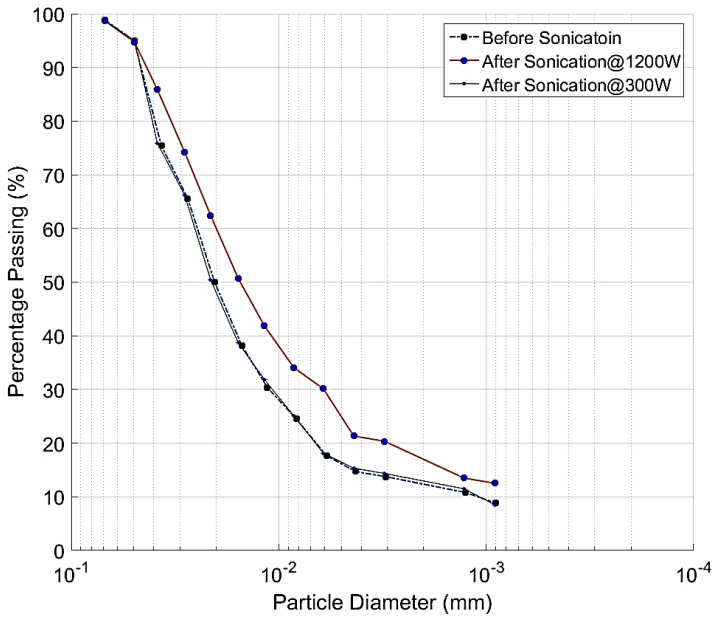

Figure 2.5 Particle size distribution of soil with and without ultrasound sonication excitement.

The red gradation line presents the sonicated soil. The sonicated soils are much finer than the original soil where percentage finer is higher compared to the original soil. The particle size distribution for the soil subjected to sonication has much finer particles compared to the original sample. The cavities collapsing close to the soil particles forming localized ultra-high forces which will break the surface of the particle. The continuous bombardment of these forces onto the soil will continuously shave off the particle surfaces. The convection cells formed within the container will push the particles into the stream created under the ultrasound probe tip.

The samples were imaged using scanning electron microscope (SEM) to ascertain the impact of the ultrasound on the soil particles. Images were obtained using a LEO 1530 VP scanning microscope. Figure 2.6 presents the SEM images of the soil particles after sonication. Impact from ultrasound breaking off the surface of the soil particle is clearly visible.

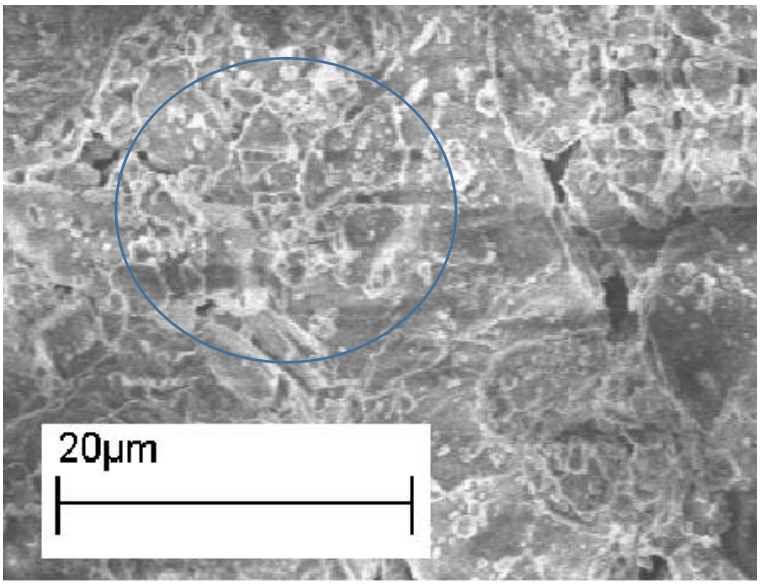

Figure 2.6 SEM images of the sediments after sonication. (EHT = 6.00kV, Signal A= Inlens, WD = 10mm)

The particles shown in the images are much finer in size where it presents the broken particles. The majority of the particle images obtained using the SEM presented high amount of particles smaller than 20µm.

2.5.3 Impact of Ultrasound on Dissolved Gases

The ultrasound propagating through the liquid creating shockwaves will have a considerable influence on nano/micro bubbles in water.

To identify the impact of sonication on dissolved gases and *nano-bubbles*. A variety of tests were performed by varying the ultrasound power, and sonication time in respect to temperatures at 15^0C and 20^0C. A chamber was filled up to 18 liters of stabilized DI water and the system generating ozone *nano-bubbles* was initiated for 6 minutes. Then 1000ml sample of ozone *nano-bubble* saturated water was used. The sample was subjected to a variation of ultrasound sonication times from 1 to 4 minutes. Each sample was subjected to ultrasound powers of 300W, 600W, and 1200W. The samples were test before and after the sonication to check the bubble size distribution (BSD), zeta potential (ZP), dissolved ozone concentration (DO_3), dissolved oxygen concentration (DO_2), and the conductivity (EC).

The first set of experiments was performed by applying 300W ultrasound power for different durations from 1 to 4 minutes. The results observed for ozone and oxygen concentrations over sonication duration is shown in Figure 2.7.

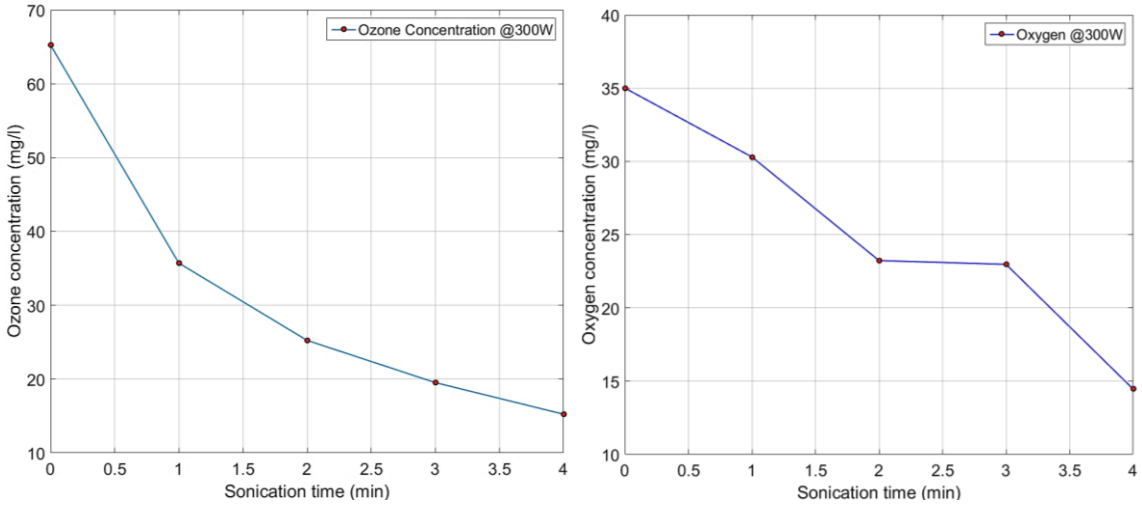

Figure 2.7 Ozone and Oxygen concentration with sonication duration at 300W at 25^0C.

Sonication of ozone *nano-bubble* saturated water using 300W power indicated the reduction in dissolved ozone gas in water with the increase in the duration of sonication. The shock waves in the water forced bubble coalescence and generate micro and macro bubbles promoting release of ozone from water much faster than *nano-bubbles* over time. The ultrasound waves propagating through the water also promoted the release of dissolved gases. The study observed similar behavior for the ultrasound power levels of 600W and 1200W. These results for dissolved oxygen concentration and ozone concentrations are shown in Figure 2.8.

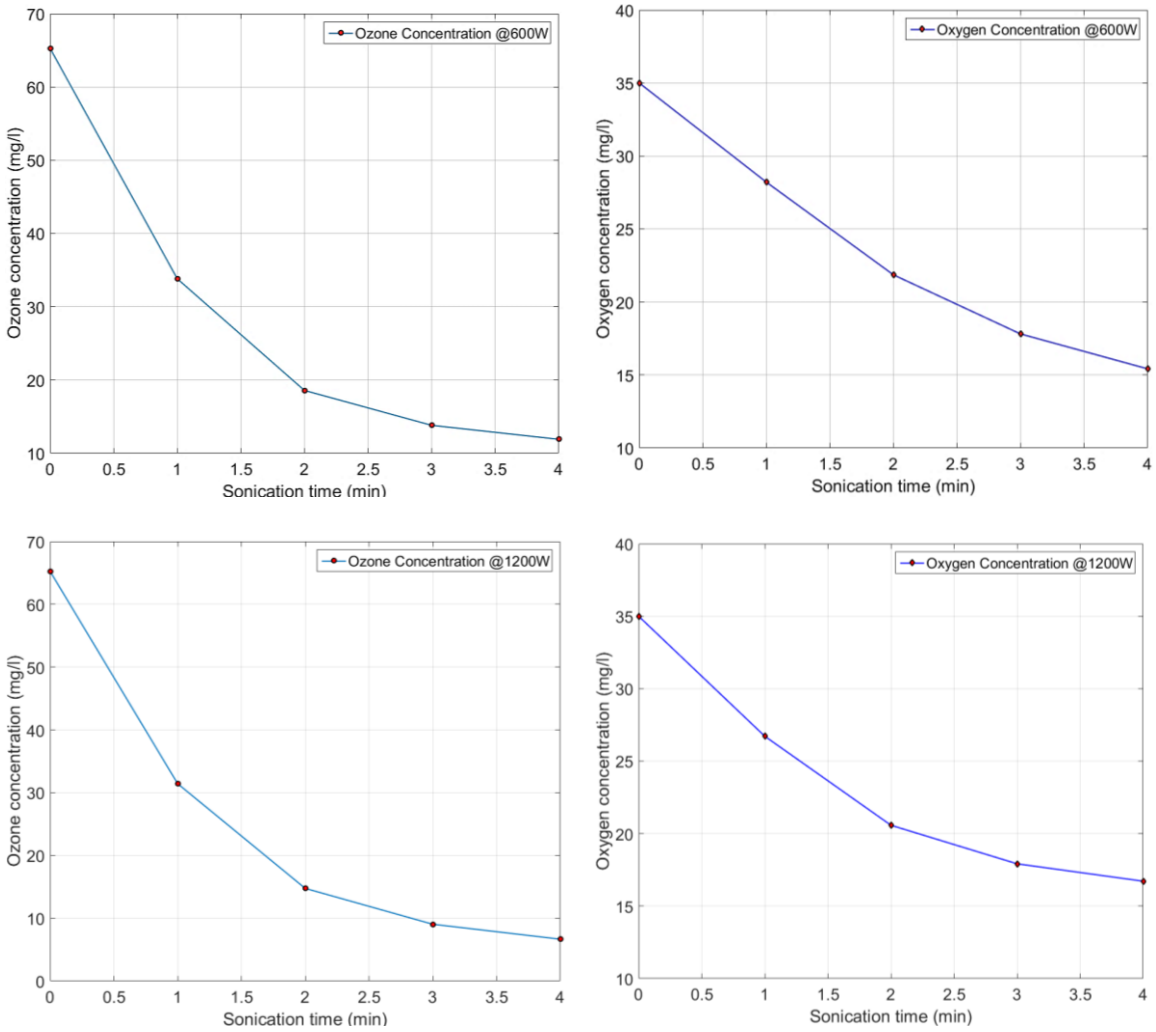

Figure 2.8 Dissolved ozone and oxygen concentrations with sonication duration at 600W and 1200W at 25^0C.

For both 300W and 600W, sonication power levels the reduction of oxygen level in water indicated a gradual decrease when the sonication period increased. However, for 1200W sonication power, the rate of reduction with the sonication duration decreased. Similar observation indicated in the data obtained shown in Table 2.1. increasing the intensity of sonication can generate hydroxyl radical that will decompose and generate oxygen, decelerating the oxygen reduction rate in liquids. In addition to the breakdown of the water molecule, the sonication seems to accelerate the decomposition of dissolved

ozone. The ozone concentrations reduced rapidly when the ultrasound power level increased. Sonication impacts negatively on the dissolved ozone in water. Increasing the reduction of dissolved ozone and decomposition by increasing the ultrasound power have a significant impact on the remediation of contaminants. The reduction of ozone in the water will reduce the possibility of oxidation of contaminants with ozone. Hence, reducing the sonication time (dwell time) 2 minutes or under will allow water to retain a considerable amount of dissolved ozone that oxidize the pollutants.

Similar set of experiments were performed using ozone *nano-bubble* saturated water at 15^0C. The sonication powers used during ultrasound agitation are 300W, 600W, and 1200W. Ozone concentration variation observed in water for sonication times of 1 to 4 minutes showed in Figure 2.9.

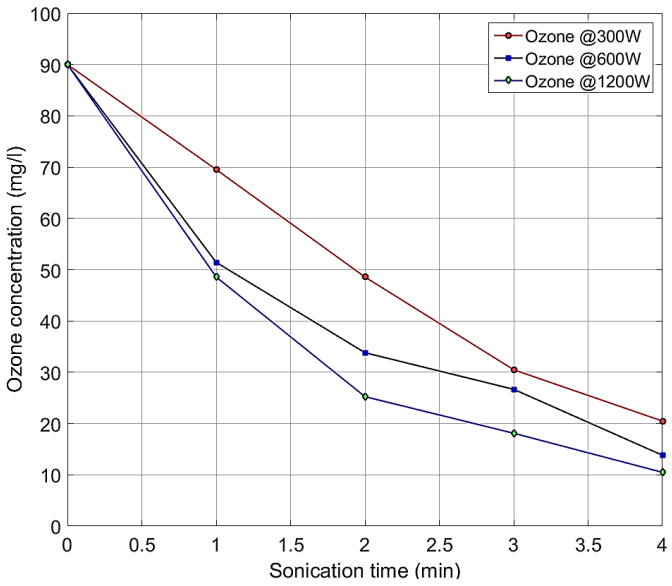

Figure 2.9 Ozone concentration variation over the sonication time at 15^0C.

Results obtained at 15^0C showed same variation as that at 25^0C. Ozone concentrations decreased when with the duration of sonication. Increasing the ultrasound

power increased the reduction in the dissolved ozone in water. The oxygen concentrations were obtained for the same sonication powers and the results are shown in Figure 2.10.

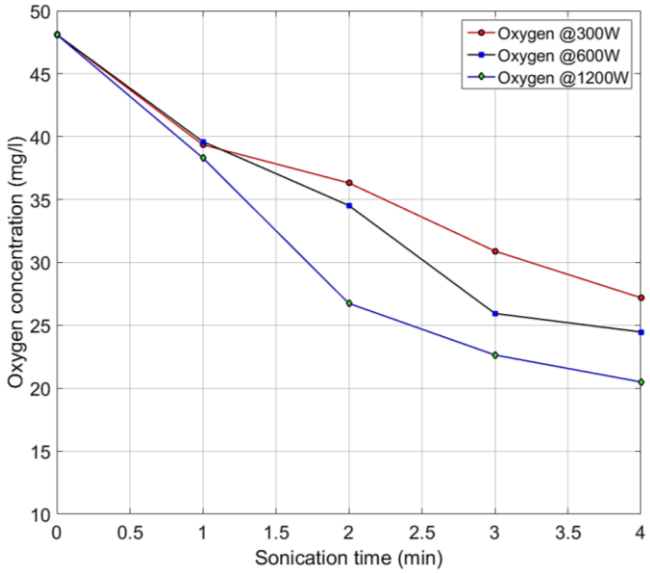

Figure 2.10 Oxygen concentration variation over sonication time at 15^0C.

Sonication reduced the oxygen concentration over time. Higher sonication power reduced high oxygen concentrations where at 1200W dissolved oxygen concentrations were 27.60 mg/l. During 1200W sonication, the observed reduction of dissolved oxygen at temperatures 15^0C and 25^0C followed similar trends.

2.5.4 Impact of Ultrasound on *Nano-bubbles*

Application of ultrasound on *nano-bubbles* saturated water increases the coalescence and generates micro bubbles. Hence, it is necessary to investigate the impact of ultrasound on *nano-bubbles*. A study conducted by researchers from the University of California, Berkley investigated the impact of sonication on bubbles near rigid surfaces. Where they observed the reflected shockwaves impacted bubble collapse (Calvisi et al., 2008 and Iloreta et al.,

2008). The bubbles deformation due to the shockwave travelling through bubbles was observed by Ohl and Ikink (2003), as shown in Figure 2.11.

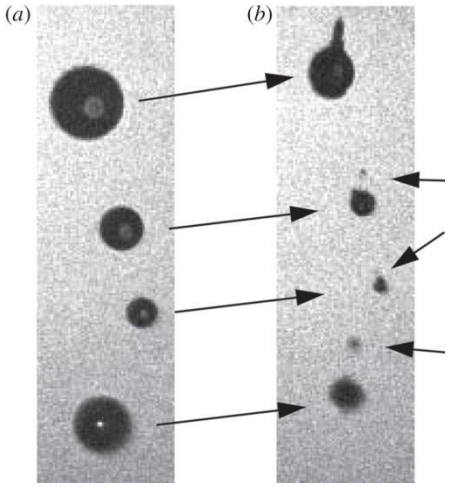

Figure 2.11 Deformation of gas bubbles due to shockwaves in water.
Source: Experimental result Replicated with permission from Ohl C. D. and Ikink R. Copyright 2003 American Physics Society.

Bubbles in Figure 2.11(a) presents the gas bubbles in water before the arrival of the shock waves, and 2.11(b) shows the gas bubbles shrinking due to the travelling shockwave through gas bubbles. This shock will force the bubbles to dissolve the entrapped gases in the liquid. In the case of ozone gas bubbles, the dissolved gases will decompose by reacting with water. The decompositions of gases will further enhance the diffusion of gases into the liquid. Outcome of interaction between bubbles in water depends on bubble size, number of bubbles, and arrangement. Experiments performed by Dear and Field (1988) studied bubbles in multiple arrangements, including three bubbles arranged perpendicular to the shock front and parallel to the shock front. The observations showed bubbles upstream of the wave shielding bubbles downstream. The study included the arrangements of bubbles in different ways, triangular, and nine bubbles which confirmed the shielding effect by the bubbles on the upstream to the downstream of the shockwave.

The same study (Dear and Field, 1988) observed bubble collapse under sonication. The observations were modeled by Klaseboer et al. (2007) using potential flow theory using the boundary-element method (BEM). The simulation included collapse of the bubble. The collapse of the bubble is shown in Figure 2.12, based on the model.

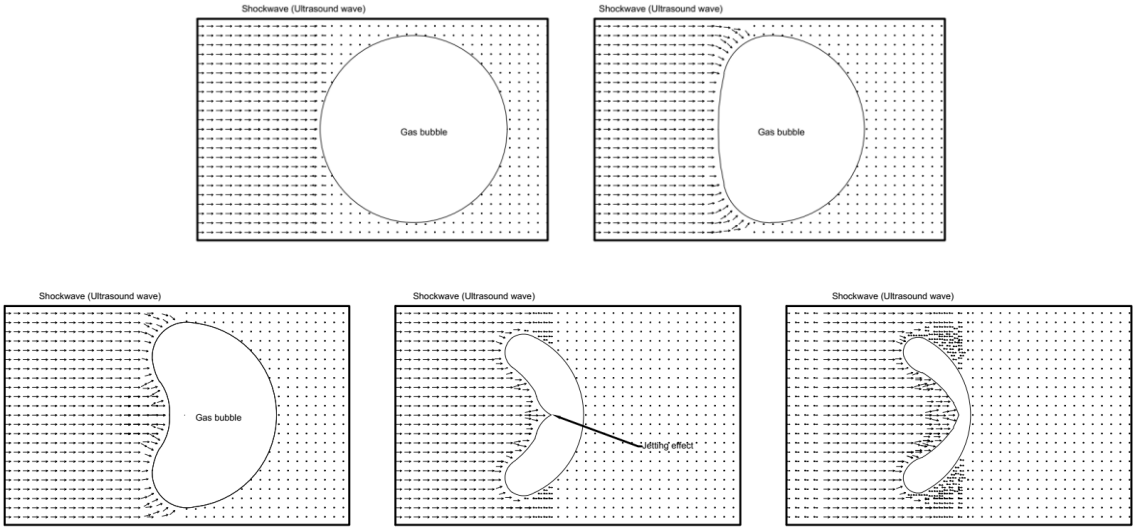

Figure 2.12 Collapse of a bubble under the pressure pulse from the shock wave redrawn based on the modeling by Klaseboer et al., (2007).
Redrawn with permission from Cambridge University Press.

The collapse of bubbles due to shockwaves depends on whether the bubbles are in the path of the shock wave or whether it escape the shockwaves. Bubbles which are in the direct path of the wave will collapse or will shrink, where some of those bubbles will cushion the wave and shield bubbles downstream of the wave. During the investigation, ozone *nano-bubbles* were subjected to different sonication powers ranging from 300W, 600W, and 1200W. The bubble size, zeta potential, and the conductivity of a *nano-bubble* after sonication were measured. Sonication was applied for 1 minute and 2 minutes. The ozone *nano-bubble* generation system operated for 6 minutes to saturate 18 liters of water. The measured diameter of *nano-bubbles* observed before and after sonication of 1 minute

are shown in Figure 2.13. Each after sonication sample was tested to identify any variations.

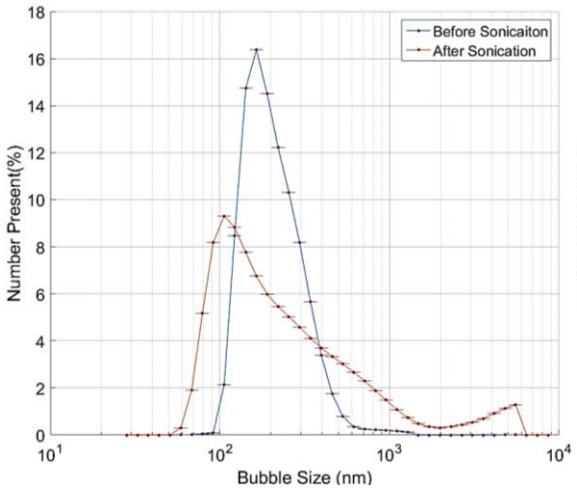

Sizes after 300W sonication

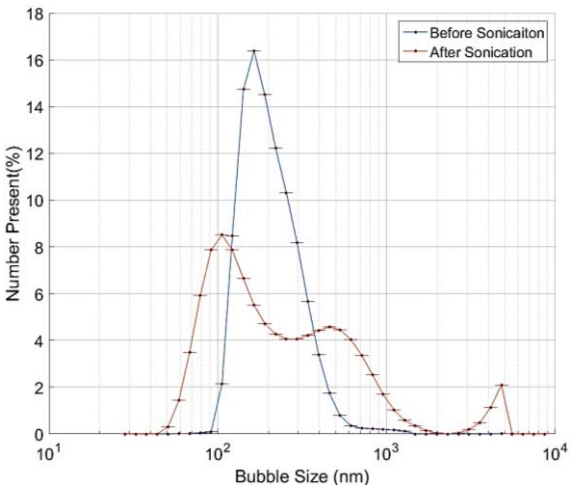

Sizes after 600W sonication

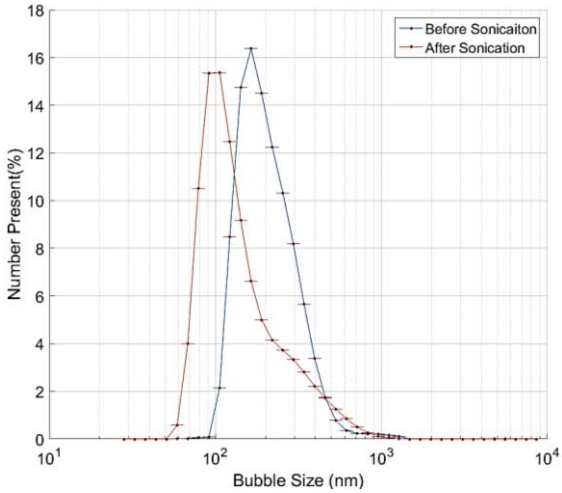

Sizes after 1200W sonication

Figure 2.13 Ozone *nano-bubble* variation before and after sonication (1 minute).

By applying ultrasound, it was detected that majority of the *nano-bubbles* after sonication became smaller in size. The observed bubbles were smaller in size, but it is not clear whether the bubbles are still filled with ozone or other dissolved gas. Based on the literature, at high sonication power levels, cavitation created micro and *nano-bubbles* that

were infused with dissolved gases and vapor. The observed smaller bubbles were due to the forced diffusion of the gases and increased decomposition of ozone in the liquid. The coalescence of the bubbles which is apparent in the results obtained and shown in Figure 2.13 with a larger diameter in the bimodal size distribution.

Another test was performed by applying ultrasound for 2 minutes for the same ultrasound power levels (300W, 600W, and 1200W). The *nano-bubbles* size distributions obtained during the experiments are shown in Figure 2.14. Further analysis of the size distribution obtained before and after sonication for 1200W power shows approximately 1/3 of bubbles became smaller.

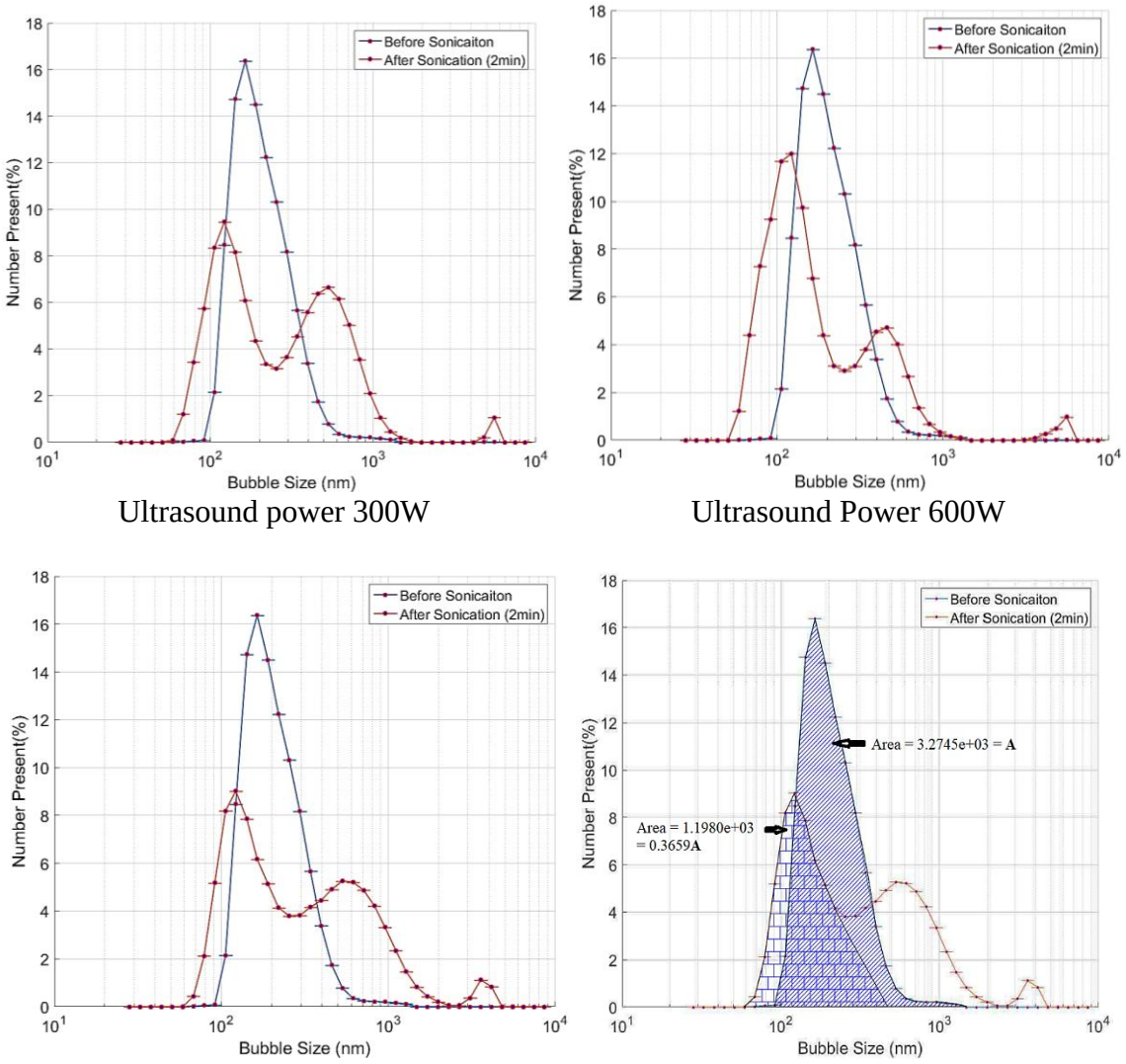

Figure 2.14 Ozone *nano-bubble* diameter before and after sonication (2 minutes).

The impact on *nano-bubbles* from sonication power indicated a decrease in bubble diameter. However, elevated ultrasound power for 2 minutes of sonication time did not show a similar variation when the bubbles were sonicated for 1 minute. In both instances, the majority of the bubbles became smaller. This confirms the hypothesis made indicating dissolved gases absconding the liquid (water) and sonication promoting the diffusion of ozone gas into water. The hypothesis developed by Dear and Fields (1988) was confirmed

by the results obtained from this investigation. The amalgamation of gas bubbles was correspondingly confirmed based on the results where all the graphs presented a second peak between 500-600nm at lower to higher power levels.

Conductivity of a liquid depends on the availability of ions in water. During ozone *nano-bubble* generation, the ion concentration in the liquid increases due to the dissolved ozone and decomposition of ozone forming hydroxy radicals. The samples were tested for the conductivity and the conductivity of the stabilized deionized water was 10µS/cm before use in ozone *nano-bubble* generation. Table 2.2 presents the conductivity obtained before and after applying ultrasound at power levels 300W, 600W and 1200W.

Table 2.2 Conductivity in Water Saturated with Ozone *Nano-bubbles* after Sonication

	Ultrasound Power (W)		
Sonication time (min)	**Conductivity at 300W (µS/cm)**	**Conductivity at 600W (µS/cm)**	**Conductivity at 1200W (µS/cm)**
0	17	17	17
1	12	13	14
2	12	13	14
3	12	13	14
4	12	13	14

During sonication the conductivity initially decreased during the 1 minute of sonication. The reduced conductivity stayed constant with the duration of the sonication which did not further reduce. However, the reduction in the conductivity with the change

in sonication power did not present similar drops. This may have contributed towards ion formation under different ultrasound intensities.

The zeta potential of the bubbles in the liquid were measured during the sonication. The zeta potential values obtained during the study are shown in Figure 2.15.

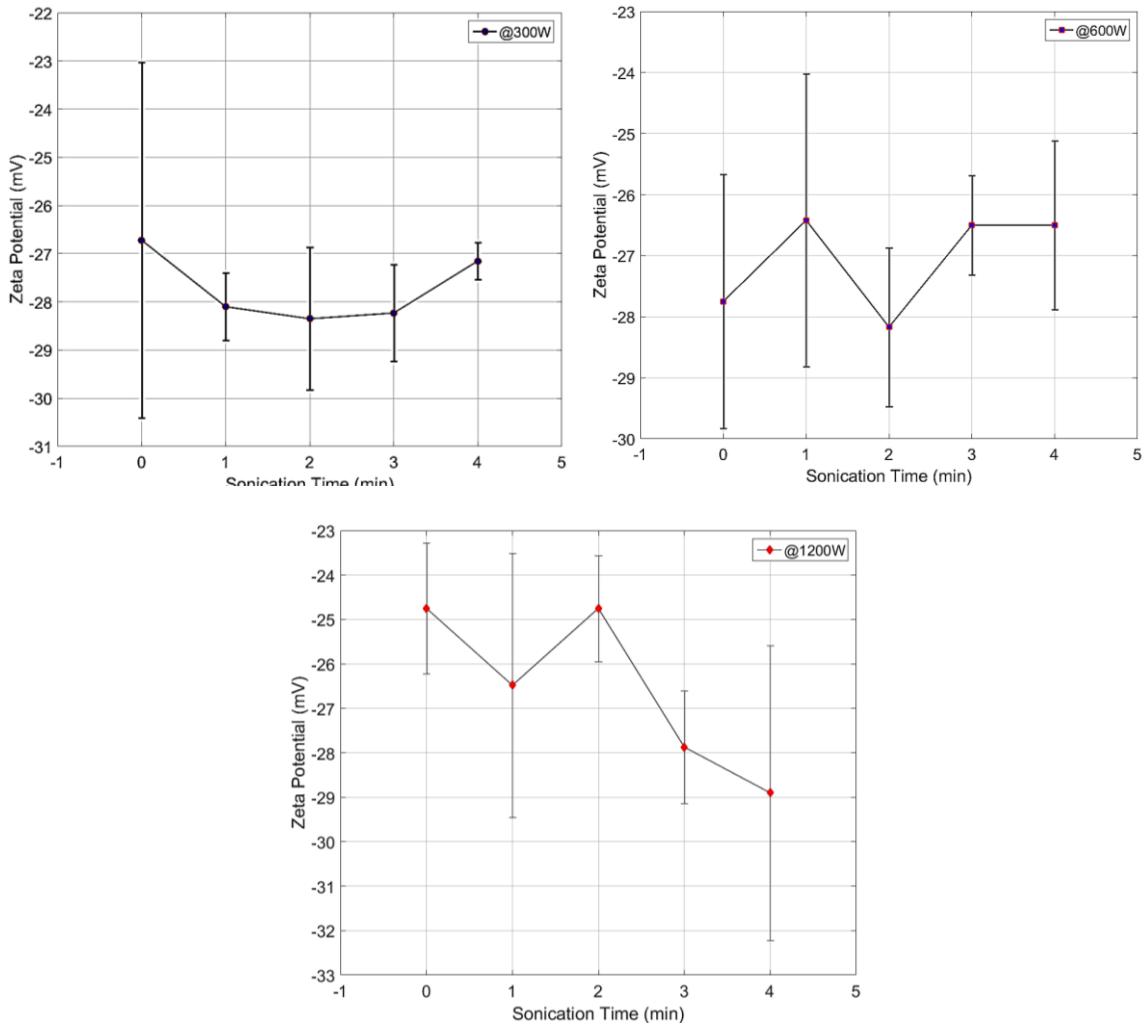

Figure 2.15 Zeta variation with sonication time and power.

Nano-bubbles did not show conclusive evidence of increasing or decreasing in zeta potential with sonication for low power levels. However, for 1200W power there was an increase in negative zeta potential values. The formation of gas cavities due to the

sonication may have impacted the zeta potentials values. Based on Figure 2.7 and 2.8, the dissolved ozone values in water are much lower than initial concentrations. The zeta potential increase at higher sonication powers can be attributed to the formation of hydroxy radicals and eventual formations of oxygen and hydrogen peroxide. This phenomenon was observed by other researchers when ultrasound was used to reduce toxins in water (Lurling et al., 2014; Weissler, 1959, and Jia et al., 2010).

2.6 Summary and Conclusions

Ultrasound can form cavities in liquid. Sonication in water will have a considerable negative impact on the dissolved gases and *nano-bubbles* in water. The dissolved ozone was removed from the water when ultrasound was applied. The reduction of dissolved ozone in water was rapid. Due to sonication, resulting bubbles observed in water were finer than bubbles observed prior to the sonication. At higher power levels, a second peak of bubbles were observed, that might be attributed to the coalescence of *nano-bubbles* due to shock waves from collapsed cavities and ultrasound shock waves. The conductivity of water increased when ozone *nano-bubbles* were formed, and it declined when ultrasound was applied. It did not indicate any conductivity change in water with the sonication duration and sonication power. The results obtained from the experiments specified, avoiding long sonication times to prevent the loss of dissolved gases, and prevent the temperature rise in water.

CHAPTER 3

OZONE *NANO-BUBBLES* AND THE BEHAVIOR

3.1 Introduction

Nano-bubbles are nano-sized gas cavities in aqueous solutions that are filled with different gases. The ordinary bubbles that are formed in aqueous solutions have a diameter ranging from 1 µm to few millimeters. These bubbles will reach equilibrium due to the capillary and buoyancy forces that predict the time of retention in an aqueous solution (See Figure 3.1) (Hu et al., 2010; 2011; Wang 2015). If the forces acting up on the bubbles are not at equilibrium they tend to rise through the liquid and burst at the surface releasing the contained gases (Takahashi 2009).

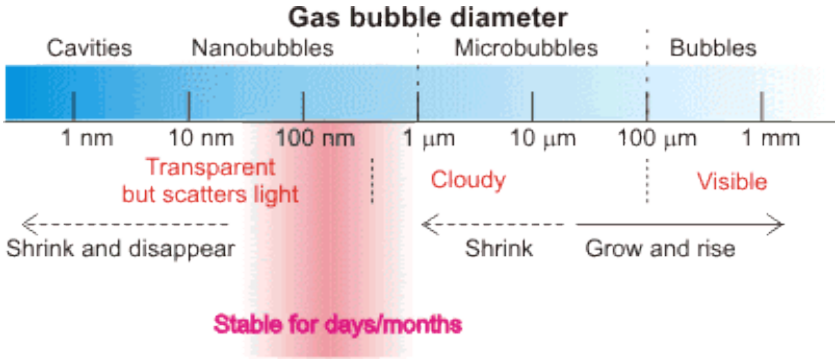

Figure 3.1 Gas bubble diameter and bubble classification for observation.
Source: (http://www1.lsbu.ac.uk/water/nano-bubble.html. Accessed on January 10, 2018)

The *nano-bubbles* with diameters close to 100nm and smaller can remain in water for an extended time period (Li et al., 2014; Agrawal et al., 2011). The uncharacteristic mechanical, physical and chemicals properties of *nano-bubbles* that are observed include finite buoyancy, high surface area to volume ratio, negative zeta potentials, greater ability to dissolve gases in water, and generation of free radicals during generation and collapse.

The sporadic properties shown by *nano-bubbles* are a focus point of many industries and researchers. Researchers have investigated numerous advantages of using *nano-bubbles* in various fields, including medicine (Choi et al., 2012.; Mondal et al., 2012; Modi et al., 2014), controlling boundary slip (Wang et al., 2009; Li et al., 2016), bioremediation (Pan et al., 2012; Li et al., 2014), water treatment by flotation (Li & Tsuge 2006), taking advantage of the high specific area of micro-and *nano-bubble*; the sterilization using ozone gas (Li & Tsuge 2006), crop production and agriculture (Ebina et al. 2013; Minamikawa et at., 2015) and carbonated drinks and as a nutritional supplement carrier (Shen et al. 2008).

3.2 *Nano-Bubble* Generation Methods

Methods of generating *nano-bubbles* include hydrodynamic, acoustic, and electro-osmotic.

3.2.1 Static Mixing Type Generator

The static mixer was designed by Original Hydrodynamic Reaction (OHR) fluid engineering institute (Uematsu, 2006) to mix multiple elements in aqueous solutions, where while mixing replace fluid with air injected from a nozzle to produce micor/*nano-bubbles.* The outlet will produce a stream of bubbles at a rate of 1500L/min. Figure 3.2 presents the OHR static mixer.

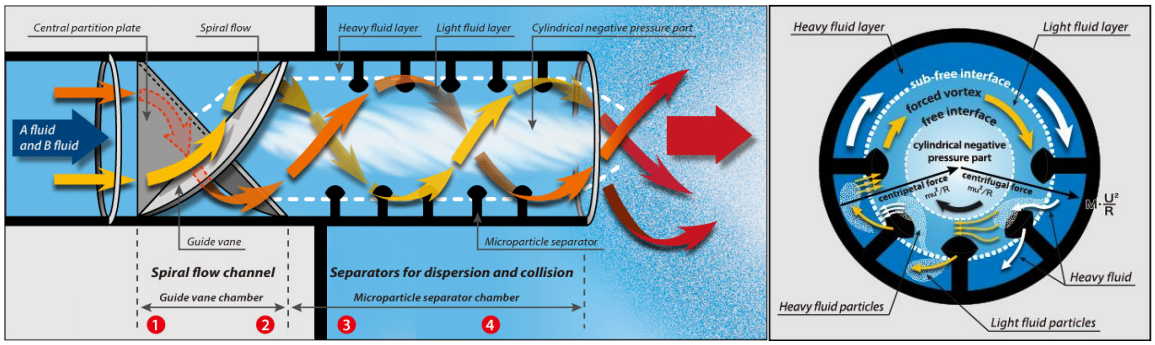

Figure 3.2 OHR static mixer.
Source: (http://www.ohr-labo.com/en/mx_compare.html. Accessed on January 10, 2018)

The forced water free vortex will encourage the gas to dissolve and shear to a fine mist of micro/*nano-bubbles* as it exits into the liquid.

3.2.2 Rotational Liquid Flow Generator

Figure 3.3 presents the rotational flow type *nano-bubble* generator that utilizes the Bernoullis theorem to create a low-pressure zone in the middle of the chamber by creating a rotational liquid flow. The pressurized circular swirling flow of water will force the bubbles to be dissolved into the liquid and sheared into micro and *nano-bubbles* at the outlet of the nozzle. These types of nozzles have the capability of dissolving higher concentration of gases in water.

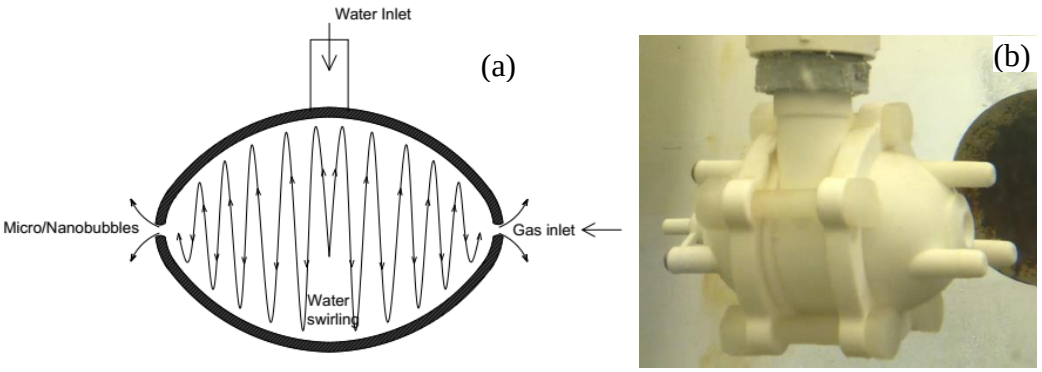

Figure 3.3 Rotational liquid flow generator.

This study uses similar type of nano-bubble generator during the investigation. Figure 3.3 (b) presents the nano-bubble generator used in the study.

3.2.3 Venturi Type Generator

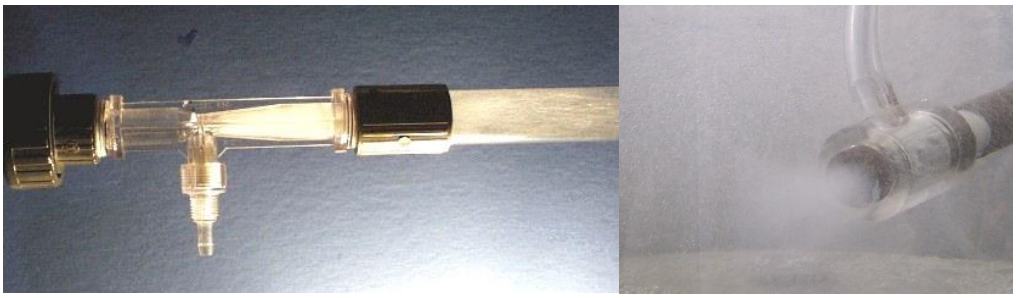

Figure 3.4 Venturi type *nano-bubble* generator.
Source:*(http://www.ozoneapplications.com/info/venturi_injection_vs_bubble_diffusers.htm,http://www.koi.com.my/forum/KOI_Talk_C1/Members_Pond_F16/gforum.cgi?do=post_editlog;post=127026;guest=&t=search_engine. Accessed on January 10, 2018)*

The venturi injection works by forcing the water to move through a bottleneck at a high pressure while injecting the gas into the bottleneck. The vacuum created by the water travelling at high speed, based on the Bernulli's theory, causes the suction to dissolve the gas into the liquid. The shock created at the outlet of the nozzle will create cavities generating micro and *nano-bubbles*.

3.2.4 Ultrasound Assisted *Nano-Bubble* Generation

Ultrasound waves travelling through liquid form microscopic cavities that are filled with vapor and gas. These cavities will settle to become gas bubbles over time depending on the type of gas dissolved in water. This indicates that the ultrasound waves provide the minimum negative pressure called Blake threshold Pressure (Harkin et al., 1999; Makuta et al., 2006). Figure 3.5 presents the cavitation from a horn type ultrasound probe creating bubbles.

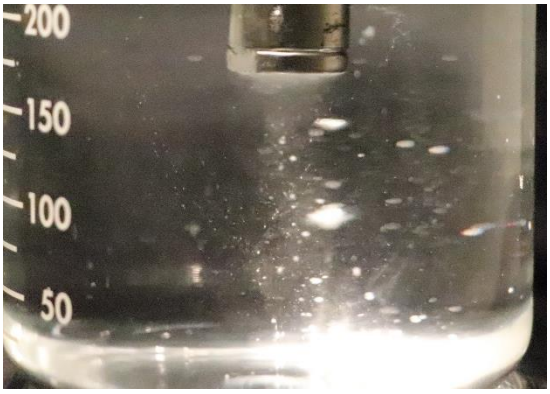

Figure 3.5 Bubble cavitation under ultrasound probe.

3.2.5 Electrolysis Bubble Generation

Using NaOH as an electrolyte, electrolysis generates oxygen and hydrogen bubbles in water. This is used in multiple industries, such as aquatic environment management. Figure 3.6 as shown is the use of electrolysis in a fish tank to increase the oxygen concentrations.

Figure 3.6 Electrolysis bubble generation in fish tank.
Source :*(https://www.aquascapeaddiction.com/articles/twinstar-nano-review-aquarium-algae-control-made-easy. Accessed on January 10, 2018)*

During electrolysis water is broken into hydrogen gas and oxygen gas. By making the surface area higher and adding vibrating fins, the process can produce much finer bubbles (Tsuge et al., 2008).

3.3 Detection and Measurement of *Nano-Bubbles*

The stability of *nano-bubbles* was a topic of research since *nano-bubbles* were first observed in aqueous media and on surfaces of hydrophobic materials. The stability and the behavior of bubbles were measured using multiple methods with varying degrees of accuracy. These methods are highly important to measure the stability and function of *nano-bubbles* in water.

3.3.1 Laser Diffraction and Scattering

The use of a laser beam directed at a liquid containing *nano-bubbles* will scatter the light in different directions. The laser beam will reflect on the surface of the bubble and it will reflect to different directions within the liquid. This diffracted laser light is detected by an array of detectors surrounding the liquid containing cell as shown in Figure 3.7.

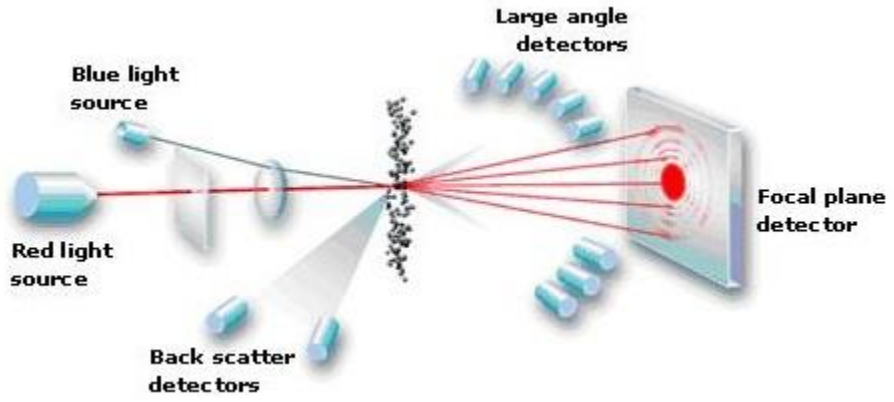

Figure 3.7 Laser diffraction and scattering to find bubble size.
Source*: (https://www.pharmaceutical-networking.com/wp-content/uploads/2016/12/Blue-Light-Source.jpg. Accessed on January 14, 2018)*

These laser light scattering detectors use the Mie scattering theory and Fraunhofer diffraction theory to calculate the bubble size based on the light scattering angle and the light distribution pattern. Figure 3.8 presents the light scattering patterns that can be observed.

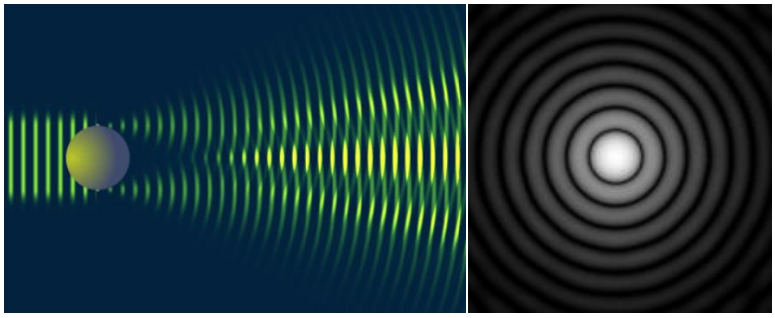

Figure 3.8 Light scattering due to a particle.
Source: *(http://www.horiba.com/fileadmin/uploads/Scientific/Documents/PSA/Webinar_Slides/TE017.pdf. Accessed on January 14, 2018)*

3.3.2 Laser Dynamic Light Scattering

The dynamic laser scattering or quasi-elactic light scattering is one of the most commonly used method of measuring sub micron level particles. The dynamic light scattering method uses the brownian motion in the bubbles in water. The larger the particle is, the slower the movement in the bubble; hence, the visocity of the liquid and the temperaure has a big impact on the output. Figure 3.9 indicate the process that is used for the dynamic light scattering.

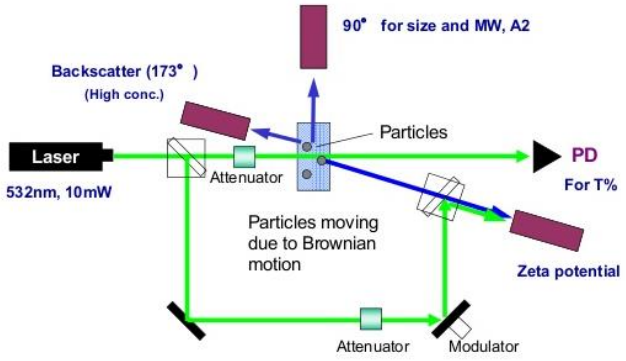

Figure 3.9 Dynamic light scattering analytical method.
Source: *(https://image.slidesharecdn.com/tr014-130116102515-phpapp01/95/method-development-for-dynamic-light-scattering-5-638.jpg?cb=1358332037. January 14, 2018)*

Rayleigh and Mie scattering are two main theories used in the bubble analysis. The cuvette containing the sample is illuminated with the laser, where the scattered beam was detected by two sensors at 173^0 and 90^0 from the beam direction. The sparkle pattern made by the cuvette at the particle detector will stay stationary while the scattered light and the diffracted laser pattern from *nano-bubbles* will change the sparkle pattern. Using detectors patterns will be detected and analyzed to determine the particle size.

The analysis of zeta potential is done by using the back-scattering detector where the laser intensity is reduced to prevent the laser penetration through the bubbles and the detector at 173^0 was used to detect the back-scatter patterns. The system uses a combination of laser Doppler velocimetry and phase analysis light scattering by applying a voltage to the sample making the *nano-bubbles* move within the sample.

3.4 *Nano-Bubble* Stability

The explanation of the stability of the nano gas bubbles in water based on regular thermodynamics seems improbable (Ushikubo et al., 2010). Ljunggren et al. (1997) theorized that a 100nm *nano-bubble* cannot last for more than 10μs in water in many temperatures based on thermodynamics. The most likely mechanisms to explain the stability of *nano-bubbles* are hydrogen bonds on the interface of the bubbles (Ohgaki et al., 2010), formation of clusters (Sedlak 2006, 2006, Jin 2007, Bunkin et al., 2012), ions available in water (Bunkin et al., 2012, Hampton et al., 2010), and supersaturated liquid next to the bubble surface (Brenner et al., 2008). From the previous studies it seems that the stability of the *nano-bubble* depends on combinations of each mechanism working together to stabilize the system.

The stability of *nano-bubbles* is supported by the electrically charged liquid-gas interface, which creates repulsions to prevent bubble coalescence (Figure 3.10). The bubble will not grow as the gases in the bubble will diffuse over time. When given a shock, bubbles tend to coalesce to create micro and macro bubbles and leave the aqueous system. Having a large amount of ions in water will contribute towards the stability of the *nano-bubble*. The negatively charged bubble surfaces compliment the surface tension of the bubble and it enhance the bubble gas pressure (Qiu et al., 2017).

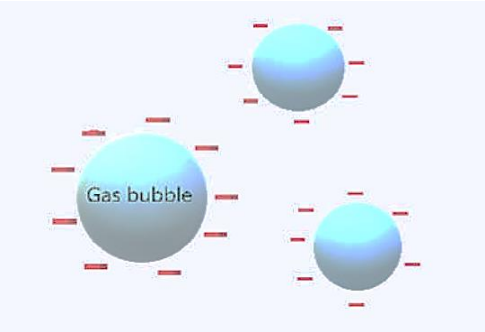

Figure 3.10 Negatively charged *nano-bubbles* in water.

Since the volume of a *nano-bubble* is so small and hence buoyancy force applied on the bubble is also small, resulting in very low rising terminal velocities in water. This will allow the gas bubbles to be impacted by the Brownian motion in the aqueous solution (Qiu et al., 2017). When the *nano-bubbles* are clustered in an aqueous solution, the formation of such clusters and the screening effect dominates the diffusion of gas in to water. The screening effect is caused by the formation of *nano-bubbles* as a cluster (Weijs & Lohse, 2013).

Nano-bubbles have large specific surface area compared to macro bubbles. When compared with the surface area of the macro and micro bubbles, *nano-bubbles* have a

higher potential to react with a pollutant. Table 3.1 presents the equivalent surface area of bubble size varying from 1mm, 1µm and 100nm for equal volume.

Table 3.1 Total Surface Area of the Bubbles (1mm, 1µm and 100nm Diameter)

Bubble Diameter (mm)	Volume of a bubble (mm^3)	Surface area of a bubble (mm^2)	Equivalent number of Bubbles	Total surface area (mm^2)
1	0.5236	3.1416	1	3.141593
0.001	5.236E-10	3.1416E-06	1E+9	3141.593
0.0001	5.236E-13	3.1416E-08	1E+12	31415.930

The total surface area of 100nm *nano-bubbles* with the same volume of gas to a 1mm bubble has 10000 times the surface area. Hence, the potential to have contact with pollutants or contaminants increases immensely. The large surface area will allow more gas to diffuse into the liquid. In order to calculate diffusion of ozone in water the equation (Equation 3.1) can be used (Johnson and Davis 1996).

$$r = 2S(C' - C_0)\sqrt{\frac{DT}{\pi}} \tag{3.1}$$

S is the surface area of the gas bubble or $S = 4\pi r^2$. C' is the concentration of O_3 in the gas-liquid interface or $C' = \frac{PC_w}{H}$. P is the pressure. C_w is the molar concentration of water. H is the Henry's constant and is assumed to be $3.90 \times 10^3\ atm$ for ozone (Kavanagh et al., 1980). C_0 is the initial concentration of the gas and D is diffusivity of ozone given as $1.76 \times 10^{-9}\ \frac{m^2}{s}$ (Johnson and Davis, 1996).

3.5 Reaction of Ozone *Nano-Bubbles* in Water

3.5.1 Ozone in Water

There are many common oxidizing agents with high oxidizing potential available and used in multitude of industries. A few of the most common oxidizers are ozone (O_3), hydrogen peroxide (H_2O_2), fluorine (F_2) and potassium permanganate ($KMnO_4$). Among the most powerful oxidizing agents for an in-situ treatment process, use of F_2 and $KMnO_4$ require special methods to remove byproducts of oxidation. Hence, the conservative and best approach is to use an oxidant such as ozone (O_3) or hydrogen peroxide (H_2O_2) that will not create toxic byproducts, does not require special precautions during use, and cost effective. Out of ozone (O_3) and hydrogen peroxide (H_2O_2), ozone is cheaper to generate.

Ozone must be electrically generated on-demand and cannot be stored for later use. Ozone is generated by irradiation of an air stream with ultra-violet (UV) light at a wavelength of 185 nm or by passing dry air or oxygen through a corona discharge (CD technology) (Figure 3.11). Interest in using ozone to remediate contaminated soils has been rising over years, especially in application for non-volatile organic compounds that are not removed by conventional soil venting (O'Mahony et al. 2006). Ozone can be utilized in both gaseous and aqueous forms (Choi et al., 2001). When utilized in the aqueous phase, ozone can be applied to the soil in a similar manner to that used in soil washing. Another benefit of using ozone is that after a short period of time ozone unreacted reverts back to atmospheric oxygen leaving no toxic residues of the oxidant in the soil (O'Mahony et al., 2006). Field studies of ozone in remediation of chlorinated compounds have been very successful and have been reported to be cost effective compared to other soil remediation methods (Masten & Davies, 1997). Ozone is also reported to be expedient for the

degradation of PAHs in soils (Choi et al., 2001; Masten & Davies 1997). Because microorganisms are only capable of degrading PAHs that are dissolved in the aqueous phase, bio-gradation of PAHs contaminated soil is limited (Bosma et al., 1996; Luthy et al., 1994). Intermediates that are extra soluble would be available to microbes for biodegradation. Hence, ozone is used to degrade PAHs into intermediates that are more soluble in the aqueous phase (Kornmüller & Wiesmann 2003). Ozone sparging in the kaolinite slurries removed 94% of Hexachlorobenzene (HCB) in 30 days. In contrast, it took 55 days to achieve the same PCB removal in river sediment slurries (Cassidy et al., 2002). Ozone also oxidizes heavy metals to their higher oxidation state making them water soluble and easy to separate by filtration (McBride 1989).

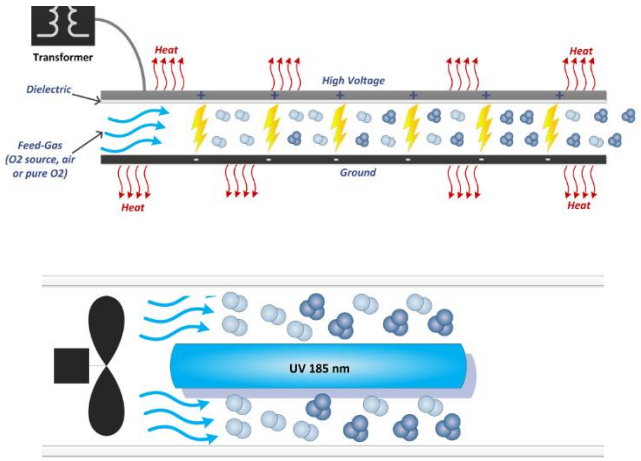

Figure 3.11 Ozone generation technologies.
Source: *(https://www.ozonesolutions.com/. Accessed on January 14, 2018)*

Ozone is a very reactive and unstable oxidant available to the chemical industry (Siegrist et al., 2011) and it reacts with organic and inorganic compounds. It is common practice to use ozone to treat wastewater. Due to its unstable form and its instability, ozone is produced at the site. Upon release of its oxidizing potential, ozone reverts back to oxygen

from which it was generated. Application of ozone does not leave a chemical residue, and under ambient conditions, it has a half-life of 10 to 20 minutes.

Once in an aqueous solution, ozone decomposition can occur due to chain reactions with radicals created by ozone reacting with water. In pure aqueous solutions, ozone slowly decomposes in multiple steps including radical formation. These set of chain reactions has been explained using two different mechanisms, by Hoigne-Staehelin-Bader (HSB) and Gordon-Thomiyasu-Fukutomi(GTF) as shown in Figure 3.12 (Langlais, et al., 1991).

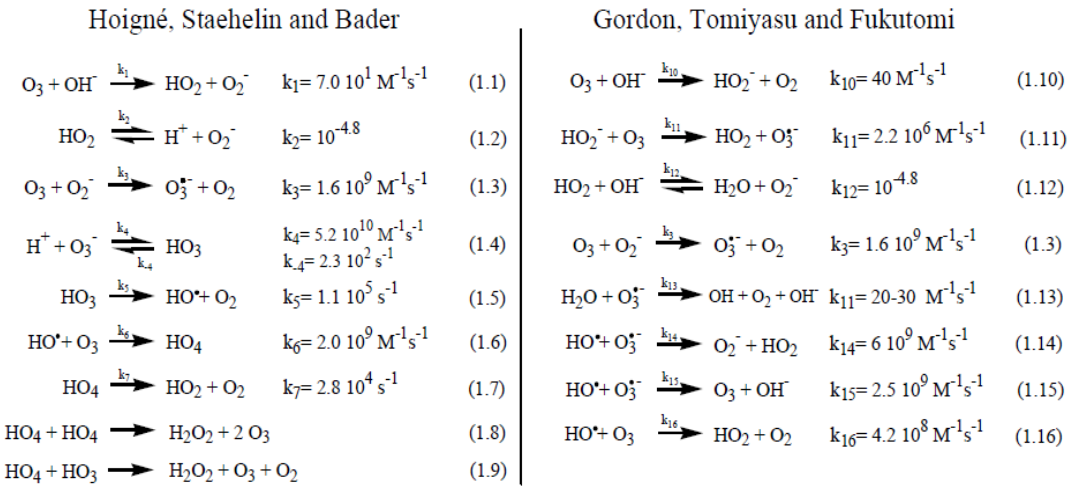

Figure 3.12 Decomposition of ozone in aqueous solutions.
Source: (Langlais, et al., 1991)

The radicals formed during the decomposition of ozone are highly unstable with a very short life span. Due to the high instability of the radicals, they possess strongest oxidation capabilities.

3.5.2 Ozone *Nano-Bubbles* in Water

Use of ozone to treat contaminated soil and waste water, and pretreatment of drinking water is a common practice (Hoigne et al., 1998, Ikehata et al., 2006). The use of *nano-bubbles*

in waste water and contaminant treatment is being researched (Takahashi 2009). Khuntia et al. (2013) investigate the possibility to use ozone micro and *nano-bubbles* to remove ammonia from drinking water. Using micro ozone bubbles, Ikeura et al. (2011) effectively removed Fenitrothion from vegetables. The removal rates were shown to be higher than regular methods, indicating that reaction between ozone and Fenitrothion was very high due to the use of ozone microbubbles. Xia and Hu (2016) investigated the use of ozone *nano-bubbles* to remediate organically contaminated industrial sites.

Industries ranging from food, soil remediation and waste water treatment have had significant success of using ozone *nano-bubbles*. Depending on the conditions and the method used in *nano-bubble* generation, the amount of ozone dissolved in water and bubbles has to be investigated.

3.6 Materials and Methods

Ozone will be produced by passing oxygen through Ozonator (Model T Series, Welsbach Ozone System Corporation, USA & A2Z Ozone Inc. Model MP-3000). Oxygen used to generate ozone in the lab was an industrial grade oxygen. The dissolved ozone was tested using the 4500-O_3 indigo Colorimetric method. A Thermo Scientific™ Evolution 201 and 220 UV-Vis spectrophotometer was used during the 4500-O_3 ozone analysis.

The *nano-bubble* was generated with micro-nano bubble nozzle (Model BT-50FR, Riverforest Corporation, USA) which implement rotational flow of water to generate *nano-bubbles*. Ozone gas will be introduced to the inlet of the utility pump (Model 4CUK6, Dayton, USA) and to the ozone *nano-bubble* nozzle to produce the ozone *nano-bubble*. To optimize the bubble generation, the pump has to generate a pressure above 42 psi. The

pump generated a constant running pressure of 55 psi during operations. The *nano-bubble* generation system is presented in Figure 3.13.

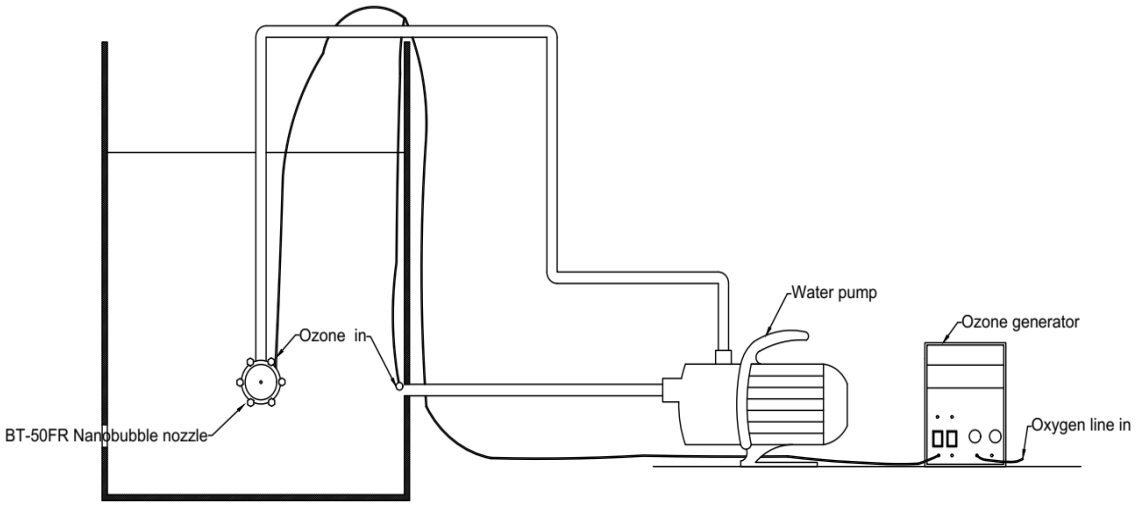

Figure 3.13 Ozone *nano-bubble* generation system.

Malvern Nano Zetasizer was used for the analysis of *nano-bubbles* and its zeta potentials. To analyze the bubble size, 12mm square polystyrene cuvettes were used and to analyze the zeta potential Folded Capillary Zeta Cell (model DTS1070) is used. Malvern nanosight ns300 was used to observe the amount of *nano-bubbles* generated.

3.7 Results and Discussion

3.7.1 Ozone *Nano-Bubble* Size Distribution and Zeta Potential in Water

Nano-bubble size distribution in water is a key factor to determine the stability of the bubbles and the amount of ozone dissolved in water. *Nano-bubbles* with a diameter around 100nm showed in water for long durations and indicated them being stable for a long period of time (Ushikubo et al., 2010). Ohgaki et al. (2010) observed the 50nm *nano-bubbles* lasting more than two weeks, where the bubbles were prepared by using nitrogen, methane

and argon. The solubility of the gases used in the study by Ohgaki is low compared to ozone where it is inevitable to have a much lower lifespan. The *nano-bubble* sizes generated by using BT-50FR *nano-bubble* was measured for the bubble size distribution, and zeta potential of the bubble. Figure 3.14 present the images obtained by using nanosight ns300. The white spots show the diffracted laser aurora of the *nano-bubbles*.

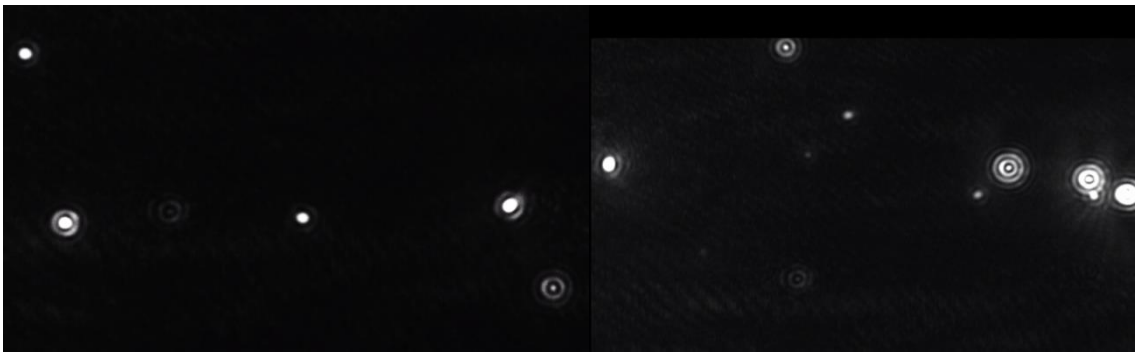

Figure 3.14 *Nano-bubbles* observed using Nanosight ns300.

Figure 3.15 shows the size distribution of *nano-bubbles* tested at 10^0C, 15^0C, 20^0C and 25^0C. The bubble diameter did not indicate temperature having a considerable impact to the diameter or the amount of bubbles generated in the water. However, the bubbles seem to be slightly larger in diameter when the temperature increases.

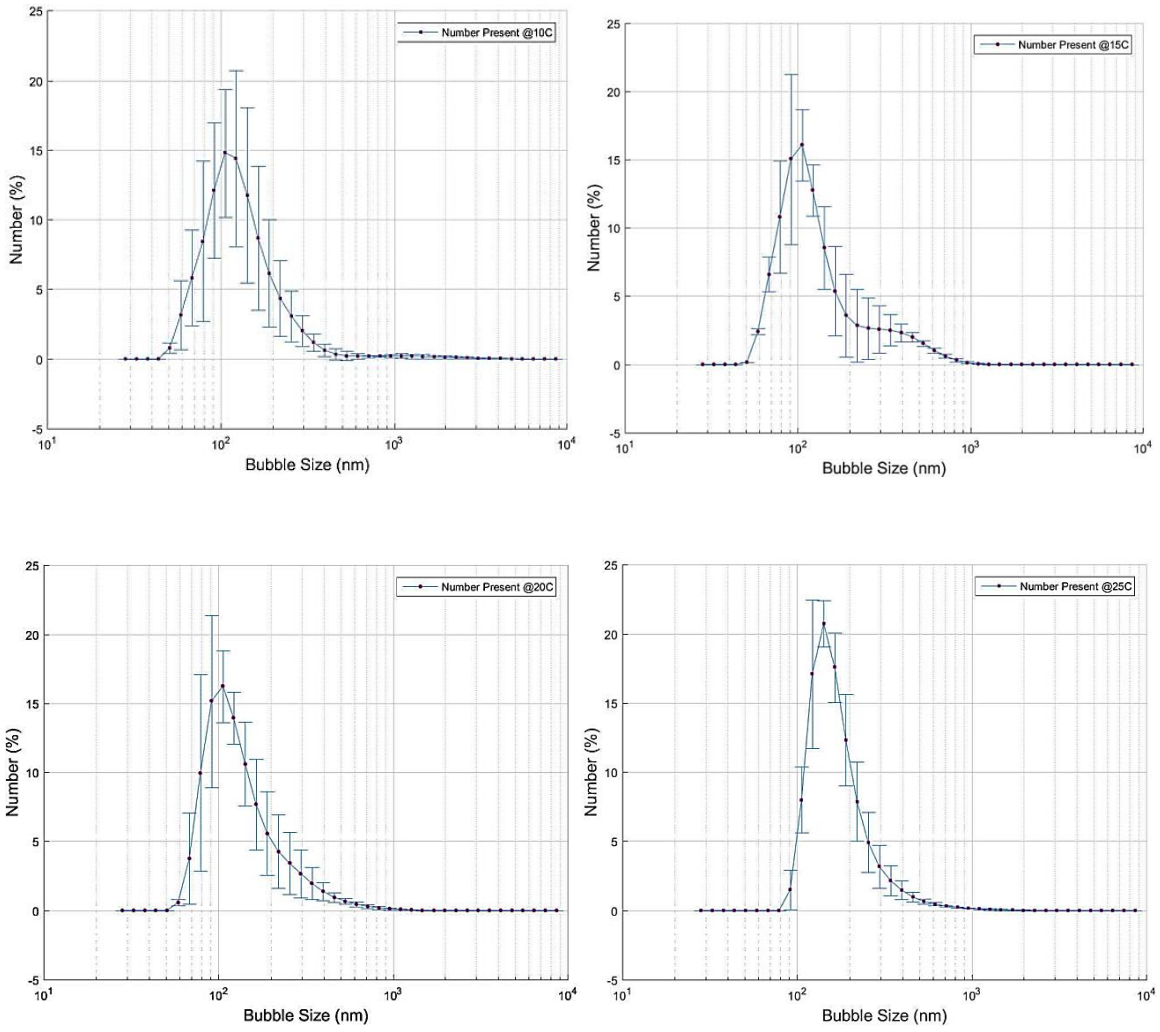

Figure 3.15 Ozone *nano-bubble* distribution (at 10^0C, 15^0C, 20^0C and 25^0C).

Ozone *nano-bubbles* generated at the same condition at 25^0C were also tested using the Malvern nanosight ns300 where the bubble size distribution. Ozone *nano-bubble* size obtained using nanosight ns300 was slightly smaller in size when compared to that obtained from the zetasizer. The results are presented in Figure 3.16

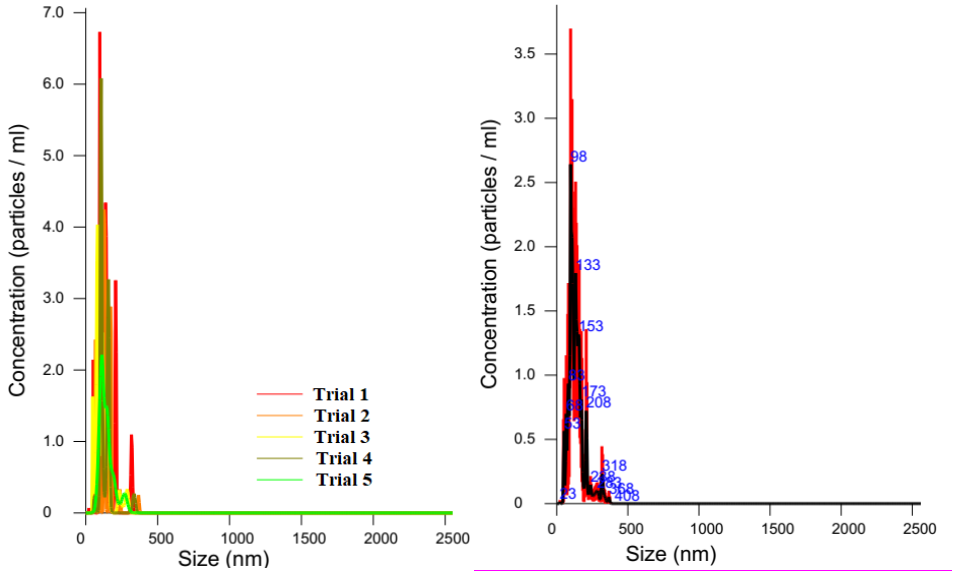

Figure 3.16 Ozone nano-bubble size distribution using Nanoparticle Tracking Analysis (NTA)

The reliability of the results was questionable due to the high vibrations detected during the analysis. However, a sample of ozone *nano-bubbles* tested using the same batch indicated slightly high bubble sizes, which was expected due to the difference in the technology.

Figure 3.17 shows the variation of zeta potential of *nano-bubbles* with temperature. The results shown in Figure 3.17 were obtained by repeating the bubble size analysis two times for each sample of ozone *nano-bubbles*. During each analysis the samples were tested three times. The average zeta potential of the ozone *nano-bubbles* was -25.4mV. The negative zeta potential decreased with the increase in temperature and bubble diameter increased with the temperature.

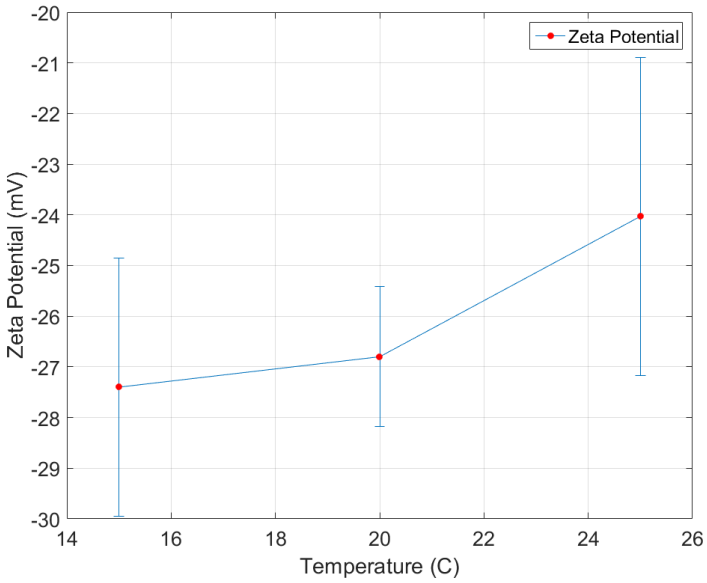

Figure 3.17 Zeta potential of *nano-bubbles* at 15^0C, 20^0C and 25^0C.

Zeta potential of the ozone *nano-bubbles* decreased with the increase of the temperature. With the increase of the temperature ions in the liquid gain energy that will increase its mobility within the liquid. Jai and Ren (2013) presented a similar observation to the zeta potential of air bubbles in water, where the bubble zeta potential decreased with the rise in temperature.

The zeta potential is influenced by the type of gas encapsulated in the gas bubbles. Gases with high potential to dissolve in water tend to present higher negative zeta potential than inert gases. The area where the diffusion takes place gets saturated with ozone gas and concentrates with diffused gas and decomposed ions. That will increase the thickness of the slipping plane increasing zeta potential. Figure 3.18 presents the gas diffusion into a liquid from a gas bubble.

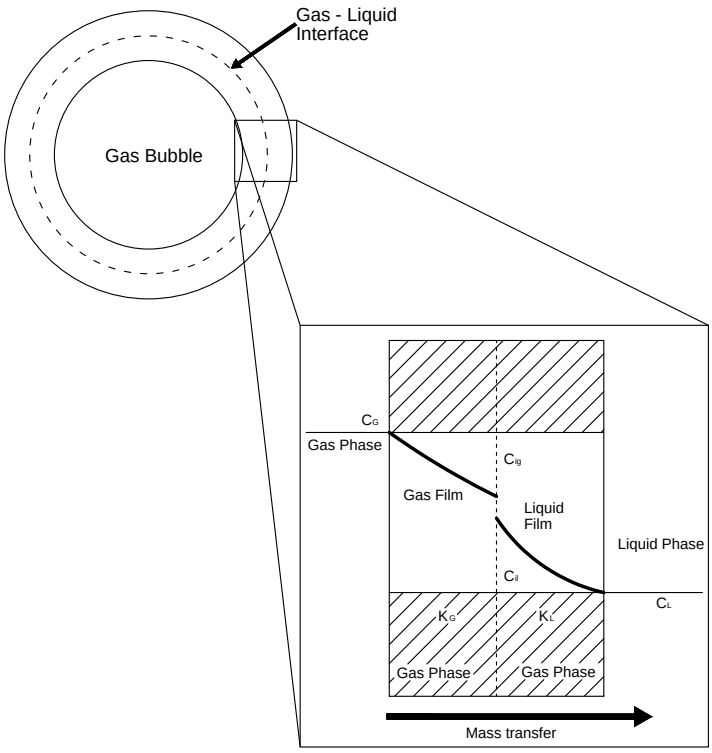

Figure 3.18 Gas diffusion from a bubble.

The diffusion rate decreases when the immediate area surrounding the bubble gets saturated with the gas in the bubble. A cluster of *nano-bubbles* saturating the immediate vicinity will slow the gas diffusion increasing the lifespan of the *nano-bubbles*. As explained by Ljunggren and Eriksson (1997), if the bubble sizes are 10nm to 100nm the bubble lifespan will be around 1µs to 100µs where the diffusion of gases to the liquid will remove the encapsulated gases to the liquid.

3.7.2 Ozone Concentration

The use of ozone *nano-bubble* generation systems will reduce the amount of ozone required to achinve high ozone concentrations in water. Reducing the amount of ozone to achieve high ozone levels in water helps many industries that require ozone during disinfection or remediation processes to reduce the amount of money spent on ozone production. *Nano-*

bubble generation systems using hydrodynamic forces to breakdown the gases to minute gas bubbles will reduce the amount of gases leaving the system by making minute bubbles that diffuse entrapped gases slowly into water. By using ozone *nano-bubbles*, it is possible to reach the maximum ozone levels in water.

During this study, experiments were carried out to ascertain the advantaged of using ozone *nano-bubbles* to dissolve ozone in water. Ozone and oxygen levels in water was measured over a span of 8 hours. The *nano-bubble* generation tank was filled to 20 liters using filtered tap water. The tank was areared using a 20mm diameter fish tank air diffuser (Figure 3.19) for 3 minutes and the *nano-bubble* generation was carried out for the same quantity of time. The samples were prepared at 10^0C, 15^0C, and 20^0C examining the impact of the temperature on the ozone concentrations and *nano-bubbles*. Ozone was delivered at a rate of 3 liter per minute at a pressure of 6.895 kPa. The samples were tested for the *nano-bubbles* sized 30 minutes after the preparation and tested after 8 hours to measure the bubble behavior and size over the time period. The two prepared samples were kept in an 800ml container which was housed in a constant temperature bath as shown in Figure 3.19. The containers were vented to the environment to prevent ozone buildup.

Figure 3.19 Diffuser used in ozonation and the constant temperature bath.

Figure 3.20 present the obtained data from the ozone levels over time for temperature at 20^0C. The ozone levels present in water when using the *nano-bubble* generator is much higher than the concentration of ozone achieved using the diffuser.

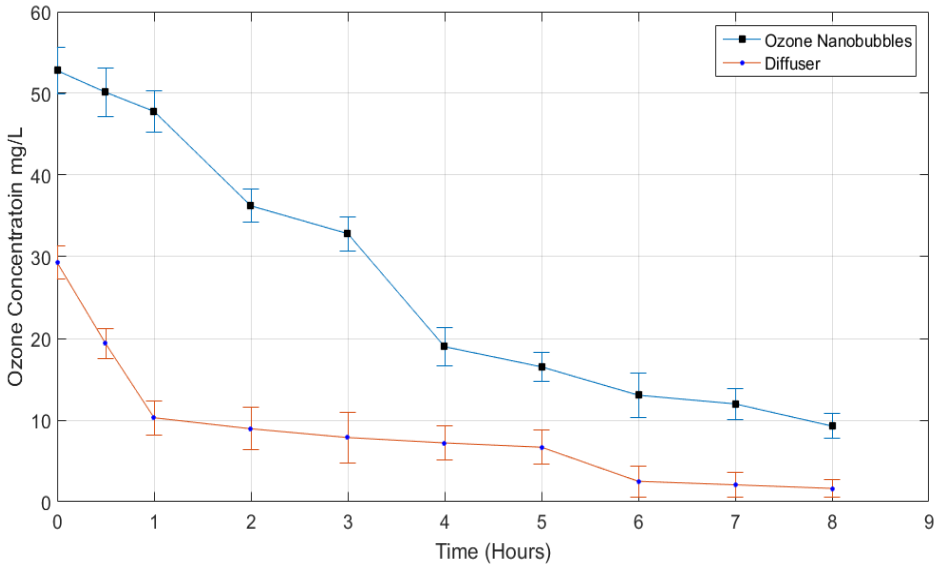

Figure 3.20 Ozone concentration over time at 20^0C.

Ozone concentration rapidly reduced when a diffuser was used to dissolve ozone in water. By using ozone *nano-bubbles*, the amount of ozone left in the system after 3 hours was much higher and was equal to the initial ozone concentrations achieved using a diffuser. During the 8 hours of observation, the ozone concentration in water dropped over time where the ozone concentration in *nano-bubble* water. This investigation proved that using *nano-bubbles* kept the system saturated with ozone for a long period. The ozone concentrations obtained at temperatures 10^0C and 15^0C are presented in Figure 3.21. The study continued to observe the ozone concentration for 8 hours.

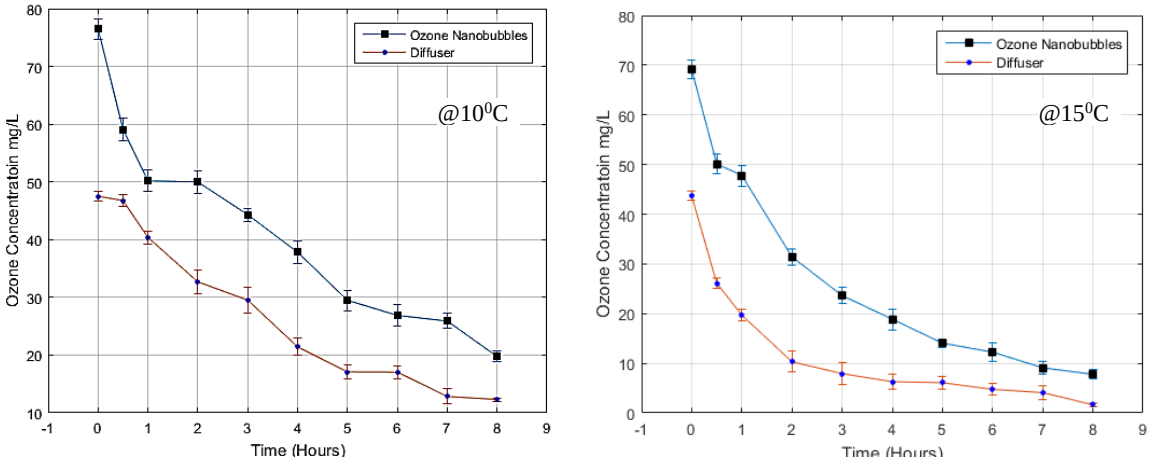

Figure 3.21 Ozone concentration variation over time at 10^0C and 15^0C for 8 hours.

At 10^0C, the ozone concentration in water reached 76.49mg/l using *nano-bubbles* where the ozone concentration using the *nano-bubbles* at a temperature of 15^0C was 69.12mg/l. The dissolved ozone levels obtained in water where ozone was dissolved using a diffuser obtained a maximum of 47.51mg/l at 10^0C and 43.69mg/l at 15^0C. Ozone concentrations obtained using diffusers depleted rapidly over time and at the end of the 8 hours the ozone concentration was 12.31mg/l and 1.64mg/l at temperatures 10^0C and 15^0C respectively. However, the ozone concentrations after 8 hours when *nano-bubbles* were used end up at 19.75mg/l and 7.78mg/l for 10^0C and 15^0C. At lower temperatures the ozone levels observed in water using *nano-bubbles* was considerably high compared to using a fish tank aerating diffuser.

Ozone decomposition and release of dissolved ozone to the overhead space were two major reasons for the decrease in dissolved ozone concentrations over time. The stability and half-life of dissolved ozone depends on ozone concentration, temperature, pH level, availability of hydroxy radicals, fluid dynamic conditions in the liquid, and availability of organic and inorganic material. Other than mentioned parameters, there are

other factors that can influence the stability. Bin (2004) suggested the use of a constant gas consumption model from gas phase to liquid (Equation 3.2) neglecting the changes in ozone concentration during ozonation of the liquid.

$$\frac{dC_L}{dt} = k_L a(C_L^* - C_L) - k_d . C_L^m \quad (3.2)$$

C_L= molar concentration of ozone in the liquid phase (mol.m^{-3}), C_L^* = equilibrium molar concentration of ozone in the liquid phase (mol.m^{-3}), $k_L a$= volumetric mass transfer coefficient in the liquid phase (s^{-1}), k_d= kinetic constant of ozone self-decomposition (s^{-1}), and C_L^m= ozone decomposition in the liquid (m, can be 1 to 2 where it will be first order or second order formation). The solubility of the gas phase and decomposition can lead to a much-complicated model which require additional data. Mechanistic approach to the decomposition require defining multiple conditions and observations. Hence, to simplify the approach for the decomposition of ozone in the liquid, a generic formula (Equation 3.3) can be derived from Equation 3.2.

$$-\frac{d[O_3]}{dt} = k_d . [O_3] \quad (3.3)$$

Keeping the temperature and pH constant, Gardoni et al., (2012) developed an empirical kinetic decomposition chart for the k_d constant. The imperial values were calculated based on the first order kinetic studies performed by Czapski et al. (1968), Rizzuti et al. (1976), Teramoto et al. (1981), Sotelo et al. (1987), Huang and Chen (1993) and Ku et al. (1996). The upper boundaries and lower boundaries were based on the studies are shown in Figure 3.22.

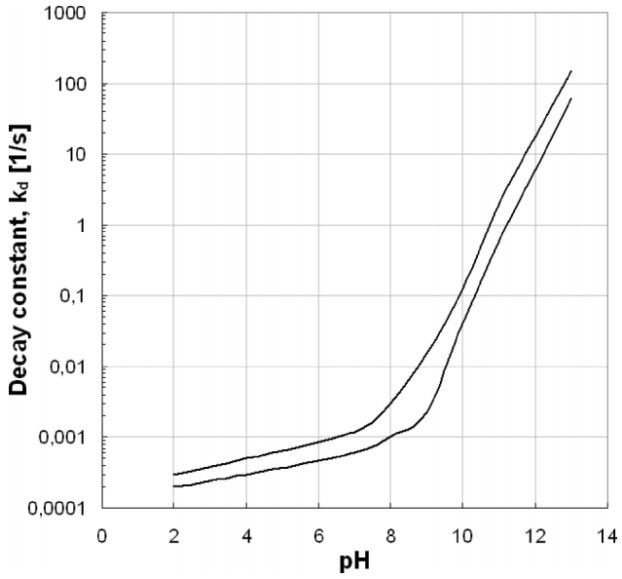

Figure 3.22 Ozone decomposition rate based on variation of pH (@20^0C).
Source: Gardoni et al., (2012) (Ozone Science and Engineering)

The pH level of the water used in the study was 7. Hence, from Figure 3.22 the decaying constant ($k_d = 0.0006\ s^{-1}$) was obtained. The ozone reduction rate from the study was obtained for each observed hour by using Equation 3.4. The concentration in water at the start of the hour and the end of the hour was used calculated the reduction rate.

$$Reduction\ rate = \frac{d[O_3]}{dt} = \frac{[C_{O_3(start)} - C_{O_3(end)}]}{3600\ s} \tag{3.4}$$

Ozone reduction rates based on the empirical theory (Equation 3.3) and experimentally observed values were calculated (Equation 3.4). The results attained are shown in Table 3.2.

Table 3.2 Ozone Reduction Rates using Empirical Calculations and Experimental Data @ 20^0C

Time (hour)	Observed Concentration (mg/l)	Average concentration (mg/l)	Reduction rate (mg/l).s^{-1}	k_d (s^{-1})	Theoretical reduction rate (mg/l).s^{-1}
0	58.12	-	-	0.0006	-
1	47.68	52.90	0.00290	0.0006	0.03174
2	31.39	39.54	0.00452	0.0006	0.02372
3	23.63	27.51	0.00216	0.0006	0.01651
4	18.87	21.25	0.00132	0.0006	0.01275
5	14.05	16.46	0.00134	0.0006	0.00987
6	12.24	13.14	0.00050	0.0006	0.00789
7	9.09	10.66	0.00087	0.0006	0.00640
8	7.78	8.44	0.00036	0.0006	0.00506

The reduction obtained from the theoretical formula are higher than the reduction observed during the experimental studies. Using an ozone sensor (A-21ZX ozone sensor, Manufactured by EcoSensors), the overhead concentration was monitored, where the ozone sensor failed to detect ozone. Henceforth, ozone *nano-bubbles* improve the ozone retention in water and prevent release of ozone from water. Ozone *nano-bubbles* slowed the decomposition of ozone in the liquid, increasing the retention time of ozone in water. The ozone decomposition (reduction rate) observed at each hour are shown in Figure 3.23.

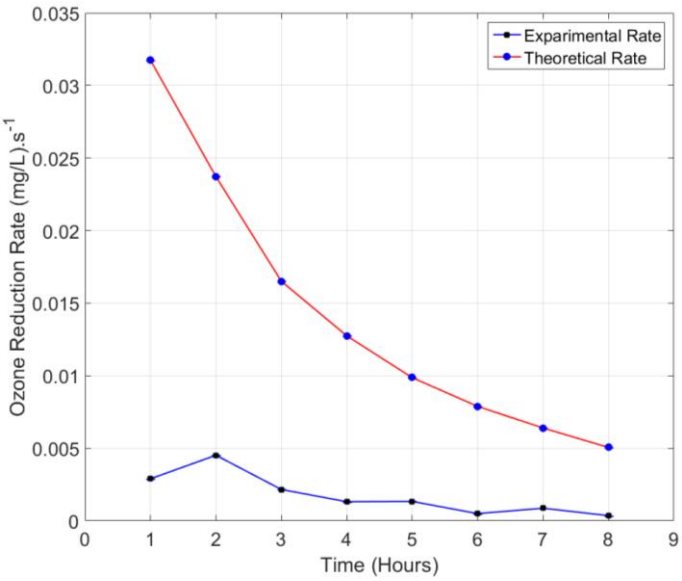

Figure 3.23 Calculated ozone reduction rates using empirical and experimental data.

Figure 3.23 shows the convincing difference between the theoretical and experimental data. When gas diffuse from a gas bubble, the immediate vicinity of the bubble surface gets saturated by the diffused gas. The ozone saturated water surrounding *nano-bubbles* slows down the gas diffusion into the liquid. Figure 3.18 confirmed the theoretical explanation used in in section Ozone *Nano-Bubble* Size Distribution and Zeta Potential in Water.

Ozone decomposition in water generates oxygen. Using ozone, the dissolved oxygen concentration in water can be raised. The decomposition of ozone is catalyzed by the OH^- in water (Bader et al., 1982, Sehested et al., 1984) where the OH^- promote the formation of radicals that will further react with water and form O_2. The study continued to investigate the concentration of oxygen during the investigation for the ozone concentrations in water by dissolving ozone using a diffuser and *nano-bubbles*. The oxygen levels were observed for 8 hours starting at 30 minutes after the process of dissolving

ozone. The oxygen levels were monitored at temperatures 10^0C, 15^0C and 20^0C. Figure 3.24 present the oxygen concentrations observed at 20^0C.

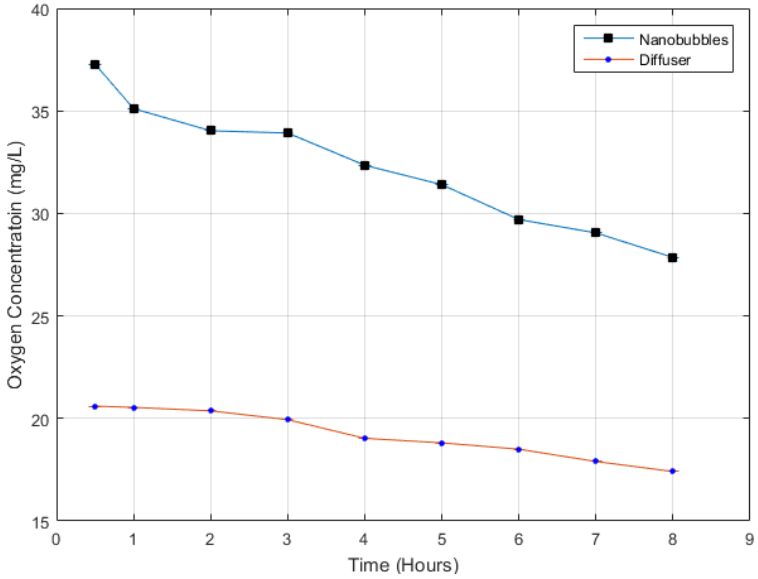

Figure 3.24 Oxygen concentration in water over time at 20^0C.

The highest oxygen levels observed in water were obtained when using a *nano-bubble* generator to dissolve ozone in water. At 30 minutes oxygen concentration reached 37.28mg/l where the oxygen level slowly decreased over time. However, compared to depletion of ozone, the rate of decline of oxygen was much slower due to the generation of oxygen during decomposition of ozone. Similar variation is observed when using a diffuser where the highest oxygen concentration observed in water was 20.60mg/l. Figure 3.25 present the oxygen concentrations observed at temperatures 10^0C and 15^0C.

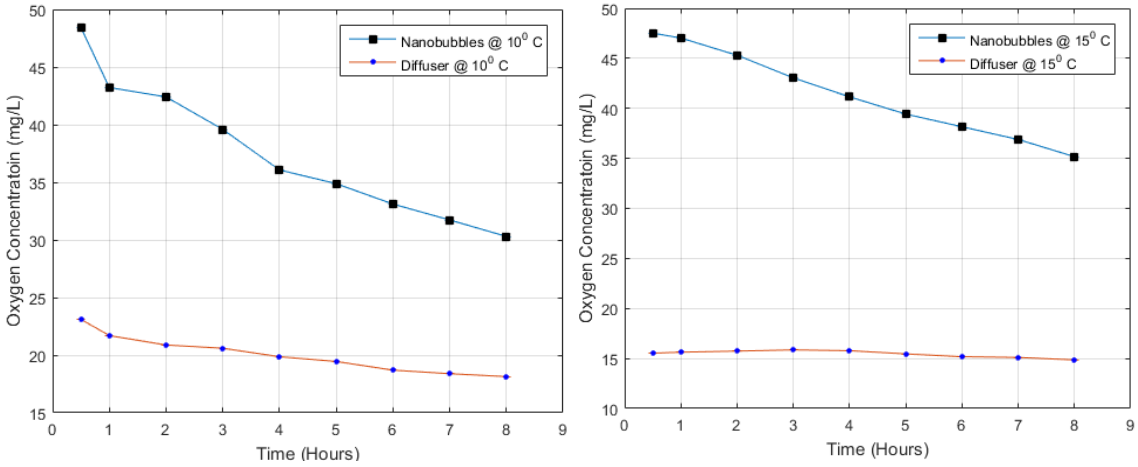

Figure 3.25 Oxygen concentration in water over time at 10^0C and 15^0C.

Observing the oxygen levels in water at 10^0C and 15^0C, attained concentrations of oxygen in water by using a *nano-bubble* generation was much higher than the regular diffuser. The oxygen levels stayed at high concentrations over the 8 hours. Observed oxygen concentrations remained twice the concentration of a regular diffuser. Devising high oxygen concentrations in water will help further decomposition of ozone that generate radicals that can oxidize pollutants and any unnecessary materials.

3.8 Ozone *Nano-Bubble* Generation Time

The foremost reason of using ozone *nano-bubbles* as an ozone delivery method to improve the ozone solubility and reduce waste. By using the BT50-FR *nano-bubble* generating nozzle, the amount of ozone that can be dissolved can vary with the temperature. As it was observed at 10^0C 76.49mg/l ozone in water and s at a temperature of 15^0C was 69.12mg/l dissolved ozone was observed in water. Hence, it is necessary to identify the optimum time it is needed to operate the *nano-bubble* generation system. The ozone *nano-bubble* generation system was operated every 2 minutes up to 8 minutes to obtain the dissolved

ozone concentration and dissolved oxygen concentration. The total volume of the stabilized DI water used in the study was 21 liters and it was kept for 24 hours prior to be used in the ozone *nano-bubble* generation. Table 3.3 present the results obtained during the *nano-bubble* generation time requirement to saturate water with ozone.

Table 3.3 Dissolved Ozone and Oxygen Concentrations Observed with System Operation Time at Temperature of 25^0C

System Operation time (min)	Conductivity (µS/cm)	Dissolved Oxygen Concentration (mg/l)	Dissolved Ozone concentration (mg/l)
0	8	9.79	0
2	59	32.38	35.24
4	58	35.12	45.24
6	58.5	35.43	54.29
8	58	36.13	65.24

Observations made by changing the duration of the *nano-bubble* operation times indicated that at time 6 minutes and time 8 minutes, the dissolved ozone concentrations were 54.29mg/l and 65.24mg/l. The dissolved ozone concentrations at minutes 6 and 8 seems to indicate that the water reaching its maximum dissolved ozone concentration. However, dissolved ozone concentration in water depends on the temperature in water. Hence, the study was repeated at a water temperature of 15^0C. The results obtained when ozone generated at 15^0C are presented in Table 3.4.

Table 3.4 Dissolved Ozone and Oxygen Concentrations Observed with System Operation Time at Temperature of 15^0C

System Operation time (min)	Conductivity (µS/cm)	Dissolved Oxygen Concentration (mg/l)	Dissolved Ozone concentration (mg/l)
0	8	9.79	0
2	59	32.38	40.00
4	58	35.12	52.38
6	58.5	35.43	90.00
8	58	36.13	89.52

Repeating the ozone *nano-bubble* generation at 15^0C indicated 90.0mg/l at 6 minutes and 89.52mg/l at 8 minutes. This investigation indicated that by operating the pump for 6 minutes it is possible to obtain the maximum dissolved ozone concentrations in the water that will be used in remediation.

High instability of ozone gas in aqueous environments makes the evaluation of solubility of ozone complicated. However, researchers were able to find the Henry's constant for the solubility of ozone in water. Using Henry's law (shown in Equation 3.5) solubility of ozone in water was calculated.

$$p = k_H.C \tag{3.5}$$

$p =$ partial pressure of the solute in the liquid (kPa), k_H= Henry's constant (L.kPa/mol) and C = concentration of the solute (mol L^{-1}) (Clever, 2014). The concentration of ozone theoretically calculated at 15^0C and 25^0C for ionic strength of 0.00, 0.05 and 0.10molL^{-1}. Ozone concentrations calculated based on Henry's law are shown in

Table 3.5. During the calculations, the ozone injection pressure into the nano-bubble chamber 1 psi (0.06805atm) was used as the partial pressure.

Table 3.5 Ozone Concentrations Calculated using Henry's Law

Temperature (^{0}C)	**Ionic Strength** (mol L^{-1})	**Henry's constant*** **(**L.atm/mol)	**Partial Pressure** (atm)	**Concentration of Ozone**	
				mol L^{-1}	mg L^{-1}
15	0.00	68.0	0.06805	0.0010	48.03
20	0.00	78.0	0.06805	0.0009	41.87
25	0.00	87.5	0.06805	0.0008	37.33
15	0.15	70.8	0.06805	0.0010	46.13
20	0.15	81.8	0.06805	0.0008	39.93
25	0.15	92.2	0.06805	0.0007	35.43

* Calculated by Clever (2014) based on Rischbieter et al., (2000).

The concentrations calculated using the Henry's constant, show the concentrations that resulted are lower than the concentrations observed with ozone *nano-bubbles*. Hence, it was clear to consider using ozone nano-bubbles will increase the ozone solubility. Ozone nano-bubbles availability as a gas in the liquid will increase the total ozone concentration in the water.

3.9 Summary and Conclusions

Nano-bubble technology has been a key technology used in many industries. Ozone *nano-bubbles* generated using the BT50FR model which uses hydrodynamic forces to generate *nano-bubbles,* and generated *nano-bubbles* with an average diameter of 100nm. The bubbles observed in the samples lasted for 14 days before disappearing from the water. The

laboratory studies investigated the behavior of *nano-bubbles* with the temperature, where *nano-bubbles* diameter increased with increasing temperature. The zeta potential of the ozone *nano-bubbles* decreased with the increase of the temperature. This might be a cause of the increase in temperature increasing the mobility of ions in water. Use of ozone *nano-bubbles* presented results with extremely high concentrations of ozone in water and the decomposition of ozone produced high oxygen concentrations in water. The ozone *nano-bubble* generation system used during the investigation reached the maximum ozone concentration by operating the system for 6 minutes.

CHAPTER 4

DECONTAMINATE ORGANIC CONTAMINANTS IN PASSAIC RIVER SEDIMENTS

4.1 Organic Contamination in Passaic River

Contamination of the Passaic River sediments was a combination of multitudes of industries releases chemicals accidentally or due to facile waste disposal laws. The types of organic contaminants available in the Passaic River range from polyaromatic hydrocarbons (PAHs), Polychlorinated biphenyl (PCBs), many other pesticides and by-products of pesticides manufacturing that are classified and non-classified chemical products (U. S. EPA, 1998; Armstrong et al., 2005). Investigations carried out by the U.S. EPA found a mixture of polyaromatic hydrocarbons with heavy and low molecular weights. Based on the data provided by the U.S. EPA indicated few locations with PAH concentrations between 300-1000 ppm. In three monitoring locations used by the U.S. EPA, the concentration of PCB was above 650 ppb where one location indicating a concentration of 2481 ppb. Few locations in the river around the 11 and 7.4-kilometer marker few hotspots with a concentration above 10ppm were discovered. Detection of 2,3,7,8-Tetra-chloro-dibenzodioxin (TCDD or 2,3,7,8-TCDD) by sampling in the Passaic River, locations with 10000 ppt and above are mainly associated with silty sediments and were found at kilometer markers of 6km, 7.24km, 7.4 km, 10.14km, 12km, and 12.23km (U. S. EPA 2014). For *Dichloro-diphenyl-dichloro-ethylene* (DDE) and *Dichloro-diphenyl-trichloroethane* (DDT), there were not many locations in the river containing high concentrations but few locations containing 1000ppb and above. The 2,3-Dehydro-2,3-Dideoxyribofuranose-5-phosphate (DDx) where found on the surface during investigations

between 2005 and 2012 (U. S. EPA 2014). Agent orange as a chemical weapon that was used in Vietnam war, was accidently released to the river during production. The 2,4-dichlorophenoxyacetic acid (2,4-D) and 2,4,5-trichlorophenoxyacetic acid which are known to chemist as one of the worst toxins and leaving traces of TCDD during production in the final product.

Due to the number of pesticide and herbicide industries next to the river, the accidental release of these chemicals were inevitable. Ulrban et al., 2009 showed high possibility of bioaccumulation due to the fish and carbs prevailing and use the sediments as a source of food. State of New Jersey and Department of Environmental Protection and Health and Senior Services posted public health statements to prevent inhabitants from consuming the fish or crabs as a source of food.

4.2 Organic Contamination and Remediation

There are many ways of remediation organic contaminated soil based on the site conditions available where most common technologies being used solvent extraction, bioremediation, phytoremediation, electrokinetic remediation, and chemical oxidation. These technologies meet many requirements before being implementing at a contaminated site. The Passaic river presents a unique condition where it requires treatment of sediments underwater, and dredging will increase the possibility of recontamination of the river. This would make phytoremediation, solvent extraction, bioremediation, and electrokinetic remediation in appropriate. Chemical oxidation is one of the remediation methods that can be adapted to the given contaminated environment. Using the proper oxidizer will allow the process to be successful for given mixture of contaminants as indicated by Lemaire et al. (2013).

Using the correct oxidizer will degrade both high and low molecular weight hydrocarbons. Interest in using ozone to remediate contaminated soils has been looked into by many researchers for the past few decades, especially in the application for non-volatile organic compounds that are not removed by conventional soil venting (O'Mahony et al., 2006). Ozone can be utilized in both gaseous and aqueous forms (Choi et al. 2001). Ozone is also reported to be expedient for the degradation of PAHs in soils (Choi et al. 2001; Masten & Davies, 1997). Several researchers investigated use of ozone to remove organic contaminants from soil (Do et al., 2009; Yu et al., 2007). Li et al. (2009) investigated the influence of soil grain size and ozonation for 20 hours to remove diesel oil from the soil. They found that the ozonation efficiency was not affected by soil water content of less than 18 w/w%. Sparging the contaminated soil with surfactants mixed with ozone where the mixture took 156h to remove phenanthrene from a 5m soil column. Xia and Hu (2016) investigated the use of ozone *nano-bubbles* with hydrogen peroxide to remediate a contaminated site in Nanjing with success.

The use of ultrasound will increase the shearing of bonds between soil particles and the organic contaminants. Meegoda et al. (2001) studied the impact of ultrasound on solvent extraction on PAH contaminated soil. The study concluded with an efficiency of 89% when solvent extraction is enhanced by including sonication. Bagal and Gogate (2012) investigate the possibility of using ultrasound to remove alachlor herbicide. They used a 20 kHz ultrasound at 100W power to remove the alachlor, where the study used the Fenton reaction to improve oxidation. They showed high efficiencies in removing alachlor from the soil. Kidak and Ince (2006) used ultrasound to destruct phenol and substituted phenol where they observed the optimum frequency range between 200–540 kHz with

power intensity increased to 75Wcm^{-2}. A study conducted by Babic et al. (1998) examined the use of ultrasonic solvent extraction, Soxhlet extraction and shake-flask extraction for their efficiency and rate of extraction. The study identified using ultrasound during solvent extraction, the rate of extraction to be higher than shake-flask and Soxhlet extraction. Ultrasound extraction, in general, has been studied in laboratory scales to remove organic contaminants from soil and sediments due to cavitation and radical formation at high energy levels. In this study they investigated the advantages of cavitation and formation of radicals to desorb the adsorption bonds between organic pollutants and soil particles releasing the compound to the liquid. Released compounds are further degraded by using ultrasound where the degraded compounds are exposed to ozone that reacts with the compounds oxidizing it further. Using *nano-bubbles* to deliver ozone to oxidize contaminants increase the possibility of reaction with ozone directly. The *nano-bubbles* contain a negative surface charge which intensifies the attraction with any compound that has a positive charge. This action will increase the possibility of bonding between chemicals with a positive charge and reaction with ozone.

4.3 Materials and Methods

The variation in contaminants and this distribution in sediments recovered from the River tend to present complications in laboratory scale experiments. Hence, as an alternative to using the Passaic River sediments during the laboratory experiments a synthetic soil was prepared based on the average distribution of the Passaic River sediments. The soil synthesized in the laboratory was a mixture of kaolin, slit (rock flour), and fine sand. The

particle size distribution of the soil used in the laboratory investigation is shown in Figure 4.1.

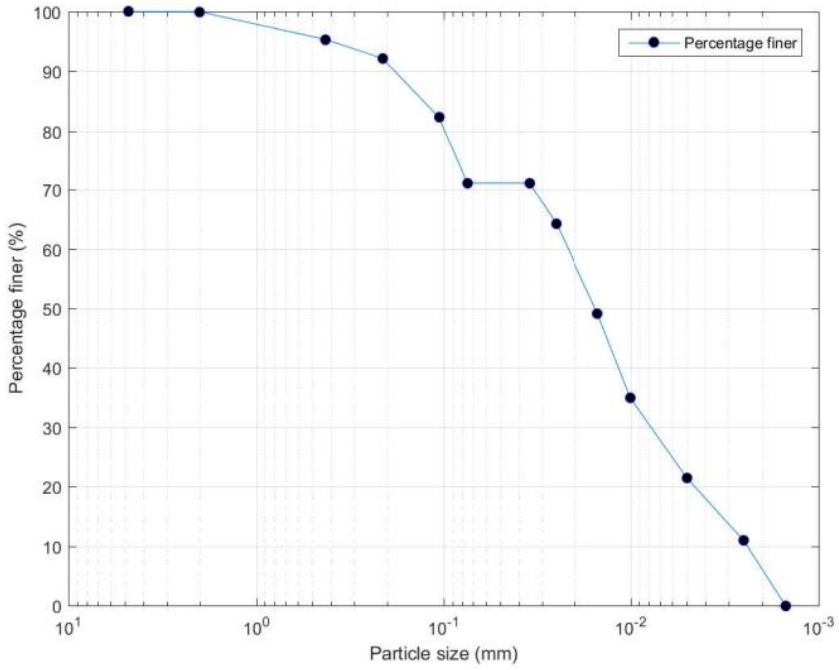

Figure 4.1 Particle size distribution of the synthetic laboratory soil.

Table 4.1 shows the typical properties of the dredged sediments obtained from the Newark harbor and Passaic River. The majority of the sediment consisted of silt and clay which has the highest tendency for absorption of organic pollutants. The clay content is 26% and silt content is 45% so the total fine fraction is 71%.

Table 4.1 Properties of the Dredged Sediments from the Newark Harbor and Passaic River

Parameter	Amount
Water Content	225%
Loss on Ignition	14%
Clay Content	26%
Silt Content	45%
pH	8.0
Total Organic Carbon	7.5%
Pesticides	~ 400 µg/kg
PCB (total)	~4,000 µg/kg
Dioxins	~5,000 µg/kg
Furans	~15,000 µg/kg
PAHs	~100,000 µg/kg
Chromium	~370 mg/kg
Lead	~600 mg/kg

Use of hazardous compound to perform experiments in the lab require a considerable amount of modifications and monitoring the disposal of waste. Hence, to avoid complications, the laboratory experiments used *p-terphenyl* (International Union of Pure and Applied Chemistry (IUPAC) name - 1,4 diphenylbenzene) to mimic the PAH contamination. The *p-terphenyl* has a melting point of 213^0C and a boiling point of 389^0C. the molecular weight of the compound is 230.31 g/mol which is classified as semi-volatile compound (Weast & Astle, 1985).

4.3.1 Sample Preparation

A 0.15g of *p-terphenyl* was measured and mixed with 50 ml of acetone (Certified ACS Reagent Grade with ≥ 99.5% purity) for 2 hours until all the *p-terphenyl* flakes are dissolved in acetone. Then 80g of synthetic soil was mixed with the *p-terphenyl* in acetone for another 2 hours until the acetone is evaporated from the soil leaving the *p-terphenyl* in the soil matrix. The soil was mixed for another 2 hours until the sample is stabilized and air dried for 24 hours prior to use.

4.3.2 Soil Remediation

The contaminated soil prepared in the lab is placed in a sediment treatment chamber (Figure 4.2). The chamber consists of a high dense polycarbonate (transparent) shell and a high-density polyethylene base. The contaminated soil was placed on the US number 325 mesh (mesh aperture of 0.044mm). For the treatment a soil to water ratio (w/w%) of 4% was used. This was maintained by using a total of 2000ml of ozone *nano-bubble* saturated water.

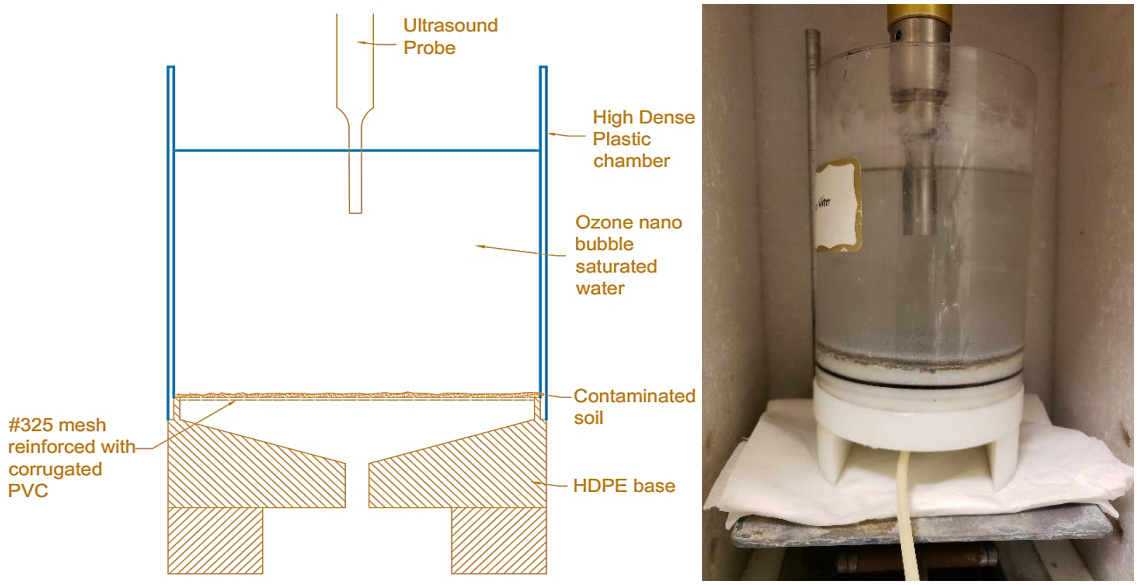

Figure 4.2 Contaminated sediment treatment chamber.

Ozone *nano-bubbles* were generated in a chamber with a capacity of 25 liters where the *nano-bubble* generation chamber is filled up to 21 liters and ozone was injected into the BT50-FR ozone *nano-bubble* generation nozzle. The ozone *nano-bubble* generation system was operated for 6 minutes to obtain the maximum ozone concentrations in water and it was pumped into the sediment treatment chamber. During the remediation process, a varying amount of ultrasound power, ultrasound dwell time, pH in water, temperature, and sonication cycle time was applied to the soil to identify the impact of each parameter on the efficiency of the soil remediation.

At the end of treatment, the soil was drained out of the chamber and dried at 60^0C for 24 hours in a temperature-controlled oven. The samples were brought back to room temperature and air dried for another 24 hours. Then the samples were prepared for the next phase of analysis to identify the removal efficiency.

4.3.3 Chemical Analysis

EPA method 3550B (U. S. EPA 1996) was used to extract *p-terphenyl* from the treated synthetic contaminated sediments. The treated and untreated synthetic soil sediments was extracted using solvent extraction enhanced with ultrasound. A sample of 20g is separated from the treated soil and the sample placed in a 250ml beaker and 100ml of acetone added to the beaker. The acetone and soil containing beaker were placed under horn type ultrasound generator with a maximum 300W power output. Sonication was applied on to the sample in short burst to prevent any changed to the chemical composition of the organic materials in the liquid. These short bursts carried with a gap of 10 minutes between each sonication to prevent temperature rise. Once the sonication process was completed, the

sample was filtered, and another 100ml of acetone is added to the soil and the process is repeated to ensure extraction of all the organic material from the treated soil.

The process was followed up by concentration using the Kuderna-Danish (K-D) triple ball concentration column (Figure 4.3). The sample was concentrated to a sample of 10ml from a 200ml original volume. The (K-D) column was washed by preventing the loss of organic contaminant during the concentration. The concentrated sample was analyzed using a gas chromatograph with mass spectrometry (GC/MS).

Figure 4.3 Kuderna-Danish concentration sample preparation for GC/MS.

Malvern Nano Zetasizer was used for ozone *nano-bubble* size distribution analysis and bubble zeta potentials. To analyze the *nano-bubble* size distribution 12mm square polystyrene cuvettes was used and to analyze the zeta potential a Folded Capillary Zeta Cell (model DTS1070) was used. A sample of *nano-bubble* was tested for each experiment to observe the *nano-bubble* size distribution and the zeta potential.

4.4 Results and Discussion

4.4.1 *Nano-Bubble* Size Distribution and Ozone Concentrations

A major contributor to the remediation was the concentration of ozone in the water and the *nano-bubble* size. During each remediation of 80g of soil, a sample of water is tested to find the concentration of ozone, bubble size distribution and the zeta potential of the bubbles. The *nano-bubble* generation system was run for 6 minutes to obtain the highest saturation of ozone in water. Hence, this ozone *nano-bubbles* concentration was use for all the tests to have highest ozone concentration in water.

Figure 4.4 shows the average *nano-bubble* distribution for temperatures of 15^0C, 20^0C, and 25^0C. A sample of ozone *nano-bubble* saturated water was tested at every 10 remediation cycles to observe any changes in *nano-bubbles* size.

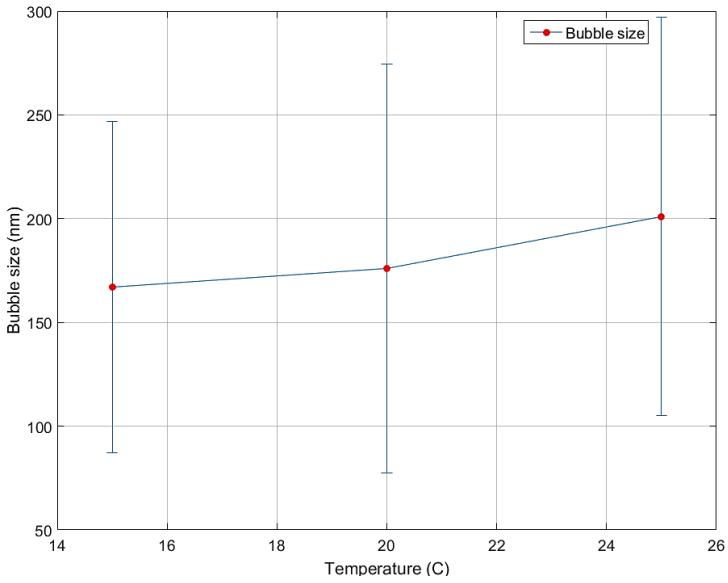

Figure 4.4 Average ozone *nano-bubble* size at temperatures 15^0C, 20^0C, and 25^0C.

By maintaining bubble generation parameters similar, except for the temperature, the average bubble diameter had a slight increase when compared with the lower

temperatures. However, the bubble diameters varied between 90 nm to 300 nm depending on the temperature and the time allowed for the bubbles to stabilize after generation. The observed bubble diameters size distribution during *nano-bubble* generation at temperatures 15^0C, 20^0C, and 25^0C are shown in Figure 4.5.

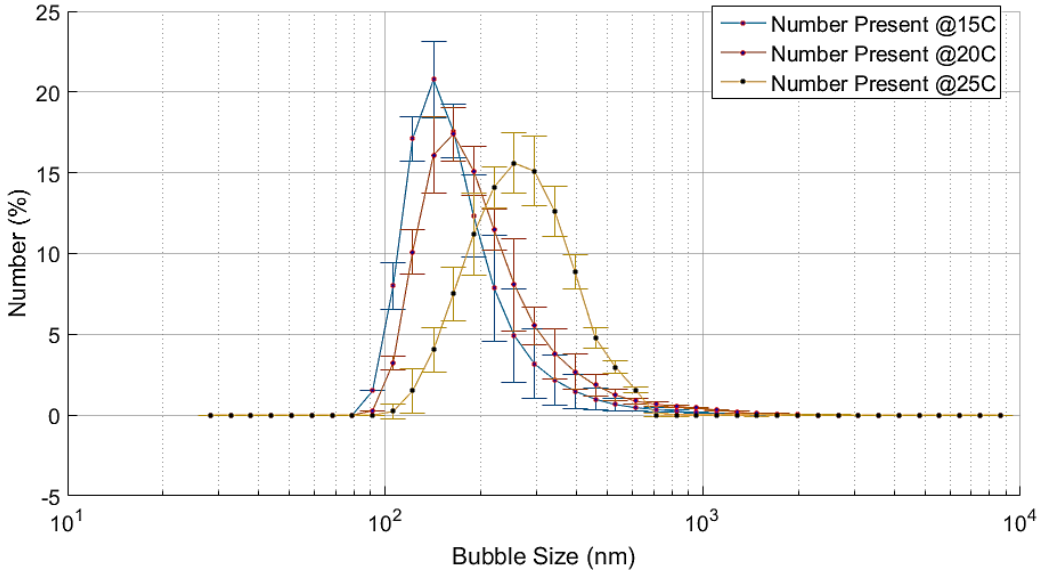

Figure 4.5 Ozone *nano-bubble* size distribution at 15^0C, 20^0C, and 25^0C.

4.4.2 Ozonation Using a Diffuser to Remediate Sediments

The initial trials were performed without using ozone *nano-bubbles* to observe the impact of ozone *nano-bubbles.* Hence, a sample of 80g of soil was placed in a 2000ml beaker where ozone is added to the system using a diffuser and treated over periods of 5, 10, 15, and 30 minutes of ultrasound application. The results obtained are presented in Table 4.2. The chamber is pre ozonated prior to the application of ultrasound and the ozonation was continued during ultrasound application to have sufficient ozone in the water. The water is ozonated after sonication to saturate the sample with ozone. Ozone was delivered at a rate of 3 liters per minute during the ozonation of water through the remediation process.

The removal efficiency of the remediation process is measured using the following formula (Equation 4.1).

$$R_{eff} = \frac{C_{in} - C_{end}}{C_{in}} \times 100 \tag{4.1}$$

Where, R_{eff}- contaminant removal efficiency, C_{in}- concentration of *p-terphenyl* before remediation and C_{end}- concentration on of the contaminants at the end of the remediation. A concentrated sample of *p-terphenyl* using the K-D column was analyzed prior to remediation and analyzed using GC/MS. The corrected area obtained using the GC/MS analysis was established for the concentration of 1875 ppm of *p-terphenyl*. The C_{in}- concentration was established using the corrected area from the intensity graph obtained from the GC/MS analysis.

Table 4.2 Removal Efficiencies Using an Ozone Gas Diffuser

Ultrasound		Ozonation (Diffuser)		Temperature		Removal Efficiency (%)
Sonication time (min)	Sonication Power (W)	Pre-ozone time (min)	Post-Ozone time (min)	Pre (^{0}C)	Post (^{0}C)	
5	600	5	0	21	-	7.97
5	600	5	0	21.1	26.9	Data lost
10	600	10	5	21.3		12.22
10	900	10	5	21.2	33.4	14.68
15	900	15	15	21.1	47.7	12.20
15*	900	15	15	22.7	26	20.08
30*	900	15	15	10	21.1	25.02
30*	900	25	15	11.2	22.6	27.05

* The treatment was performed in segments of 3-minute sonication cycles.

The results obtained during the remediation of the synthetic soil indicated that sonication for long period of time impacting the final removal efficiency. With 900W sonication power increased the water temperature rapidly. This lead to low ozone levels in water as observed in Chapter 3. To avoid the negative impact of high temperatures in water, the sonication was carried out in segments. When the sonication was segmented, the removal efficiencies improved and with larger sonication times higher removal efficiencies were obtained.

High-intensity sonication caused different mixing patterns. Hence, this research used three different horn types with tip diameters of 12.7mm, 19.05mm and 25.4mm. During the investigation, each type of probe was used observe the mixing pattern. The visual observations indicated a substantial increase in the convection flow with the smaller

(12.7mm) probe. However, at higher power levels, the tip damaged. Hence, to minimize the damage and to keep significant mixing capabilities, the probe with 19.06mm diameter was used throughout the study.

4.4.3 Impact of Ultrasound Power on Remediation

After use of the ozone diffuser to remediate contaminated sediments, the study moved to use ozone *nano-bubbles* to remediate the contaminated soil. The initial remediation was conducted by placing the contaminated soil in a beaker and then filling the chamber with ozone saturated water followed by sonication. The sonication started at 600 W and the power levels were increased to 900W, 1050W, and 1200W, and removed efficiencies were calculated after applying ultrasound for specified time intervals.

Table 4.3 shows the results obtained when ozone *nano-bubbles* were used to remediate the *p-terphenyl* contaminated soil. The soil was remediated in segments of 2 minutes of sonication cycles. Contaminated soil was sonicated at a temperature of 20^0C using varying the ultrasound power levels. The sonication was applied for a period of 30 minutes. The ozone *nano-bubble* generation time was maintained for 6 minutes. The pH level in the ozone saturated water was maintained at 7.

Table 4.3 Impact of Ultrasound Power on Removal Efficiency

Sonication Power (W)	Ave. Temperature		Removal Efficiency (%)
	Pre (^{0}C)	Post (^{0}C)	
600	20.1	24.7	21.62
600	20.2	25.1	22.01
900	20.0	25.6	38.86
900	20.1	26.0	41.59
1050	19.9	26.3	57.23
1050	20.2	26.6	56.26
1200	20.0	27.0	64.62
1200	20.3	27.3	63.89

By increasing the ultrasound power to remediate soil, the removal efficiency increased considerably. Using the same ultrasound power did not show same removal efficiency where there was a difference of 0.73%. Also, the difference in removal efficiency between 1050W and 1200W did not show considerable improvement. Each experiment was repeated to investigate the possibilities for the uneven removal of *p-terphenyl*. Observations of unequal removal efficiencies showed the possibility for the ultrasound not reaching certain sections of soil particles to desorb the bonding of soil and *p-terphenly*. To avoid unequal distribution of ultrasound, the remediation chamber was moved throughout the sonication cycle allowing the soil to be directly under the ultrasound probe.

During the GC/MS analysis, it was observed that ozone is reacting with the benzene ring of the *p-terphenyl*. The GC/MS results indicated the broken bonds that contained oxygen molecules and the evidence of the broken benzene rings as shown in Figure 4.6.

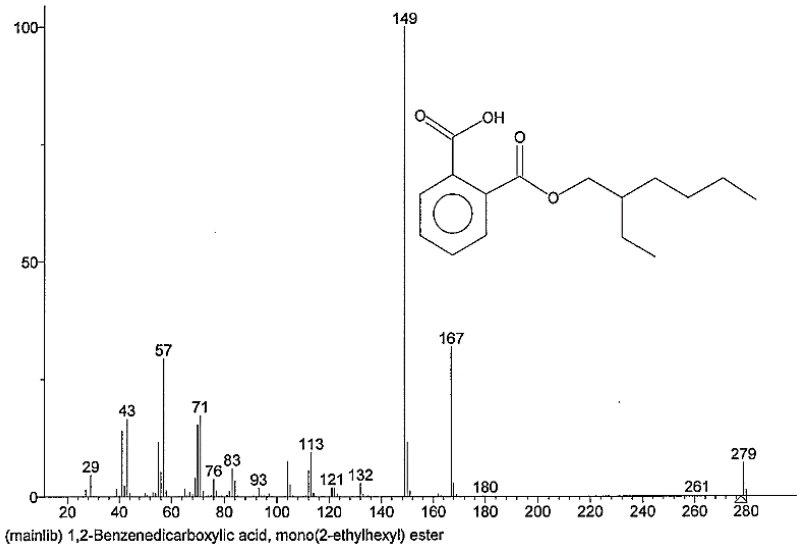

Figure 4.6 Formation of esters from broken *p-terphenyl* benzene rings.

Formation of esters with different constructions observed throughout the GC/MS analysis indicating the reaction of ozone and *p-terphenyl*. Similar observations reported by Taber and Nakajima (2001) during ozonation of hydrocarbons.

4.4.4 Impact of Ozone *Nano-bubble* Delivery on Remediation

It was detected that with ultrasound dissolved ozone concentration and ozone *nano-bubbles* were reduced. Hence, to minimize the impact of reduction in dissolved ozone during sonication, instead of adding 2000ml of ozone *nano-bubble* solution a 1000ml of ozone *nano-bubble* saturated water was added to the chamber. The 1000ml filled chamber (containing contaminated soil) was sonicated. At the end of sonication another 1000ml of ozone *nano-bubble* saturated water was added to the chamber (containing contaminated

soil). Agitated soil was allowed to settle for 20 minutes before draining the water through the opening at the bottom of the chamber.

The results obtained after changing the ozone delivering method is shown in Table 4.4. Similar to the previous experiment tests were performed with ultrasound power 600W, 900W, 1050W, and 1200W. Ozone *nano-bubbles* were generated at a temperature of 20^0C and the sonication was initiated at the same temperature.

Table 4.4 Impact of Ozone *Nano-bubble* Delivery on Removal Efficiency

Sonication Power (W)	**Temperature**		**Removal Efficiency (%)**
	Pre (^{0}C)	**Post (^{0}C)**	
600	20	23.1	22.25
600	20.1	23.6	26.14
900	20	23.9	41.19
900	20	23.5	42.36
1050	20.3	24.2	59.15
1050	20.1	24.1	60.66
1200	19.8	24.2	68.71
1200	20.1	24.3	70.79

Comparing the results obtained by varying the application of ozone *nano-bubble* showed only a slight improvement in removal efficiency of *p-terphenyl*. Each experiment was repeated to find the change in removal efficiency due to the non-uniform application of ultrasound power.

4.4.5 Impact of Total Remediation Time on Efficiency

During the investigations, it was observed that by carry out the many remediation cycles improved the removal efficiency. Increasing the duration of total remediation increased the removal efficiency of *p-terphenyl* at the end of the process. Hence, the remediation process was carryout at a power of 1050W and 1200W at pH level of 7 for total duration of 30, 60, and 120 minutes. The results obtained from the treatment are presented in Table 4.5.

Table 4.5 Removal Efficiency of p-Terphenyl Varying the Time

Ultrasound			Average ozone concentration (mg/l)	Removal efficiency (%)
Power (W)	**Duration per cycle (min)**	**Total sonication time (min)**		
1050	2	30	66.73	60.66
1050	2	60	66.73	72.65
1050	2	120	66.73	81.50
1200	2	30	69.20	70.79
1200	2	60	69.20	77.65
1200	2	120	69.20	82.43
1200	2	180	69.20	85.04
1200	2	240	69.20	91.50

The long treatment duration reduced the concentration of *p-terphenyl* in the synthetic soil sample. However, the longer treatment also showed the breakage of soil particles and showing the change in soil gradation. With high ultrasound power for remediation increases the break in the adsorption bonds between soil as well as breakage of *p-terphenyl* crystals. The broken Benzene rings in the *p-terphenyl* compound allowed

ozone to oxidize the compound further and faster. Hence, exposing the compound to intense sonication power for many remediation cycles can increase the possibility of removing organic pollutants. The broken benzene rings accelerate ozone oxidation of the compound.

4.4.6 Impact of Temperature on Removal Efficiency

One key observation made during ozone *nano-bubble* generation was elevated dissolved ozone concentrations obtained at low water temperatures. Creating a high ozone saturated environment would allow the formation of hydroxyl radicals that would react with contaminants in water. Hence, the experiments were conducted at difference temperatures of 15^0C, 20^0C, and 25^0C. The ultrasound power levels were at 900W and 1200W during the experiments. The ultrasound was applied for 30 minutes duration by using 2 minutes sonication cycles. The results obtained during the experiments are presented in Table 4.6.

Table 4.6 Removal Efficiency of p-Terphenyl Varying the Temperature

Ultrasound		Ave. Temperature (^{0}C)		Removal efficiency (%)	Difference in efficiency (% difference)
Sonication Power (W)	Duration per cycle (min)	Pre (^{0}C)	Post (^{0}C)		
900	2	15	17.1	63.65	7.09
900	2	20	21.9	58.30	1.74
900	2	25	27.0	56.56	0
1200	2	15	17.6	71.90	3.26
1200	2	20	22.2	69.87	1.23
1200	2	25	27.4	68.64	0

At 30 minutes of total sonication, the total remediation time was 600 minutes ((20 minutes allowing the soil to settle + 20 minutes of slow drainage of effluent from the chamber) ×15 (a total of 30 minutes with 2 minutes cycle) sonication cycles). The results showed at low temperatures there is a slight improvement in removal efficiency of *p-Terphenyl* from the soil. As shown in Table 4.5 with decreased in 10^0C of temperature there was 7.09% improvement with 900W and 3.26% improvement with 1200W power.

4.5 Summary and Conclusions

Experiments were performed to targeting to identify the effectiveness of combining ultrasound with ozone *nano-bubbles* to remove PAH from contaminated sediments, where *p-terphenyl* was used to mimic contamination from PAHs in soil. Initial experiments were performed by ozonating the contaminated soil/water solution using a diffuser. The removal efficiency of *p-terphenyl* obtained using a diffuser to ozonate contaminated soil reached a

maximum efficiency of 20.05%. The next set of experiments were performed with ozone *nano-bubbles*. The experiments were performed by varying ultrasound power, sonication time, temperatures at experiments conducted, and approach to ozone *nano-bubbles* delivery process. Increasing the sonication power and sonication time showed higher removal efficiencies. The prolonged remediation of contaminated synthetic soil reached 91.50% after a total sonication time of 240 minutes.

CHAPTER 5

REMEDIATION OF CHROMIUM CONTAMINATED PASSAIC RIVER SEDIMENTS

5.1 Inorganic Contaminants in Passaic River Sediments

Major industries including metal refineries were present along the shoreline of the Passaic River from the start of the first world war and during the second world war becoming a hub for metal refining. The refineries used ore to extract the metals including Arsenic (As), chromium (Cr), copper (Cu), lead (Pb), cadmium (Cd), mercury (Hg), nickel (Ni) and zinc (Zn). The byproducts from these refineries were disposed on land and in wetlands of the Passaic River estuary (Iannuzzi and Weinning, 1995; Crawford et at., 1995; U. S. EPA 1998). Based on the Passaic River sediment samples collected during a U. S. EPA investigation in 1995 and investigated by Feng et al., (2005) showed high metal concentrations at 3 to 5 km kilometer markers along the river. The chromium concentrations in sediments ranged from 7900 µg/kg to 58900 µg/kg and lead concentrations ranging from 4400 µg/kg to 751000 µg/kg. Observed mercury concentration ranged from 100 µg/kg to 10700 µg/kg, and zinc concentrations ranged from 20500 µg/kg to 1620000 µg/kg. Jung (2017) showed average Chromium concentrations of 173± 24 ppm in Passaic river sediments based on nine sampling sites in 2015 and ten sampling sites in 2016. The same study showed that Passaic river sediments contained 333±168ppm of lead, 485±183 ppm of zinc, and 6±5 ppm of arsenic. Table 5.1 presents the U. S. EPA hazardous waste screening criteria (TCLP) and guidelines for the unrestricted soil use (for chronic human health-based soil cleanup objectives) based on New York State Department of Environmental Conservation (NY SDEC).

Table 5.1 U. S. EPA and NY SDEC Guidelines for Land use and Brownfield Sites (TCLP)

	U. S. EPA	**NY SDEC for unrestricted use** (mg/kg)		
Contaminant	**Requirement for cleanup** (mg/kg)	**Carcinogenic**	**Adult non-carcinogenic**	**Child non-Carcinogenic**
Arsenic (Ar)	0.11	0.11	24	2.2
Chromium	11	-	-	-
Chromium (Cr III)	-	-	410	18
Chromium (Cr VI)	-	250	250	11
Copper (Cu)	270	-	12000	500
Lead (Pb)	200	-	-	-
Mercury (Hg)	1	-	0.81	0.81
Nickel (Ni)	72	26000	1600	72
Zinc (Zn)	1100	-	25000	1100

Based on reported results of heavy metals in Passaic river sediments, most heavy metal concentrations are beyond the safe concentrations. When heavy metals enter aquatic environments, they are adsorbed by the colloidal particles and sedimented. These sediments can promote the bioaccumulation that can enter the food chain in the river ecosystem. River biota are impacted due to the non-biodegradability of heavy metals accumulated in sediments. These can impact the ecosystem in the long-term even with low concentrations (Pehlivan et al., 2009). Soil physical properties are also influenced by the heavy metal availability and bonding. The fine particles (colloidal particles) have the highest heavy metal availability in soil. The ligand between heavy metal ion and the soil colloids with high surface area can hold more heavy metals (Marques et al., 2009). Th high

surface area of soil particles and high pH levels in the water decreased the mobility of heavy metal ions. A study conducted by Mcbride and Martinez (2000) observed reduction in solubility of cadmium, copper, arsenic, molybdenum, and lead in agricultural soils when heavy metals were added via sewage sludges. However, they did not observe any change in the solubility of nickel and zinc. In natural environments heavy metal ions do not undergo any chemical or microbial degradation unless a highly oxidizing environment is presented (Kirpichtchikova et al., 2006).

5.2 Soil Treatment Using Ultrasound

Most remediation methods developed for heavy metal contaminated soil are time and energy consuming. A study conducted by Meegoda and Perera (2001) observed that using ultrasound, the soil washing and extraction of heavy metals being highly efficient and less time consuming. The process of remediation included applying a vacuum pressure to extract the liquid in the reactive chamber. Kyllonen et al. (2004) identified the capability of using ultrasound to process the minerals where they used ultrasound to separate lead and zinc from soil at an industrial scale. Newman et al., (1996) studied the use of ultrasound to remove bricks imbedded with copper oxide and showed 40% reduction of copper oxide; when used conventional methods were used with the same conditions achieved 6% reduction of copper oxide. Using ultrasound to remove inorganic contaminants in the soil can always be adopted at large scale due to the flexibility of designing ultrasound transducers. Hamdaoui et al., (2005) used ultrasound to desorb heavy metals from activated carbon with heavy metals. Modeling of desorption kinetics during the removal of heavy

metals from activated carbon indicated increase of surface diffusivity of the carbon by ultrasound.

5.3 Heavy Metal Oxidation Using Ozone

Use of advanced oxidation methods to oxidize heavy metals can help to mobilize the heavy metals making it easy to remove them from the sediments. Most heavy metals when brought to higher oxidation level, increased the mobility in water (O'Mahony et al., 2006). Hence, by converting the heavy metals to a higher oxidation state, it is feasible to remove the heavy metal from sediments. Of the available oxidizers, the use of ozone is one of the preferred highly reactive oxidizers used in the water treatment industry. Interest in using ozone to remediate contaminated soils has been rising over years, especially for the application of non-volatile organic compounds that cannot be removed by conventional soil venting (O'Mahony et al., 2006). Ozone oxidizes heavy metals to their higher oxidation state making them water soluble and easy to separate by filtration (Seo et al., 2010). Using ozone and UV to leach Ethylenediaminetetraacetic acid-lead (EDTA-Pb) from soil, Fingzar and Lestan, (2006) showed 58.4% lead removed from the soil. Rodman et al. (2006) studied the use of advance oxidation methods which included O_3 to form Cr(VI) using Cr(III) propionate. This study was also used as a pretreatment method to analyze the mobility of Cr(VI) by oxidation of ozone and to use the data to develop an analytical method.

5.4 Materials and Methods

Sediments from the Passaic River is contaminated with a verity of organic and inorganic pollutants. This range of organic and inorganics and their concentrations makes the remediation complicated as contaminants concentrations are not uniform within sediments. Hence, to perform laboratory experiments a synthetic soil was synthesized in the laboratory based on the particle size distributions obtained from field samples. The soil was a mixture of rock flour, kaolin, and sand that represent the physical properties of the river sediments and details are provided in chapter 4.

5.4.1 Sample Preparation

One gram of $CrCl_3.6H_2O$ was mixed with 50 ml of DL water and stirred until the $CrCl_3$ is dissolved in DI water. The dissolved $CrCl_3$ was mixed with 80g of the synthetic soil for one hour and kept at a temperature of 40^0C to evaporate the excess water. Then the sample was heated at 850^0C to create adsorption bonds between chromium and soil particles for 3 hours in a high-temperature oven. The soil mixed with $CrCl_3$ was heated in an oxygen-less environment by purging nitrogen during and after heating until the sample reached the room temperature. The oven was switched off and the samples were kept in the oven until they reach the room temperature. The color of the final sample stayed the same as the initial color of the sample before heating after heating showed the oxygen less environment was created in the oven. Figure 5.1 shows samples before heat treatment and the final sample used in the laboratory experiments.

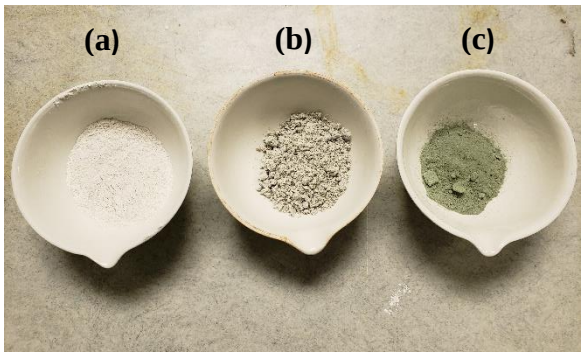

Figure 5.1 Sample preparation and the final sample before remediation ((a) Sample before mixing with $CrCl_3$, (b) Sample after adding $CrCl_3$, (c) Heat treated sample).

When $CrCl_3$ was mixed with the synthetic soil, the color of the soil used in the experiment turned to a dark grey in color. Once the soil was heated in the high temperature over for 3 hours at 850^0C the soil color turned to darker green as presented in Figure 5.1.

5.4.2 Chemical Analysis

The chromium contaminated, and treated samples were dried at 40^0C. A sample of 1.0g was collected from the remediated and dried soil. The 1g of soil was digested using 10ml of trace metal grade nitric acid (67 to 70% w/w). The sample was heated until the full soil sample was dissolved in the nitric acid. Then the solution was diluted by adding 990ml of deionized water bring the total solution volume to 1000ml. The samples were tested using Atomic Absorption Spectrometry (AAS) and Inductively Coupled Plasma Mass Spectrometry (ICP-MS). Figure 5.2 shows the sample preparation method and analysis of the chromium contaminated soil. The nitric acid (67 to 70% w/w) was added to the dried treated sediments and the it was stirred and placed on the hot plate at 50^0C allowing nitric acid to digest the soil.

Figure 5.2 Chromium contaminates sample preparation for testing.

The dissolved ozone was tested using the 4500-O_3 indigo Colorimetric method. Using a Thermo Scientific™ Evolution 201 and 220 UV-Vis spectrophotometer during the 4500-O_3 ozone analysis. Dissolved oxygen levels in water were tested using an Orion Star A329 optical dissolved oxygen and pH monitor. The monitor is capable of measuring oxygen levels in water from 0.00 to 90.00mg/L with an accuracy of ±0.2mg/L.

Ozone *nano-bubbles* were tested every 10 remediation cycles to see the bubble size distribution of the *nano-bubbles* and to observe the zeta potential of the bubbles. Malvern Nano Zetasizer was used for the analyze of the size distribution and zeta potentials of *nano-bubbles*. To analyze the bubble size, 12mm square polystyrene cuvettes were used and to analyze the zeta potential, Folded Capillary Zeta Cell (model DTS1070) was used. The cells used to analyze the *nano-bubbles* are shown in Figure 5.3.

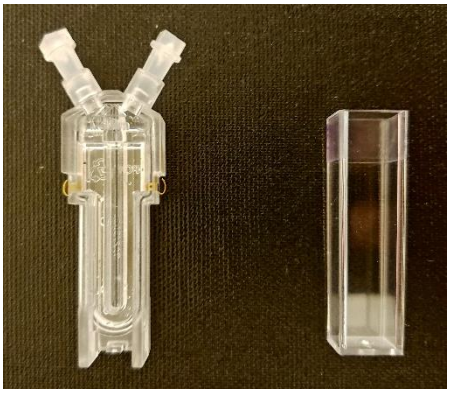

Figure 5.3 Folded capillary zeta cell (model DTS1070) and 12mm square polystyrene cuvettes.

5.4.3 Soil Remediation

A sample of 40g of Synthetic soil contaminated with Chromium Chloride was placed in the reaction chamber (Figure 5.4). The sample size used in the investigation was kept at 40g to reduce the contaminant effluent. The remediation chamber is made of high dense polyethylene base and high dense polycarbonate shell. The soil was placed at the bottom and the soil was subjected to varying amounts of ultrasound power and dwell time, ozone *nano-bubble* saturated water, temperature, and pH level. The soil was drained out of the chamber through the valve on the side of the chamber that included a filtering mesh. The soil was collected to a 20-liter container and the soil that escaped the reaction chamber was allowed to sediment. The sedimented soil was returned to the reaction chamber by filtering the water to minimize the soil lost during the experiment.

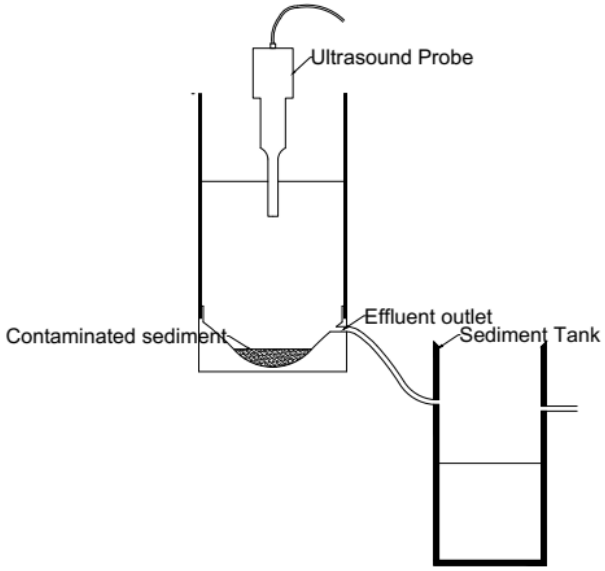

Figure 5.4 Contaminant remediation setup.

5.5 Results and Discussion

5.5.1 Ozone *Nano-Bubbles* in Water

Nano-bubbles are essential ingredients of the proposed remediation. Hence, the bubble size distribution and zeta potential of bubbles were measured. The bubble generation was carried out at different temperatures and the bubbles were tested after 30 minutes generation allowing the system to stabilize. The Zeta potential of the bubbles impact the stability of the *nano-bubbles* and their capability to oxidized heavy metals. The bubble generation was carried out for 6 minutes, which helped to obtain maximum ozone levels in water. The tested bubble sizes are shown in Figure 5.5.

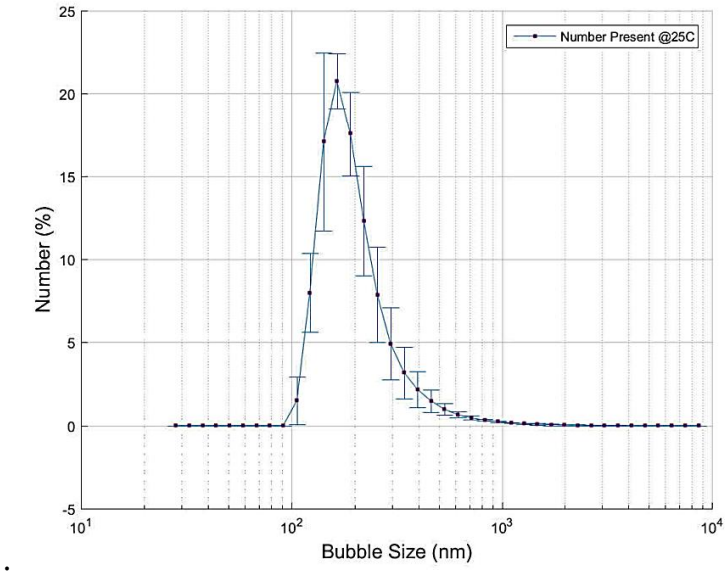

Figure 5.5 Ozone *nano-bubble* size distribution.

The *nano-bubbles* were tested 6 times and the bubble size distribution indicates a number of bubbles with a diameter of 200nm, and the bubble diameter varied between 90nm to 600nm. These variations indicated stable bubbles and ozone saturated water. The average zeta potential for the ozone *nano-bubbles* was -27.3 mV. Hu and Xia (2018) showed ozone *nano-bubbles* with high zeta potential values, where the measured zeta potential varied between -20mV to -26 mV. To identify the *nano-bubble* size variation with the temperature during the experiment, the bubbles were tested at temperatures 15^0C, 20^0C, and 25^0C. The results obtained are shown in Figure 5.6.

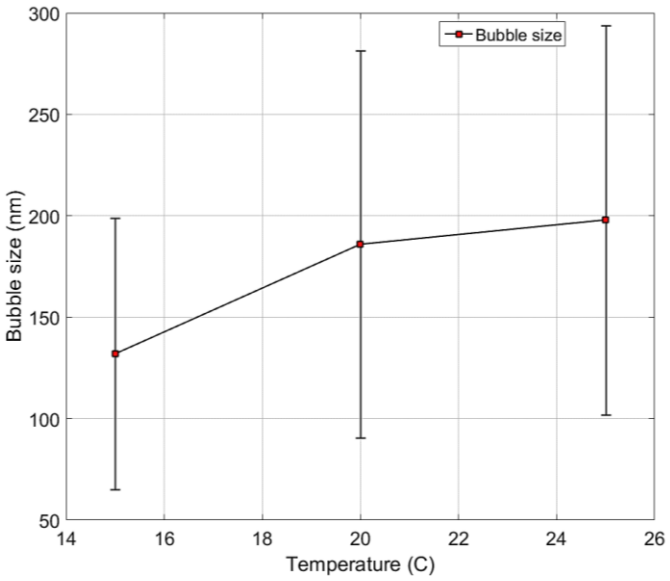

Figure 5.6 Ozone *nano-bubble* variation with temperature.

The bubble diameter did not show significant change with the rise of temperature. The bubble diameter increased slightly as shown in Figure 5.6. Increase in temperature in water used in *nano-bubble* generation had contributed to the increase in bubble diameter. The growing bubble size with the temperature rise was also reported by Callaghan et al., (2014).

5.5.2 Remediation of Chromium Contaminated Sediments

Remediation of chromium contaminated soil was performed in a chamber with a 3-liter volume. The remediation chamber was filled with ozone *nano-bubble* saturated water and ultrasound was applied to the soil and water mixture varying the ozone generation temperature, pH level, ultrasound power, and dwell time. During the investigation, the impact of ultrasound on *nano-bubbles* was investigated and showed by applying ultrasound for long durations had a negative impact on the dissolved gases and *nano-bubbles* in water. Hence, to avoid such negative impact, ultrasound was applied in segments of 1 to 2 minutes

during remediation. The removal efficiency of the chromium was determined by using equation 5.1.

$$R_{eff} = \frac{Cr_{in} - Cr_{end}}{C_{rin}} \times 100 \tag{5.1}$$

Where, Cr_{in} is the chromium concentration of initial specimen, Cr_{end} is the chromium concentration at the end of the experiment. The initial chromium concentration of the samples was 3253 ppm.

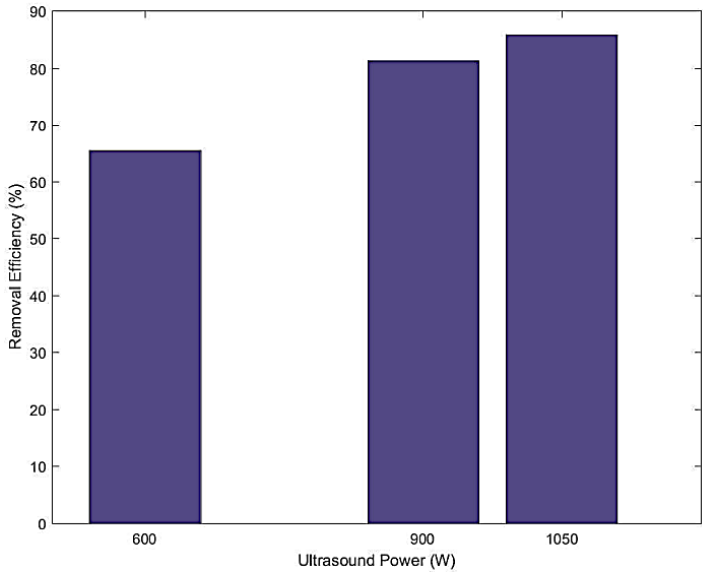

Figure 5.7 Sonication power and removal efficiency at 20^0C.

Higher sonication power levels showed higher removal efficiencies. The sonication was performed at 20^0C and 2-minute intervals to prevent the increase in temperature. A total of 30 minutes of sonication was applied to the sample which took a total of 600 minutes for treatment. Figure 5.7 presents the results obtained by varying the ultrasound power while keeping the duration of the treatment, ozone concentration and the

temperature constant. The lower power levels showed low removal efficiencies. This was also reported by Meegoda and Perera (2001) and Park and Son (2017).

The high concentrations of chromium in the sample required long treatment durations. This study used a very high concentration of chromium in soil to represent actual conditions and to determine optimum treatment conditions to remove heavy metals from the sediments.

Figure 5.8 shows the results obtained by changing the total remediation duration using the same ultrasound power. The ultrasound power was kept at 1050W and the total sonication time was varied to 60 and 120 minutes where the sonication was applied at 2 minute cycles.

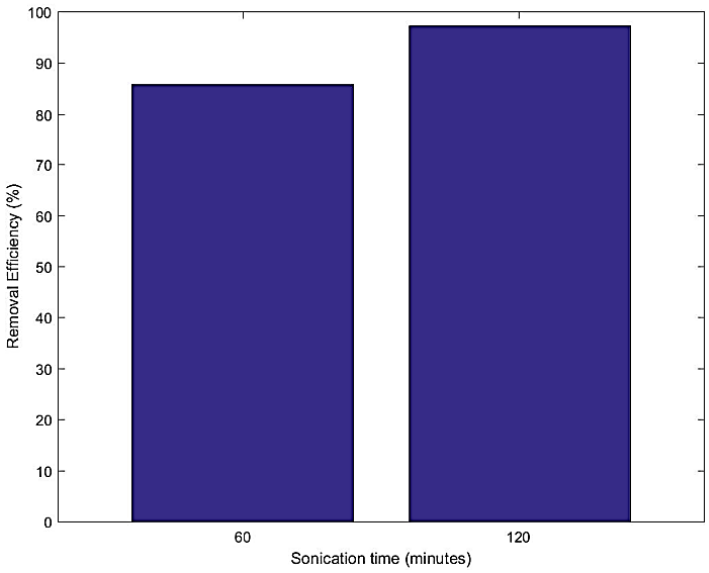

Figure 5.8 Removal efficiency with time.

Due to the high concentrations, the removal took long duration remediation cycles. The removal efficiency of the chromium reached 97.54% at 120 minutes of sonication with a total remediation time of 1800 minutes.

The pH level in water can significantly contribute the heavy metal removal rate. Park and Son (2017) showed high removal efficiencies at low pH levels. This study performed experiments at pH levels of 4, 7, and 10 to evaluate the impact of pH on removal efficiency.

In this test, a sample of soil is collected at the end of 10 minutes of total sonication using 2-minute sonication cycles. For this specific experiment initial chromium contamination level was tripled at 16.714 mg/g (16714 ppm) in the synthetic contaminated soil. Figure 5.9 shows the results. The chromium concentration in the soil reduced over time for all the pH levels but the reduction rate was much high at lower pH levels. The reduction level is much lower at high pH level. Having a low pH level in the water would enhance whereas removal of the remediation performed at high pH levels would not effectively remove the chromium from the soil.

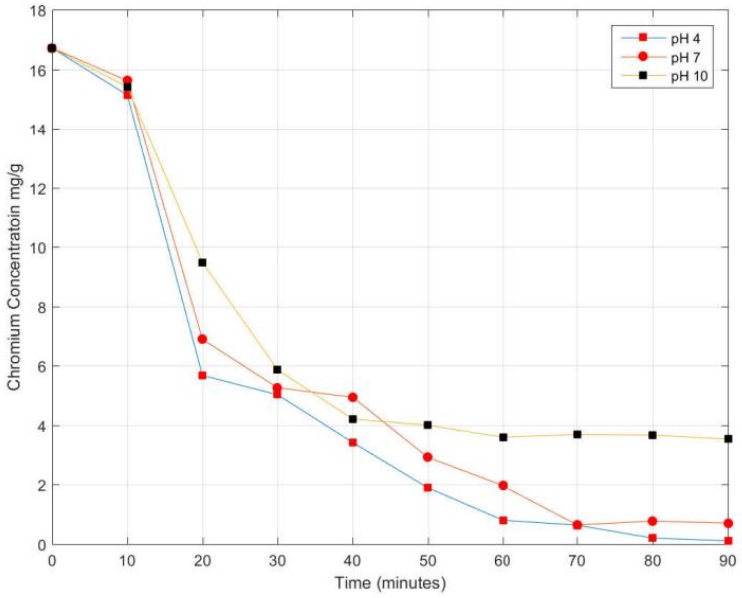

Figure 5.9 Chromium concentration with time (pH4, pH7 and pH 10).

The chromium removal efficiency reached 99% for pH value of 4. At pH 10 the removal efficiency was low because the chromium starts to precipitate by creating $Cr(OH)_3$ which is not water soluble. Chromium in an alkaline environment tend to precipitate making it difficult to separate from soil. Hence, creating an acidic environment for the removal of chromium will increase the removal efficiency.

To identify the individual contribution to chromium removal from ultrasound and ozone *nano-bubbles* three samples of 40g of sample were treated at 20^0C at pH level 7. The results observed are shown in Figure 5.10. The three tests were conducted at the same time with similar conditions where the ultrasound power was kept at 1200W.

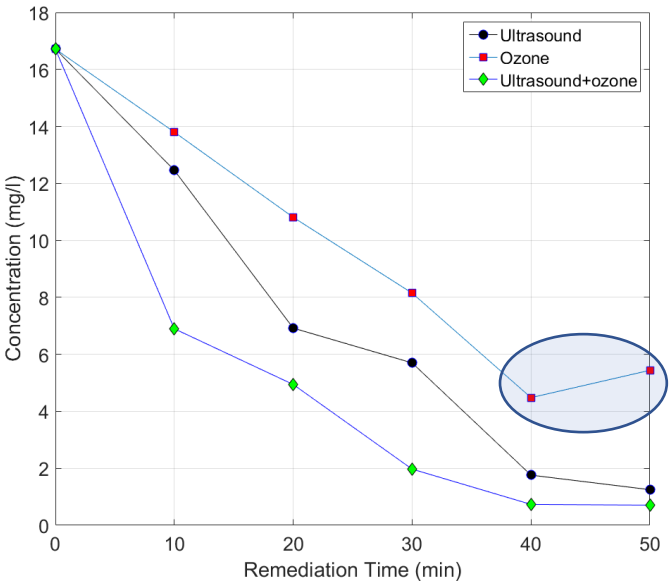

Figure 5.10 Chromium concentration over time when ultrasound and ozone *nano-bubbles* were applied separately.

Ultrasound has a significant impact on remediation of metals than simply using ozone *nano-bubbles*. The ozone *nano-bubble* treated sample did not have agitation. Therefore, combining the two technologies improved the remediation. However, the reduction in soil color which indicated a reaction between chromium and ozone showed a

difference. In Figure 5.10 for ozone treated soil, there was a rise in concentration after 50 minutes of treatment. The sudden increase in chromium concentration was a result of improper mixing of soil. Careful examination of only ozone nano-bubble treated soil showed a color variation as shown in Figure 5.11 (b). Soil collected from the top showed reduced color (circled in Figure 5.11 (b)) and soil at the bottom of the chamber showed dark green color (squared in Figure 5.11 (b)). Differential exposure to ozone nano-bubble saturated water due to lack of agitation resulted in a sudden increase in the chromium concentration. Figure 5.11 (a) shows the effluent collected in the sedimentation tank. The bright yellow color in the effluent demonstrates chromate in liquid. The oxidation number of the chromium in the chromate ion is chromium (VI). The formation of the chromate ion during the use of ozone *nano-bubbles* only experiments confirmed the oxidation of chromium (III).

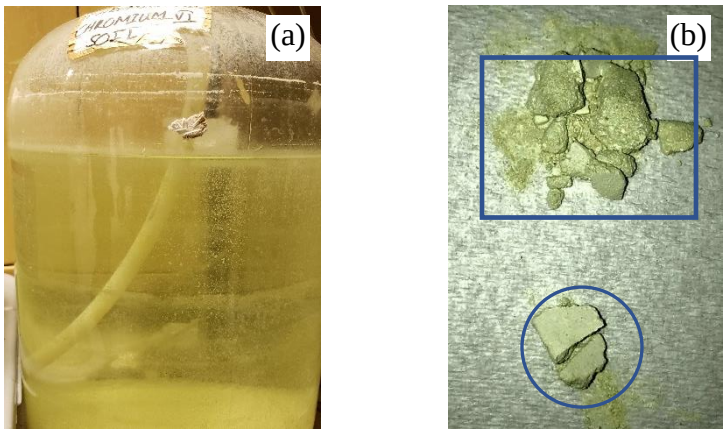

Figure 5.11 (a) Luminesce green effluent and (b) ozonated soil with unequal treatment.

During the investigation, the ultrasound transducer used was a horn type transducer. The distance between the transducer and the contaminated soil has a visible impact on the results obtained for the chromium removal efficiencies. When the ultrasound probe was

kept at distance of 5cm above the contaminated sediments, the removal efficiency improved by 2.5-7%. A few experiments were conducted by varying the distance of the ultrasound probe. During the test, the distance of the probe was varied from 5cm to 10cm. The arrangement is shown in Figure 5.12.

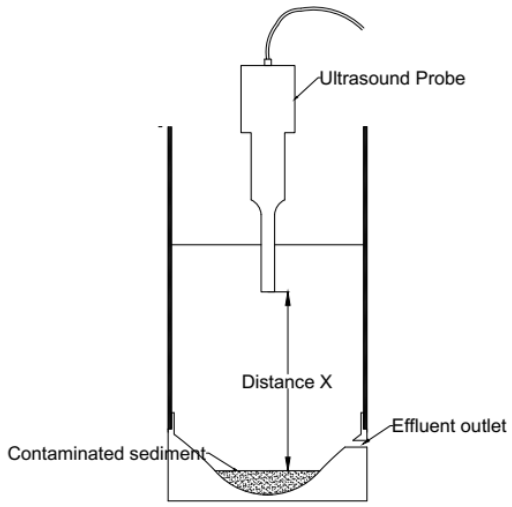

Figure 5.12 The distance varied during the investigation.

The results obtained by varying the distance of the ultrasound probe from the contaminated soil are presented in Table 5.2. During the study the ultrasound power was varied between 900W, and 1200W. The temperature was kept at 20^0C and the pH level was maintained at 7 during ozone *nano-bubble* generation and remediation. Remediation was carried out for a total sonication time of 30 minutes.

Table 5.2 Impact Removal Efficiency Due to the Probe Distance from the Contaminated Sediments

Ultrasound Power (W)	**Sonication cycle duration** (min)	**Distance from the Sediments** (cm)	**Removal efficiency** (%)
900	1	5	84.48
900	1	10	78.94
900	2	5	88.89
900	2	10	82.03
1200	1	5	92.78
1200	1	10	87.73
1200	2	5	91.54
1200	2	10	89.03

By reducing the distance between the probe and the contaminated sediments, the removal efficiency increased. At higher sonication power levels, the distance between soil and probe was not significant. At lower power levels, the distance between the ultrasound probe and the contaminated sediments made a difference of 6.89%. The shape of the remediation chamber ensured falling soil returned to a location just under the probe, which was subjected to sonication. The amount of ultrasound power dissipated due to cavities in water before it reaches the sediments was minimized by moving the probe closer to the contaminated soil. When sonication was performed for 1 minute or 2 minutes, sonication cycles showed varying final removal efficiencies even when the total sonication time was similar. The number of treatment cycles for the 2-minute sonication cycles are half of the total treatment cycles used for 1 minute sonication cycle. This phenomenon can be due to

the hydroxyl ion formation being close to the ultrasound probe that was carried by the acoustic streaming which impacted the contaminated soil. The radical formation using a 20kHz ultrasound probe was imaged by Chen et al., (2006) where the increase in the removal efficiency was observed.

5.5.3 SEM Imaging

Scanning Electron Microscope imaging was carried out on the chromium contaminated soil to identify the impact on the soil and to observe the chromium adsorption on to the soil particles. The SEM images captured before remediation are shown in Figure 5.13.

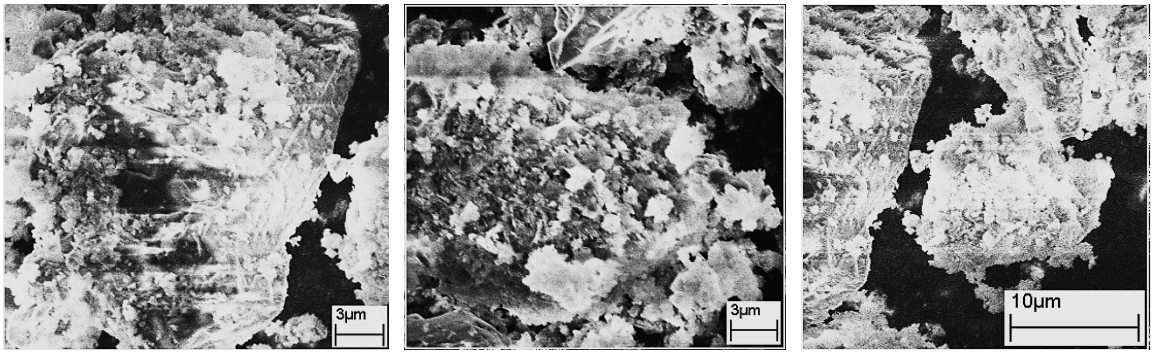

Figure 5.13 SEM imaging – chromium contaminated soil.

Results from SEM images show the chromium deposits on the soil particles. The deposits surrounding soil particles created adsorption bonds. Remediation of these sediments breaks the adsorption bonds and oxidizes the chromium. SEM imaging was performed on partially remediated sediments (after 15 minutes of total sonication). The images obtained are shown in Figure 5.14.

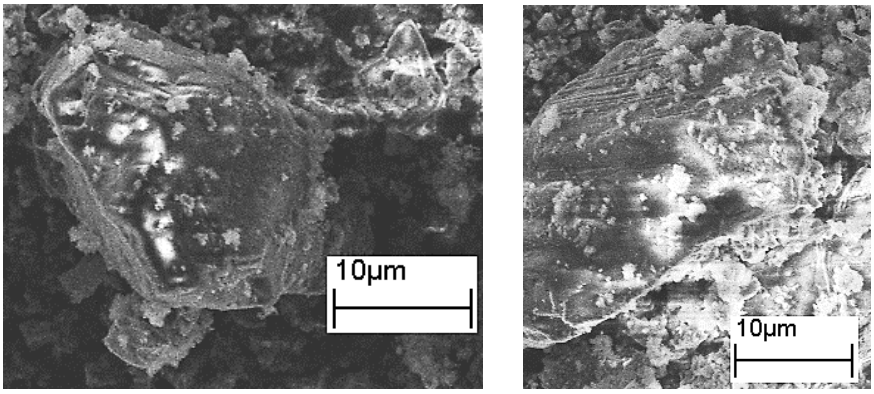

Figure 5.14 Chromium contaminated soil after 15 minutes of sonication.

5.6 Summary and Conclusion

The Chromium contaminated soil showed high removal efficiencies when ultrasound and ozone *nano-bubbles* were applied together. Changing the pH level in the reaction chamber showed increased removal efficiency at lower pH. When the impact of removal efficiencies of ultrasound and ozone *nano-bubbles* was separately compared, ultrasound produced higher removal efficiencies. However, the removal efficiency of ultrasound combined with ozone *nano-bubbles* had a higher removal efficiency when compared with the removal efficiency of individual technologies. The removal of chromium from silty soil was higher when compared to that for clay fraction.

CHAPTER 6

CONCLUSIONS AND RECOMMENDATIONS

6.1 Conclusions

The present study presents a novel, flexible in-situ technology to decontaminate the contaminated Passaic River sediments. This technology involves the use of ultrasound combined with ozone *nano-bubbles* to desorb contaminants from the Passaic River sediments and oxidizing them to less harmful products to be extracted from the sediments. Preliminary studies indicated some undesirability due to incompatibility between the two technologies, especially the increase in temperature due to the application of ultrasound that reduced the dissolved ozone. Investigations were carried out to recognize the most effective way of using ozone *nano-bubbles* with ultrasound to successfully remove and oxidize contaminated sediments. The study first investigated the feasibility to decontaminate sediments using a macro-bubble diffuser to dissolve ozone instead of ozone *nano-bubbles*. Then comprehensive study of ozone *nano-bubbles* performance with ultrasound was performed with the contribution of ozone *nano-bubbles* in dissolving ozone in water, and their impacts over time. The focus of the study was to identify the feasibility of using ultrasound and ozone *nano-bubbles* to remove organic and inorganic contaminants from sediments. Hence, multiple experiments were performed to determine the removal efficiency of organic contaminant removal, where the investigation used *p-terphenyl*. To study the impact of the technology on the inorganics in sediments, the study used chromium. The major findings from the research are summarized as follows:

1. Heat generation increased with higher sonication power levels. However, the percentage of energy loss to the total energy was lower for higher power levels.
2. Ultrasound has a negative impact on the *nano-bubbles* in water. At elevated ultrasound power levels substantial amount of *nano-bubbles* coalesced to form micro-bubbles and the remaining bubbles became smaller when compared to the initial bubble size.
3. For higher power levels of 1200W ultrasound promoted decomposition of ozone in water and increased the oxygen levels in water. At low power levels ultrasound caused a reduction in dissolved ozone as well as oxygen in water. The conductivity of water also reduced after sonication.
4. The zeta potential of bubbles did not indicate a certain pattern of variation with ultrasound power and sonication time.
5. Use of ozone *nano-bubbles* to dissolve ozone in water is highly effective. The bubbles in water remained for 21 days in a closed system. *Nano-bubbles* reached ozone concentrations of 76.49 mg/l at 10^0C, 69.12 mg/l at 15^0C and 52.79 mg/l at 20^0C, which was achieved by operating the BT50-FR nano-bubble nozzle for 6 minutes. The experimental values were much higher than the theoretically calculated values.
6. The diameter of ozone *nano-bubbles* increased slightly with elevated temperatures of 15^0C, 20^0C and 25^0C. The zeta potential observed for ozone *nano-bubbles* increased with temperature (negative zeta potential decreased). The average zeta potential at 15^0C was -27.4 mV, - 26.80 mV at 20^0C and -24.03mV at 25^0C.
7. *Nano-bubbles* improved the ozone retention time in water, after 8 hours the ozone levels in water rose to 10mg/l. Oxygen levels were above 25mg/l after 8 hours when ozone *nano-bubbles* were used.

8. Ultrasound and ozone *nano-bubbles* remediated contaminated sediments. The final best removal efficiency of the p-Terphenyl contaminated soil was 91.50-%. This was observed when carrying out the remediation for a total sonication time of 240 minutes by feeding ozone nano-bubble saturated water in segments.
9. Ultrasound and ozone *nano-bubbles* effectively remediated metal contaminated sediments. The final removal efficiency of chromium was 99%. Use of ozone and ultrasound increased the removal rate of chromium from the soil, when compared with the remediation only by each technology.

6.2 Recommendations for Future Work

1. Use of ozone *nano-bubbles* improved, enhanced, and reduced the amount of ozone needed to remove contaminants from sediments. Hence, this technology can be used to treat of both drinking water and waste water.
2. In this research only 20kHz ultrasound source was used. It is necessary to understand the impact of remediation of using a higher frequency of ultrasound sources to remediate contaminated soil with a cocktail of contaminants ranging from organics to inorganics.
3. The study used a single horn type ultrasound transducer. Further studies, should investigate having multidirectional transducers with high gains.
4. The impact of external pressure on the ultrasound was not investigated during the study and when applying ultrasound underwater, the impact of the external pressure on remediation should be known.

5. Pilot scale study requires multiple ultrasound probes housed in the containment chamber working together to cover the total area within the chamber. Hence, the interferences by ultrasound transducers has to be investigated.
6. Future study should explore the most efficient arrangement of ultrasound probes, where combining multidirectional and unidirectional ultrasound probes to sonicate the sediments.
7. Future study should also explore the Nano-filtration system to precipitate the extracted heavy metals from the effluent water.

REFERENCES

Aboobaker, N., Blackmore, D. Meegoda, J.N. . (2005). Mathematical Modeling of the Movement of Suspended Particles Subjected to Acoustic and Flow Fields. *Applied Mathematical Modeling, 29*(5), 515 - 532.

Aboobaker, N., Meegoda, J. N., & Blackmore, D. (2003). Fractionation and Segregation of Suspended Particles Using Acoustic and Flow Fields. *Journal of Environmental Engineering, 129*(5), 427-434. doi:10.1061/(ASCE)0733-9372(2003)129:5(427)

Armstrong, T. N., Iannuzzi, T. J., Thelen, J. B., Ludwig, D. F., Firstenberg, C. E. (2005). Characterization of Chemical Contamination in Shallow-Water Estuarine Habitats of an Industrialized River. Part II. Metals. *Soil & Sediment Contamination, 14*(1), 35-52.

Agarwal, A., Ng, W. J., & Liu, Y. (2011). Principle and Applications of Microbubble and Nanobubble Technology for Water Treatment. *Chemosphere, 84*(9), 1175-1180.

Babić, S., Petrović, M., & Kaštelan-Macan, M. (1998). Ultrasonic Solvent Extraction of Pesticides from Soil. *Journal of Chromatography A, 823*(1), 3–9.

Bader, H., & Hoigne, J. (1982). Determination of Ozone in Water by the Indigo Method; a Submitted Standard Method. *Ozone: Science & Engineering*. 4(4), 169-176.

Bagal, M. V., & Gogate, P. R. (2012). Sonochemical Degradation of Alachlor in the Presence of Process Intensifying Additives. *Separation and purification technology*, *90*, 92-100.

Bin, A. K., (2004). Ozone Dissolution in Aqueous Systems Treatment of the Experimental Data. *Experimental Thermal and Fluid Science*, 28, 395- 405.

Bosma, T. N., Middeldorp, P. J., Schraa, G., & Zehnder, A. J. (1996). Mass Transfer Limitation of Biotransformation: Quantifying Bioavailability. *Environmental Science & Technology*, *31*(1), 248-252.

Brenner, M. P., & Lohse, D. (2008). Dynamic Equilibrium Mechanism for Surface Nanobubble Stabilization. *Physical Review Letters*, *101*(21), 214505.

Bunkin, N. F., Yurchenko, S. O., Suyazov, N. V, & Shkirin, A. V. (2012). Structure of the Nanobubble Clusters of Dissolved Air in Liquid Media. *Journal of Biological Physics*, *38*(1), 121–152.

Callaghan, A. H., Stokes, M. D., & Deane, G. B. (2014). The Effect of Water Temperature on Air Entrainment, Bubble Plumes, and Surface Foam in a Laboratory Breaking-Wave Analog. *Journal of Geophysical Research: Oceans*, *119*, 7463–7482.

Calvisi, M. L., Iloreta, J. I., & Szeri, A. J. (2008). Dynamics of Bubbles Near a Rigid Surface Subjected to a Lithotripter Shock Wave. Part 2. Reflected Shock Intensifies Non-Spherical Cavitation Collapse. *Journal of Fluid Mechanics*, *616*, 63–97.

Camel, V., & Bermond, A. (1998). The Use of Ozone and Associated Oxidation Processes in Drinking Water Treatment. *Water Research*, *32*(11), 3208–3222.

Cassidy, D., Hampton, D., & Kohler, S. (2002). Combined Chemical (Ozone) and Biological Treatment of Polychlorinated Biphenyls (PCBs) Adsorbed to Sediments. *Journal of Chemical Technology and Biotechnology*, *77*(6), 663–670.

Chen, D., Weavers, L. K., & Walker, H. W. (2006). Ultrasonic Control of Ceramic Membrane Fouling: Effect of Particle Characteristics. *Water research*, *40*(4), 840-850.

Chen, D. (2012). Applications Of Ultrasound in Water and Wastewater Treatment. In D. Chen, S. K. Sharma, & A. Mudhoo (Eds.), *Handbook on application of ultrasound: sonochemistry for sustainability*. Boca Raton, FL: CRC Press, Taylor & Francis Group.

Chen, X., Wang, W., Li, S., Xue, J., Fan, L., Sheng, Z., & Chen, Y. (2010). Optimization of Ultrasound-Assisted Extraction of Lingzhi Polysaccharides Using Response Surface Methodology and its Inhibitory Effect on Cervical Cancer Cells. *Carbohydrate Polymers*, *80*(3), 944-948.

Cho, S.-H., Kim, J.-Y., Chun, J.-H., & Kim, J.-D. (2005). Ultrasonic Formation of Nanobubbles and Their Zeta-Potentials in Aqueous Electrolyte and Surfactant Solutions. *Colloids and Surfaces A: Physicochemical and Engineering Aspects*, *269*(1), 28–34.

Choi, H., Kim, Y. Y., Lim, H., Cho, J., Kang, J. W., & Kim, K. S. (2001). Oxidation of Polycyclic Aromatic Hydrocarbons by Ozone in The Presence of Sand. *Water Science and Technology: A Journal of the International Association on Water Pollution Research*, *43*(5), 349–356.

Choi, J. C., Mega, T. L., German, S., Wood, A. B., & Watson, R. L. (2012). Electrokinetically Altered Normal Saline Modulates Ion Channel Activity. *Biophysical Journal*, *102*(3), 683a.

Chu, L. B., Xing, X. H., Yu, A. F., Zhou, Y. N., Sun, X. L., & Jurcik, B. (2007). Enhanced Ozonation of Simulated Dyestuff Wastewater by Microbubbles. *Chemosphere*, *68*(10), 1854–1860.

Chung, H. I. and Kamon, M. (2005). Ultrasonically Enhanced Electrokinetic Remediation for Removal of Pb and Phenanthrene in Contaminated Soils. *Engineering Geology* 77, 233–242.

Clever, D., Lang, J., & Schröder, D. (2014). Model Hierarchy-Based Optimal Control of Radiative Heat Transfer. *International Journal of Computational Science and Engineering 2, 9*(5-6), 509-525.

Crawford, D. W., Bonnevie, N. L., & Wenning, R. J. (1995). Sources of Pollution and Sediment Contamination in Newark Bay, New Jersey. *Ecotoxicology and Environmental Safety*, *30*(1), 85–100.

Crum, L. A. (1975). Bjerknes Forces on Bubbles in A Stationary Sound Field. *The Journal of the Acoustical Society of America*, *57*(6), 1363–1370.

Czapski, G., Samuni, A., Yelin, R. (1968). The Disappearance of Ozone in Alkaline Solution. *Israel Journal of Chemistry*, 6(6) DOI 10.1002/ijch.196800123

Dear, J., & Field, J. (1988). A Study of The Collapse of Arrays of Cavities. *Journal of Fluid Mechanics*, *190*, 409-425.

Do, S. H., Jo, J. H., Jo, Y. H., Lee, H. K., & Kong, S. H. (2009). Application of a Peroxymonosulfate/Cobalt (PMS/Co(II)) System to Treat Diesel-Contaminated Soil. *Chemosphere*, *77*(8), 1127–1131.

Dumoulin, C., & Deraemaeker, A. (2017). Design Optimization of Embedded Ultrasonic Transducers for Concrete Structures Assessment. *Ultrasonics*, *79*, 18–33.

Ebina, K., Shi, K., Hirao, M., Hashimoto, J., Kawato, Y., Kaneshiro, S.,Yoshikawa, H. (2013). Oxygen and Air Nanobubble Water Solution Promote the Growth of Plants, Fishes, and Mice. *Public Library of Science One*, 8(6), e65339.

Eriksson, M. (2005). *Ozone chemistry in aqueous solution -Ozone decomposition and stabilization*. Royal Institute of Technology, Stockholm.

Feng, H., Onwueme, V., Jaslanek, W. J., Stern, E. A., & Jones, K. W. (2005). Lower Passaic River sediment pollution study using GIS, New Jersey, USA. (No. BNL--73671-2005-CP). Brookhaven national laboratory (US).

Finžgar, N., & Leštan, D. (2006). Advanced Oxidation for Treatment of Aqueous Extracts from EDTA Extraction of Pb and Zn Contaminated Soil. *Journal of Environmental Engineering*, *132*(10), 1376-1380.

Furukawa, M., & Tokunaga, S. (2004). Extraction of Heavy Metals from a Contaminated Soil Using Citrate-Enhancing Extraction by Ph Control and Ultrasound Application. *Journal of Environmental Science and Health, Part A*, *39*(3), 627–638.

Gardoni, D., Vailati, A., and Canziani, R., (2012). Decay of ozone in water: A Review, *Ozone: Science and Engineering*, 34, 233-242

Gillis, C. A., Bonnevie, N. L., & Wenning, R. J. (1993). Mercury Contamination in the Newark Bay Estuary. *Ecotoxicology and Environmental Safety*, *25*(2), 214–226.

Hamdaoui, O., Djeribi, R., & Naffrechoux, E. (2005). Desorption of Metal Ions from Activated Carbon in the Presence of Ultrasound. *Industrial and Engineering Chemistry Research*, *44*(13), 4737–4744.

Hampton, M. A., & Nguyen, A. V. (2010). Nanobubbles and the Nanobubble Bridging Capillary Force. *Advances in Colloid and Interface Science*, *154*(1), 30–55.

Harkin, A., Nadim, A., & Kaper, T. J. (1999). On Acoustic Cavitation of Slightly Subcritical Bubbles. *Physics of Fluids*, *11*(2), 274–287.

Hemelrijck, G. K., Deraemaeker, A., Aggelis, D. G., & Karaiskos, G. (2015). Monitoring of Concrete Structures Using the Ultrasonic Pulse Velocity Method. *Smart Materials and Structures*, *24*(11), 113001.

Hoigné, J. (1998). Chemistry of Aqueous Ozone and Transformation of Pollutants by Ozonation and Advanced Oxidation Processes. In J. Hrubec (Ed.), *Quality and Treatment of Drinking Water II* (pp. 83–141). Berlin, Heidelberg: Springer Berlin Heidelberg.

Hu, L., Wu, X., Liu, Y., Meegoda, J. N., & Gao, S. (2010). Physical Modeling of Air Flow During Air Sparging Remediation. *Environmental Science & Technology*, *44*(10), 3883-3888.

Hu, L., Meegoda, J. N., Du, J., Gao, S., & Wu, X. (2011). Centrifugal Study of Zone of Influence During Air-Sparging. *Journal of Environmental Monitoring*, *13*(9), 2443-2449.

Hu, L., & Xia, Z. (2018). Application of Ozone Micro-Nano-Bubbles to Groundwater Remediation. *Journal of Hazardous Materials*, *342*, 446–453.

Huamao L., Yuhua L., & Zhouhua L. (1997). The Heating Phenomenon Produced by an Ultrasonic Fountain. *Ultrasonics Sonochemistry*, *4*(2), 217–218.

Huang, T.C., and Chen, D.H., (1993). Kinetics of Ozone Decomposition in Aqueous Solution with and without Ultraviolet Radiation. *Journal of the Chinese Institute of Chemical Engineers*, 24, 207–213.

Iannuzzi, T. J., & Wenning, R. J. (1995). Distribution and Possible Sources of Total Mercury in Sediments from the Newark Bay Estuary, New Jersey. *Bulletin of Environmental Contamination and Toxicology*, *55*(6), 901–908

Ik Chung, H., & Kamon, M. (2005). Ultrasonically Enhanced Electrokinetic Remediation for Removal of Pb and Phenanthrene in Contaminated Soils. *Engineering Geology*, 77(3), 233–242.

Ikeura, H., Kobayashi, F., Tamak, M., (2011). Removal of Residual Pesticides in Vegetables using Ozone Microbubbles. *Journal of Hazardous Materials.* 186(1), Pages 956-959

Iloreta, J. I., Fung, N. M., & Szeri, A. J. (2008). Dynamics of Bubbles Near a Rigid Surface Subjected to a Lithotripter Shock Wave. Part 1. Consequences of Interference Between Incident and Reflected Waves. *Journal of Fluid Mechanics*, *616*, 43–61.

Jia, C., Zhu, X., Chen, L., He, M., Yu, P., & Zhao, E. (2010). Extraction of Organophosphorus Pesticides in Water and Juice Using Ultrasound-Assisted Emulsification–Mixroextraction. *Journal of separation science*, *33*(2), 244-250.

Jia, W., Ren, S., & Hu, B. (2013). Effect of Water Chemistry on Zeta Potential of Air Bubbles. *International Journal of Electrochemical Science*, *8*, 5828–5837.

Jin, F., Ye, J., Hong, L., Lam, H., & Wu, C. (2007). Slow Relaxation Mode in Mixtures of Water and Organic Molecules: Supramolecular Structures or Nanobubbles? *The Journal of Physical Chemistry B*, *111*(9), 2255–2261.

Johnson, P. N., & Davis, R. A. (1996). Diffusivity of Ozone in Water. *Journal of Chemical & Engineering Data*, *41*(6), 1485–1487.

Jung, B. H., (2017). Nutrients and Heavy Metals Contamination in an Urban Estuary of Northern New Jersey. *Geoscience*. 7, pp. 108.

Karaiskos, G., Deraemaeker, A., Aggelis, D. G., & Hemelrijck, D. V. (2015). Monitoring of Concrete Structures using the Ultrasonic Pulse Velocity Method. *Smart Materials and Structures*, *24*(11), 113001.

Kavanaugh, M. C., & Trussell, R. R. (1980). Design of Aeration Towers to Strip Volatile Contaminants from Drinking Water. *Journal (American Water Works Association)*, *72*(12), 684–692.

Khuntia, S., Majumder, S. K., & Ghosh, P. (2015). Quantitative Prediction of Generation of Hydroxyl Radicals from Ozone Microbubbles. *Chemical Engineering Research and Design*, *98*, 231-239.

Kidak, R., & Ince, N. H. (2006). Ultrasonic Destruction of Phenol and Substituted Phenols: A Review of Current Research. *Ultrasonics Sonochemistry*, *13*(3), 195–199.

Kim, Y. U., & Wang, M. C. (2003). Effect of Ultrasound on Oil Removal From Soils. *Ultrasonics*, *41*(7), 539–542.

Kimura, T., Sakamoto, T., Leveque, J.-M., Sohmiya, H., Fujita, M., Ikeda, S., & Ando, T. (1996). Standardization of Ultrasonic Power for Sonochemical Reaction. *Ultrasonics Sonochemistry*, *3*(3), S157–S161.

Kirpichtchikova, T. A., Manceau, A., Spadini, L., Panfili, F., Marcus, M. A., & Jacquet, T. (2006). Speciation and Solubility of Heavy Metals in Contaminated Soil Using X-Ray Microfluorescence, EXAFS Spectroscopy, Chemical Extraction, and Thermodynamic Modeling. *Geochimica et Cosmochimica Acta*, *70*(9), 2163–2190.

Klaseboer, E., Fong, S. W., Turangan, C. K., Khoo, B. C., Szeri, A. J., Calvisi, M. L., Sankin, G. N., & Zhong, P. (2007). Interaction of Lithotripter Shockwaves with Single Inertial Cavitation Bubbles. *Journal of Fluid Mechanics*, *593*, 33–56.

Kojima, Y., Asakura, Y., Sugiyama, G., & Koda, S. (2010). The Effects of Acoustic Flow and Mechanical Flow on the Sonochemical Efficiency in a Rectangular Sonochemical Reactor. *Ultrasonics Sonochemistry*, *17*(6), 978–984.

Kornmüller, A., & Wiesmann, U. (2003). Ozonation of Polycyclic Aromatic Hydrocarbons in Oil/Water-Emulsions: Mass Transfer and Reaction Kinetics. *Water Research*, *37*(5), 1023-1032.

Ku, Y., W.J. Su, and Shen, Y. S., (1996). Decomposition Kinetics of Ozone in Aqueous Solution. *Industrial Engineering Chemistry Research*, 35, 3369–3374

Kyllonen, H., Pirkonen, P., Hintikka, V., Parvinen, P., Gronroos, A., & Sekki, H. (2004). Ultrasonically Aided Mineral Processing Technique for Remediation of Soil Contaminated by Heavy Metals. *Ultrasonics Sonochemistry*, *11*(3–4), 211–216.

Laborde, J. L., Hita, A., Caltagirone, J. P., & Gerard, A. (2000). Fluid Dynamics Phenomena Induced by Power Ultrasounds. *Ultrasonics*, *38*(1), 297–300.

Langlais, B., Reckhow, D. A., & Brink, D. R. (Eds.). (1991). *Ozone in Water Treatment: Application and Engineering*. CRC Press.

Lee Meyerson, A., Luther, G. W., Krajewski, J., & Hires, R. I. (1981). Heavy Metal Distribution in Newark Bay Sediments. *Marine Pollution Bulletin*, *12*(7), 244–250.

Lee, K., Park, E., & Seong, W. (2009). High Frequency Measurements of Sound Speed and Attenuation in Water-Saturated Glass-Beads of Varying Size. *The Journal of the Acoustical Society of America*, *126*(1), EL28-EL33.

Lemaire, J., Buès, M., Kabeche, T., Hanna, K., & Simonnot, M. O. (2013). Oxidant Selection to Treat an Aged PAH Contaminated Soil by in Situ Chemical Oxidation. *Journal of Environmental Chemical Engineering*, *1*(4), 1261–1268.

Lenntech B. V. (n.d.). Chromium and Water: Reaction Mechanisms, Environmental Impact and Health Effects. Retrieved February 1, 2018, from https://ww. w.lenntech.com/periodic/water/chromium/chromium-and-water.htm

Li, D., Jing, D., Pan, Y., Wang, W., & Zhao, X. (2014). Coalescence and Stability Analysis of Surface Nanobubbles on The Polystyrene/Water Interface. *Langmuir*, *30*(21), 6079-6088.

Li, D., Jing, D., Pan, Y., Bhushan, B., & Zhao, X. (2016). Study of the Relationship Between Boundary Slip and Nanobubbles on a Smooth Hydrophobic Surface. *Langmuir*, *32*(43), 11287-11294.

Li, P., & Tsuge, H. (2006). Ozone Transfer in a New Gas-Induced Contactor with Microbubbles. *Journal of chemical engineering of Japan*, *39*(11), 1213-1220.

Li, P., Tsuge, H., & Itoh, K. (2009). Oxidation of Dimethyl Sulfoxide in Aqueous Solution using Microbubbles. *Industrial and Engineering Chemistry Research*, *48*(17), 8048–8053.

Lim, M., Ashokkumar, M., & Son, Y. (2014). The Effects of Liquid Height/Volume, Initial Concentration of Reactant and Acoustic Power on Sonochemical Oxidation. *Ultrasonics Sonochemistry*, *21*(6), 1988–1993.

Ljunggren, S., & Eriksson, J. C. (1997). The Lifetime of a Colloid-Sized Gas Bubble in Water and the Cause of the Hydrophobic Attraction. *Colloids and Surfaces A: Physicochemical and Engineering Aspects*, *129–130*, 151–155.

Lürling, M., Meng, D., & Faassen, E. J. (2014). Effects of Hydrogen Peroxide and Ultrasound on Biomass Reduction and Toxin Release in the Cyanobacterium, Microcystis Aeruginosa. *Toxins*, *6*(12), 3260-3280.

Luthy, R. G., Dzombak, D. A., Peters, C. A., Roy, S. B., Ramaswami, A., Nakles, D. V, & Nott, B. R. (1994). Remediating Tar-Contaminated Soils at Manufactured Gas Plant Sites. *Environmental Science & Technology*, *28*(6), 266A–276A.

Magnuson, M. L., Kelty, C. A., & Kelty, K. C. (2001). Trace Metal Loading on Water-Borne Soil and Dust Particles Characterized Through the use of Split-Flow Thin-Cell Fractionation. *Analytical Chemistry*, *73*(14), 3492–3496.

Makuta, T., Takemura, F., Hihara, E., Matsumoto, Y., & Shoji, M. (2006). Generation of Micro Gas Bubbles of Uniform Diameter in an Ultrasonic Field. *Journal of Fluid Mechanics, 548*, 113-131.

Marques, A. P. G. C., Rangel, A. O. S. S., & Castro, P. M. L. (2009). Remediation of Heavy Metal Contaminated Soils: Phytoremediation as a Potentially Promising Clean-Up Technology. *Critical Reviews in Environmental Science and Technology*, *39*(8), 622–654.

Mason, T. J., & Lorimer, J. P. (1988). *Sonochemistry: Theory, applications and uses of ultrasound in Chemistry*. Chichester: Ellis Horwood.

Mason, T. J., Collings, A., & Sumel, A. (2004). Sonic and Ultrasonic Removal of Chemical Contaminants from Soil in the Laboratory and on A Large Scale. *Ultrasonics Sonochemistry*, *11*(3), 205–210.

Masten, S. J., & Davies, S. H. R. (1997). Efficacy of In-Situ for the Remediation of PAH Contaminated Soils. *Journal of Contaminant Hydrology*, *28*(4), 327–335.

Matsumoto, M., & Tanaka, K. (2008). Nano Bubble—Size Dependence of Surface Tension and Inside Pressure. *Fluid Dynamics Research*, *40*(7–8), 546-553. doi:http://dx.doi.org/10.1016/j.fluiddyn.2007.12.006

McBride, M. B. (1989). Reactions Controlling Heavy Metal Solubility in Soils. In *Advances in soil science*. Springer, New York, NY; pp. 1-56

Mcbride, M. B., & Martínez, C. E. (2000). Copper Phytotoxicity in a Contaminated Soil: Remediation Tests with Adsorptive Materials. *Environmental Science and Technology*, *34*(20), 4386–4391.

Meegoda, J. N., & Perera, R. (2001). Ultrasound to Decontaminate Heavy Metals in Dredged Sediments. *Journal of Hazardous Materials*, *85*(1), 73–89.

Meegoda, J. N., & Veerawat, K. (2002). Ultrasound to Decontaminate Organics in Dredged Sediments. *Soil and Sediment Contamination: An International Journal*, *11*(1), 91–116.

Meegoda, J. N., Ho, W., & Frederick, R. M. (1996). Ultrasound Enhanced Soil Washing. In *Proceedings of the 3rd International Symposium on Environmental Geotechnology, Technomic*. Pennsylvania.

Meegoda, J. N., Ho, W., Bhattacharjee, M., Wei, C., Cohen, D. M., Magee, R. S., & Frederick, R. M. (1995). Ultrasound Enhanced Soil Washing. *In 27th Mid-Atlantic Industrial & Hazardous Waste Treatment Conference, Leigh University, Bethlehem. Pennsylvania.*

Minamikawa, K., Wagai, R., Nishimura, S., & Yagi, K. (2015). Heterotrophic Denitrification Constrains the Upper Limit of Dissolved N_2O-Nitrate Concentration Ratio in Agricultural Groundwater. *Nutrient cycling in agroecosystems*, *101*(2), 181-191.

Mishra, K. P., & Gogate, P. R. (2011). Intensification of Sonophotocatalytic Degradation of P-Nitrophenol at Pilot Scale Capacity. *Ultrasonics Sonochemistry*, *18*(3), 739–744.

Mondal, S., Martinson, J. A., Ghosh, S., Watson, R., & Pahan, K. (2012). Protection of tregs, suppression of Th1 and Th17 cells, and amelioration of experimental allergic encephalomyelitis by a physically-modified saline. *PLOS ONE*, *7*(12), e51869.

Mora, A. P. de, Ortega-Calvo, J. J., Cabrera, F., & Madejón, E. (2005). Changes in Enzyme Activities and Microbial Biomass After "In Situ" Remediation of a Heavy Metal-Contaminated Soil. *Applied Soil Ecology*, *28*(2), 125–137.

Morra, M. J., Blank, R. R., Freeborn, L. L., & Shafii, B. (1992). Size Fractionation of Soil Organo-Mineral Complexes using Ultrasonic Dispersion. *Soil Science*, *152*, 294–303.

Na, S., Park, Y., Hwang, A., Ha, J., Kim, Y., & Khim, J. (2007). Effect of Ultrasound On Surfactant-Aided Soil Washing. *Japanese Journal of Applied Physics*, *46*(7S), 4775.

Newman, A. P., Lorimer, J. P., Mason, T. J., & Hunt, K. R. (1997). An Investigation into the Ultrasonic Treatment of Polluted Solids. *Ultrasonics Sonochemistry*, *4*(2), 153–156.

Nomura, S., & Nakagawa, M. (1993). Ultrasonic Enhancement of Heat Transfer on Narrow Surface. *Transactions of the Japan Society of Mechanical Engineers Series B*, *59*(563), 2232–2237.

O'Mahony, M. M., Dobson, A. D. W., Barnes, J. D., & Singleton, I. (2006). The Use of Ozone in the Remediation of Polycyclic Aromatic Hydrocarbon Contaminated Soil. *Chemosphere*, *63*(2), 307–314.

Oh, Y. K., Park, S. H., & Cho, Y. I. (2002). A Study of The Effect of Ultrasonic Vibrations on Phase-Change Heat Transfer. *International Journal of Heat and Mass Transfer*, *45*(23), 4631–4641.

Ohgaki, K., Khanh, N. Q., Joden, Y., Tsuji, A., & Nakagawa, T. (2010). Physicochemical Approach to Nanobubble Solutions. *Chemical Engineering Science*, *65*(3), 1296–1300.

Ohl, C. D., & Ikink, R. (2003). Shock-Wave-Induced Jetting of Micron-Size Bubbles. *Physical Review Letters*, *90*(21), 214502.

Pan, G., & Yang, B. (2012). Effect of Surface Hydrophobicity on the Formation and Stability of Oxygen Nanobubbles. *Chemphyschem : A European Journal of Chemical Physics and Physical Chemistry*, *13*(8), 2205–2212.

Pang, Y. L., Abdullah, A. Z., & Bhatia, S. (2011). Review on Sonochemical Methods in the Presence of Catalysts and Chemical Additives for Treatment of Organic Pollutants in Wastewater. *Desalination*, *277*(1), 1–14.

Park, B., & Son, Y. (2017). Ultrasonic and Mechanical Soil Washing Processes for the Removal of Heavy Metals from Soils. *Ultrasonics Sonochemistry*, *35*, 640–645.

Qiu, J., Zou, Z., Wang, S., Wang, X., Wang, L., Dong, Y., (2017). Formation and Stability of Bulk Nanobubbles Generated by Ethanol–Water Exchange.

Pehlivan, E., Özkan, A. M., Dinç, S., & Parlayici, Ş. (2009). Adsorption of Cu^{2+} and Pb^{2+} Ion on Dolomite Powder. *Journal of Hazardous Materials*, *167*(1), 1044–1049.

Rai, D., Sass, B. M., & Moore, D. A. (1987). Chromium(III) Hydrolysis Constants and Solubility of Chromium(III) Hydroxide. *Inorganic Chemistry*, *26*(3), 345–349.

Rizzuti, L., V. Augugliaro, and Marucci, J., (1976). Ozone Absorption in Alkaline Solutions. *Chemical Engineering Science*, 31, 877–880

Rodman, D. L., Carrington, N. A., & Xue, Z. L. (2006). Conversion of Chromium (III) Propionate to Chromium (VI) by the Advanced Oxidation Process: Pretreatment of a Biomimetic Complex for Metal Analysis. *Talanta*, *70*(3), 668-675.

Sedlák, M. (2006). Large-Scale Supramolecular Structure in Solutions of Low Molar Mass Compounds and Mixtures of Liquids: I. Light Scattering Characterization. *The Journal of Physical Chemistry B*, *110*(9), 4329–4338.

Sedlák, M. (2006). Large-Scale Supramolecular Structure in Solutions of Low Molar Mass Compounds and Mixtures of Liquids: II. Kinetics of the Formation and Long-Time Stability. *The Journal of Physical Chemistry B*, *110*(9), 4339–4345.

Sehested, K., Holcman, J., Bjergbakke, E., & Hart, E. J. (1984). A Pulse Radiolytic Study of the Reaction Hydroxyl + Ozone in Aqueous Medium. *The Journal of Physical Chemistry*, *88*(18), 4144–4147.

Seo, S. H., Sung, B. W., Kim, G. J., Chu, K. H., Um, C. Y., Yun, S. L., Ko, K. B. (2010). Removal of Heavy Metals in an Abandoned Mine Drainage Via Ozone Oxidation: A Pilot-Scale Operation. *Water Science and Technology: A Journal of the International Association on Water Pollution Research*, *62*(9), 2115–2120.

Shen, Y., Longo, M. L., & Powell, R. L. (2008). Stability and Rheological Behavior of Concentrated Monodisperse Food Emulsifier Coated Microbubble Suspensions. *Journal of colloid and interface science*, *327*(1), 204-210.

Siegrist, R. L., Crimi, M., & Brown, R. A. (2011). In Situ Chemical Oxidation: Technology Description and Status. *In situ chemical oxidation for groundwater remediation* (pp. 1-32). Springer, New York, NY.

Son, Y., Cha, J., Lim, M., Ashokkumar, M., & Khim, J. (2011). Comparison of Ultrasonic and Conventional Mechanical Soil-Washing Processes for Diesel-Contaminated Sand. *Industrial & Engineering Chemistry Research*, *50*(4), 2400–2407.

Son, Y., Lim, M., Ashokkumar, M., & Khim, J. (2011). Geometric Optimization of Sonoreactors for the Enhancement of Sonochemical Activity. *The Journal of Physical Chemistry C*, *115*(10), 4096–4103.

Son, Y., Lim, M., Khim, J., & Ashokkumar, M. (2012). Attenuation Of UV Light in Large-Scale Sonophotocatalytic Reactors: The Effects of Ultrasound Irradiation and Tio2 Concentration. *Industrial & Engineering Chemistry Research*, *51*(1), 232–239.

Sotelo, J. L., Beltran, F. J., Benitez, F. J., & Beltran-Heredia, J. (1987). Ozone Decomposition in Water: Kinetic Study. *Industrial & Engineering Chemistry Research*, *26*(1), 39–43.

Sumikura, M., Hidaka, M., Murakami, H., Nobutomo, Y., & Murakami, T. (2007). Ozone Micro-Bubble Disinfection Method for Wastewater Reuse System. *Water Science and Technology: A Journal of the International Association on Water Pollution* Research, 56(5), 53–61.

Suslick, K. S. (1990). Sonochemistry. *Science, 247*(49), 1439-1445.

Taber, D. F., & Nakajima, K. (2001). Unsymmetrical Ozonolysis of a Diels-Alder Adduct: Practical Preparation Of A Key Intermediate for Heme Total Synthesis. *Journal of Organic Chemistry*, *66*(7), 2515–2517.

Takahashi, M., Chiba, K., & Li, P. (2007). Formation of Hydroxyl Radicals by Collapsing Ozone Microbubbles Under Strongly Acidic Conditions. *The Journal of Physical Chemistry B*, *111*(39), 11443–11446.

Takahashi, M., Chiba, K., & Li, P. (2007). Free-Radical Generation from Collapsing Microbubbles in the Absence of a Dynamic Stimulus. *The Journal of Physical Chemistry B*, *111*(6), 1343–1347.

Takahashi, M., & Li, P. (2009). Base and Technological Application of Micro-Bubble and Nano-Bubble. *Mater. Integr*, *22*, 2-19.

Tang, W. Z. (2003). *Physicochemical Treatment of Hazardous Wastes*. Boca Raton, FL: CRC Press, Taylor & Francis Group.

Teramoto, M., S. Imamura, N. Yatagai, Y. Nishikawa, and Teranishi, H., (1981). Kinetics of the Self-Decomposition of Ozone and the Ozonation of Cyanide Ion and Dyes in Aqueous Solutions. *Journal of Chemical Engineering Japan*, 14, 383–388.

The Louis Berger Group, Inc. (2014). *Remedial Investigation Report for the Focused Feasibility Study of the Lower Eight Miles of the Lower Passaic River*. Kansas City District.

Thompson, L. H., & Doraiswamy, L. K. (1999). Sonochemistry: Science and Engineering. *Industrial & Engineering Chemistry Research*, *38*(4), 1215–1249.

Tsuge, H., Ogawa, T., & Ohmasa, R. (2008). Microbubble Formation by Electrolysis Using a New Mixing Equipment with Low Frequency Vibratory Fins. *Journal of Chemical Engineering of Japan*, *41*(7), 557–561.

Uematsu, H (2006) Advantage and Possibility of OHR Microbubbles, *Journal of Resources and Environment*, 42, 100-103

Urban, J. D., Tachovsky, J. A., Haws, L. C., Staskal, D. W., & Harris, M. A. (2009). Assessment of Human Health Risks Posed by Consumption of Fish from the Lower Passaic River, New Jersey. *Science of the total environment*, *408*(2), 209-224.

U. S. EPA (1986). Method 3050: Acid Digestion of Sediment, Sludges and Soils, *Test Methods for the Evaluation of Solid Waste: Laboratory Manual Physical Chemical Methods: vol. IA*. Washington, DC 20460: Office of Solid Waste; 1986.

U. S. EPA, (1991). *Methods for Aquatic Toxicity Identification Evaluations: Phase I Toxicity Characterization Procedures, second ed. EPA/600/6- 91/003, National Effluent Toxicity Environmental Research Laboratory Report 18-90*, United States Environmental Protection Agency Environmental Research Laboratory, Duluth, MN.

U. S. EPA, (1991). *Sediment Toxicity Identification Evaluations: Phase I (characterization), Phase II (identification), and Phase II (confirmation) Modifications of effluent Procedures, EPA 600/6-91/007.* United States Environmental Protection Agency Environmental Research Laboratory, Duluth, MN.

U. S. EPA, (1991). *Toxicity Identification Evaluation: Characterization of Chronically Toxic Effluents, Phase I, EPA/600/6-91/005.* United States Environmental Protection Agency Environmental Research Laboratory, Duluth, MN.

U. S. EPA (1996). SW-846 Manual, Method 3550B, Rev. 2: Ultrasonic Extraction. US Environmental Protection Agency. Retrieved July 2, 2015, from http://www.epa.gov/epaoswer/hazwaste/test/pdfs/3550b.pdf

U. S. EPA, 1998. Sediment Quality of NY/NJ Harbor System. An Investigation under the Regional Environmental Monitoring and Assessment Program (R-EMAP), EPA/902-R-98/001, United States Environmental Protection Agency.

U. S. EPA, (2002). Supplemental guidance for developing soil screening levels for superfund sites. Office of Solid Waste and Emergency Response, Washington, D.C. Retrieved March 12, 2015, from http://www.epa.gov/superfund/health/conmedia/soil/index.htm

U. S. EPA, (2014). Cleaning up the Nation's Hazardous Wastes Sites. Retrieved March 12, 2015, from http://www.epa.gov/superfund/

Ushikubo, F. Y., Furukawa, T., Nakagawa, R., Enari, M., Makino, Y., Kawagoe, Y., … Oshita, S. (2010). Evidence of the existence and the stability of nano-bubbles in water. *Colloids and Surfaces A: Physicochemical and Engineering Aspects*, *361*(1), 31–37.

Vajnhandl, S., & Majcen Le Marechal, A. (2005). Ultrasound in textile dyeing and the decolouration/mineralization of textile dyes. *Dyes and Pigments*, *65*(2), 89–101.

von Sonntag, C., & von Gunten, U. (2012). *Chemistry of ozone in water and wastewater treatment* (Illustrated reprint). IWA Publishing.

Walker, W. J., McNutt, R. P., & Maslanka, C. K. (1999). The potential contribution of urban runoff to surface sediments of the Passaic River: Sources and chemical characteristics. *Chemosphere*, *38*(2), 363–377.

Wang, Y., Bhushan, B., & Zhao, X. (2009). Improved nanobubble immobility induced by surface structures on hydrophobic surfaces. *Langmuir*, *25*(16), 9328–9336.

Wang, Y., Liu, G., Hu, H., Li, T. Y., Johri, A. M., Li, X., & Wang, J. (2015). Stable encapsulated air nanobubbles in water. *Angewandte Chemie*, *127*(48), 14499-14502.

Weast, R. C., & Astle, M. J. (1985). *CRC Handbook of Data on Organic Compounds. Volumes I and II*. Boca Raton, FL: CRC Press.

Weijs, J. H., & Lohse, D. (2013). Why Surface Nanobubbles Live for Hours. *Physical Review Letters*, *110*(5), 054501.

Weissler, A. (1959). Formation of Hydrogen Peroxide by Ultrasonic Waves: Free Radicals. *Journal of the American Chemical Society*, *81*(5), 1077–1081.

Wu, T. N., & Shi, M. C. (2010). pH-affecting sonochemical formation of Hydroxyl radicals under 20 KHz ultrasonic irradiation. *Sustain. Environ. Res*, *20*(4), 245–250.

Xia, Z., & Hu, L. (2016). Remediation of organic contaminated industrial sites by Ozone micro-nano bubbles. In *5th Geo-Chicago Conference: Sustainable Waste Management and Remediation, Geo-Chicago 2016* (pp. 371–380). Chicago; United States.

Yu, D. Y., Kang, N., Bae, W., & Banks, M. K. (2007). Characteristics in Oxidative Degradation by Ozone for Saturated Hydrocarbons in Soil Contaminated with Diesel Fuel. *Chemosphere*, *66*(5), 799–807.

Ziembowicz, S., Kida, M., & Koszelnik, P. (2017). Sonochemical Formation of Hydrogen Peroxide. In *Multidisciplinary Digital Publishing Institute Proceedings*. Vol. 2(5), pp. 188.

Zou, Z., & Meegoda, J. N. (2018). A Validation of the Ultrasound Wave Velocity Method to Predict Porosity of Dry and Saturated Cement Paste. *Advances in Civil Engineering*, 1-8.